AD-A118 439 PENNSYLVANIA STATE UNIV UNIVERSITY PARK APPLIED RESE--ETC F/G 13/1
DISCRETE FREQUENCY NOISE AND ITS REDUCTION IN SMALL AXIAL-FLOW --ETC(U)
MAR 82 J M FITZGERALD N00024-79-C-6043
UNCLASSIFIED ARL/PSU/TM-82-76 NL

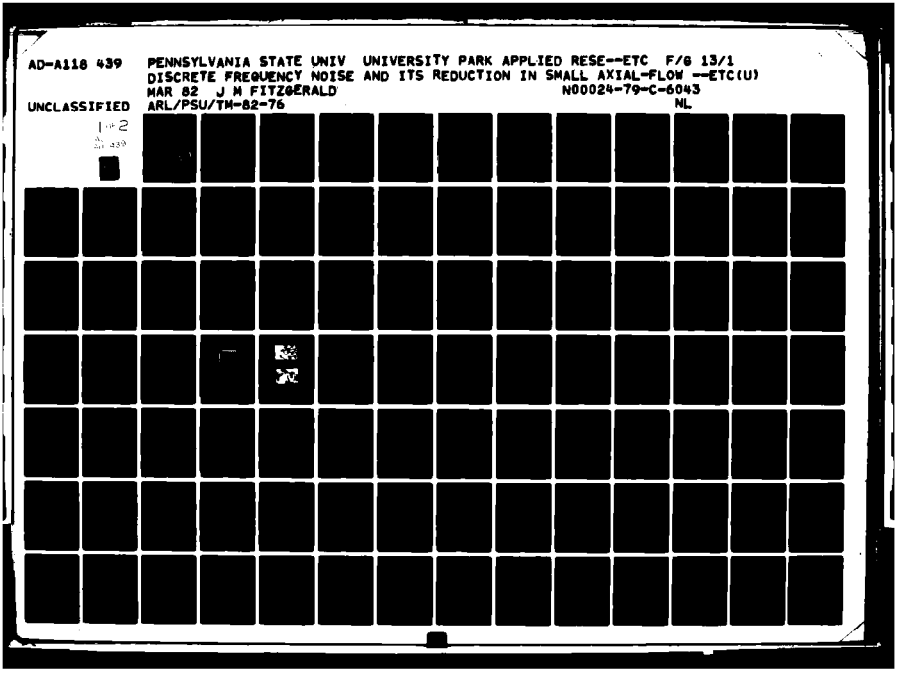

(6)

DISCRETE FREQUENCY NOISE AND ITS REDUCTION IN SMALL AXIAL-FLOW FANS

James M. Fitzgerald

Technical Memorandum
File No. TM 82-76
2 March 1982
Contract No. N00024-79-C-6043

Copy No. 42

The Pennsylvania State University
APPLIED RESEARCH LABORATORY
Post Office Box 30
State College, PA 16801

Approved for Public Release
Distribution Unlimited

NAVY DEPARTMENT

NAVAL SEA SYSTEMS COMMAND

UNCLASSIFIED

SECURITY CLASSIFICATION OF THIS PAGE (When Data Entered)

REPORT DOCUMENTATION PAGE		READ INSTRUCTIONS BEFORE COMPLETING FORM
1. REPORT NUMBER TM 82-76	2. GOVT ACCESSION NO. AD-A118439	3. RECIPIENT'S CATALOG NUMBER
4. TITLE (and Subtitle) DISCRETE FREQUENCY NOISE AND ITS REDUCTION IN SMALL AXIAL-FLOW FANS		5. TYPE OF REPORT & PERIOD COVERED Technical Memorandum 6. PERFORMING ORG. REPORT NUMBER
7. AUTHOR(s) James Michael Fitzgerald		8. CONTRACT OR GRANT NUMBER(s) N00024-79-C-6043
9. PERFORMING ORGANIZATION NAME AND ADDRESS Applied Research Laboratory Post Office Box 30 State College, PA 16801		10. PROGRAM ELEMENT, PROJECT, TASK AREA & WORK UNIT NUMBERS
11. CONTROLLING OFFICE NAME AND ADDRESS Naval Sea Systems Command Washington, DC 20362		12. REPORT DATE March 2, 1982 13. NUMBER OF PAGES 147 pages
14. MONITORING AGENCY NAME & ADDRESS(if different from Controlling Office)		15. SECURITY CLASS. (of this report) Unclassified 15a. DECLASSIFICATION/DOWNGRADING SCHEDULE

16. DISTRIBUTION STATEMENT (of this Report)

Approved for public release. Distribution unlimited
Per NAVSEA- April 5, 1982.

17. DISTRIBUTION STATEMENT (of the abstract entered in Block 20, if different from Report)

18. SUPPLEMENTARY NOTES

19. KEY WORDS (Continue on reverse side if necessary and identify by block number)

thesis, fan, noise

20. ABSTRACT (Continue on reverse side if necessary and identify by block number)

The discrete frequency noise radiated from representative types of axial-flow fans used in electronic equipment is studied in detail. Narrow-band analysis of the discrete frequency noise radiated by these types of fans has been conducted in a free-field environment. The far-field sound pressure level, radiated directivity, and total radiated power of the discrete frequency noise is presented. The influence of operating point on the sound radiated from the fans is determined. The discrete frequency noise dominates the characteristic acoustic spectra at high flow coefficients.

DD FORM 1 JAN 73 1473 EDITION OF 1 NOV 65 IS OBSOLETE

UNCLASSIFIED

SECURITY CLASSIFICATION OF THIS PAGE (When Data Entered)

20.-Abstract

The radiated directivity of the discrete frequency noise is generally uniform. Based on the data collected and on the theoretical aspects presented, the principal source of the discrete frequency noise is identified for each of the fans as the interaction of the fan rotor with a circumferentially distorted, nonuniform flow. This undesirable flow field is generated by the shroud surrounding the rotor and the rotor-shroud support structure. The flow field produces unsteady rotor blade loads which generate propagating acoustic pressure distributions.

A collection of prototype design modifications are developed for each representative fan to reduce the radiated discrete frequency noise by improving the uniformity of the local flow field. The principal source of the discrete frequency noise is identified for each of the fans as the interaction of the fan rotor with a circumferentially distorted, nonuniform flow. This undesirable flow field is generated by the shroud surrounding the rotor and the rotor-shroud support structure. The flow field produces unsteady rotor blade loads which generate propagating acoustic pressure distributions.

A collection of prototype design modifications are developed for each representative fan to reduce the radiated discrete frequency noise by improving the uniformity of the local flow field. The principal modifications are: the improvement in the circumferential symmetry of the rotor annulus, inlet, and outlet; the reduction of the potential field generated by stationary objects in the rotor annulus; and the addition of flow modifiers to the rotor blades. A modified prototype configuration is developed for each representative fan which is based on the acoustic performance obtained with the various design modifications. Without degradation in aerodynamic performance, reduction of the sound power levels of the discrete tones radiated from the representative fans is achieved.

ABSTRACT

The discrete frequency noise radiated from representative types of axial-flow fans used in electronic equipment is studied in detail. Narrow-band analysis of the discrete frequency noise radiated by these types of fans has been conducted in a free-field environment. The far-field sound pressure level, radiated directivity, and total radiated power of the discrete frequency noise is presented. The influence of operating point on the sound radiated from the fans is determined. The discrete frequency noise dominates the characteristic acoustic spectra at high flow coefficients. The radiated directivity of the discrete frequency noise is generally uniform. Based on the data collected and on the theoretical aspects presented, the principal source of the discrete frequency noise is identified for each of the fans as the interaction of the fan rotor with a circumferentially distorted, nonuniform flow. This undesirable flow field is generated by the shroud surrounding the rotor and the rotor-shroud support structure. The flow field produces unsteady rotor blade loads which generate propagating acoustic pressure distributions.

A collection of prototype design modifications are developed for each representative fan to reduce the radiated discrete frequency noise by improving the uniformity of the local flow field. The principal modifications are: the improvement in the circumferential symmetry of the rotor annulus, inlet, and outlet; the reduction of the potential field generated by stationary objects in the rotor annulus; and the addition of flow modifiers to the rotor blades. A modified prototype configuration is developed for each representative fan which

is based on the acoustic performance obtained with the various design modifications. Without degradation in aerodynamic performance, reduction of the sound power levels of the discrete tones radiated from the representative fans is achieved.

TABLE OF CONTENTS

TABLE OF CONTENTS (continued)

LIST OF TABLES

LIST OF FIGURES

LIST OF FIGURES (continued)

LIST OF FIGURES (continued)

NOMENCLATURE

a	coaxial duct inner wall radius
a_o	speed of sound
$\overline{A}$	complex constant
b	coaxial duct outer wall radius
B	blade number
$\overline{B}$	complex constant
BPF	blade-passing frequency
D_n	n^{th} amplitude harmonic of the spatial variation in blade force divided by the steady force
D_T	rotor blade tip diameter
$f_{m\mu}$	cut-off frequency of the m,μ mode in a duct
F_{jB}	amplitude of the j^{th} component of force
F_s	amplitude of the s^{th} component of force
j	Fourier series counting index for the force distribution
J_m	Bessel function of the first kind of order m
k	wave number
$k_{m\mu}$	value of k_r for the m,μ mode in a duct
k_r	radial wave number
k_z	axial wave number
$\overline{L}_p$	sound pressure level averaged over space
L_w	sound power level
m	azimuthal mode number
M_m	circumferential Mach number of m-lobed pressure distribution
M_m^*	critical tip Mach number
n	counting index for the spatially modulated force distribution

N	rotational speed in revolutions per minute
OASPL	overall sound pressure level
p	pressure
p'	fluctuating component of pressure
$P_{m,\mu}$	far-field acoustic pressure due to the m,μ mode radiating from a duct face
Q	air flow rate in cubic meters per minute
r	radius in polar cylindrical coordinates
r_t	microphone measuring radius
R	far-field radius from a duct face
s	Fourier series counting index for force distribution based on rotor order
SPL	sound pressure level
t	time
u_i	velocity in tensor notation
u_i'	fluctuating component of velocity
u_r'	acoustic particle velocity in the radial direction
x_i	distance in tensor notation
Y_m	Bessel function of the second kind of order m
z	axial distance in polar cylindrical coordinates
θ	angle in polar cylindrical coordinates
ρ	density
ρ'	fluctuating component of density
ρ_o	ambient density
ϕ	flow coefficient
ϕ_j	phase of the j^{th} component of force
ϕ_s	phase of the s^{th} component of force

μ	ascending index identifying the members of a series of eigenvalues for each value of m
ψ	far-field angle from a duct face
ψ_n	phase of the n^{th} component of the spatial force variation
ω	frequency in radians per second
$\bar{\omega}$	speed of rotation of a flow distortion relative to the fixed axis of a rotor
Ω	rotational speed of a rotor
Ω_m	($=\omega/m$) angular velocity of an m-lobed pressure distribution
∇^2	Lapacian operator

ACKNOWLEDGEMENTS

This work was performed at the Applied Research Laboratory of The Pennsylvania State University under an agreement with International Business Machines Corporation (Purchase Order No. S-925751-Q-LX-A-C18). Additional support was provided from the U. S. Naval Sea Systems Command for the fabrication of the Anechoic Chamber and supporting test apparatus. The author gratefully acknowledges the guidance and insight supplied by his adviser, Dr. Gerald C. Lauchle, and by Dr. Donald E. Thompson, through the course of this project. The author also wishes to thank Dr. Robert E. Henderson for assisting on the thesis committee and reviewing the manuscript. Appreciation is expressed to the many staff members of the Garfield Thomas Water Tunnel who rendered assistance in many forms, particularly during assembly of the test facility and development of the prototype modifications for the representative fans. Lastly, the author wishes to thank Mr. Andrew Boggess and Mr. Michael Edwards of Rotron, Inc., located in Woodstock, New York, for providing assembly piece parts of the fans and permitting the use of their performance test apparatus.

CHAPTER I

INTRODUCTION

1.1 Origin and Importance of Study

During the past few years, an enormous growth in the use of modern electronic equipment has occurred. Devices such as small personal computers, large computers, printers, terminal-oriented equipment, and electronic test equipment are common in the workplace of most people and in growing use at home. For proper operation and protection of their internal components, these devices incorporate various forms of cooling apparatus including small axial-flow fans. In many applications, the noise produced by these small cooling fans dominates the overall noise generated by electronic equipment.

The acoustic spectrum of axial-flow fans is characterized by a broadband component of sound on which is superimposed a series of discrete frequency peaks. Kryter and Pearsons [1] have shown that the judged noisiness of sound containing audible discrete tones is substantially greater than the judged noisiness of pure random noise. Thus, the discrete frequency noise generated by small axial-flow cooling fans is annoying to users of electronic equipment and reduces the acceptance of this equipment into common working and living environments.

To insure the growth in use of electronic equipment, it is imperative that the annoying factors associated with its use are minimized. This thesis is concerned with the reduction of discrete frequency noise generated by small axial-flow cooling fans.

1.2 Objective

The basic objective of this project is to demonstrate that the discrete frequency noise generated by representative axial-flow cooling fans commonly used in electronic equipment may be reduced. It is implied that the reduction of this noise be achieved without degradation of the aerodynamic performance of these fans.

1.3 Scope and Method of the Investigation

The project described here may be broadly classified into four phases. Prior to execution of these phases, selection of representative fans was necessary. Table I lists the four fans selected for study with their general application ratings. A more detailed description of these fans, including photographs, is given in Appendix A. Further reference to each of the fans will be in accordance with the model name assigned by the manufacturer; i.e., the "Tarzan."

The first phase of the project was the development of the basic theories and mechanisms responsible for discrete frequency noise generation by these types of fans. This work is a direct extension of the knowledge previously promulgated by other studies on larger scale axial-flow devices and is described in Chapter II.

The next phase was the characterization of the noise radiated by the representative fans. A test facility was designed and constructed for this purpose. The origins of the radiated discrete tones were identified based on the developed theory and the characteristics of the noise.

The third phase was the redesign of the representative fans to reduce the discrete frequency noise. Various elements of each fan

TABLE I

REPRESENTATIVE FANS FOR STUDY

Fan Model	Application Range		
	Airflow	Static Pressure Rise	Number of Blades
Rotron Tarzan TN 3A3	0 - 160 (l/s)	0 - 22 (mm-H_2O)	5
Rotron Patriot PT 77 B3	0 - 113 (l/s)	0 - 20 (mm-H_2O)	5
Rotron Muffin XL MX 2A1	0 - 50 (l/s)	0 - 7.5 (mm-H_2O)	3
Rotron Muffin	0 - 50 (l/s)	0 - 7.5 (mm-H_2O)	3

design were modified on a prototype basis. The modifications were based on the identified origins of the discrete tones and the results obtained by previous studies.

The final phase of the project consisted of acoustic test and evaluation of the modifications. Following evaluation on an individual basis, the modifications were combined and collectively evaluated. This was conducted until the best combination of modifications was obtained. The acoustic and aerodynamic characteristics of the resulting modified fan assemblies were determined.

Chapter III describes the experimental approach taken to execute each phase of the project, and Chapter IV presents the results obtained. The fundamental conclusions drawn from the study are presented in Chapter V.

CHAPTER II

THEORETICAL CONSIDERATIONS

2.1 Approach

Axial-flow fans principally generate aerodynamic sound. The study of aerodynamic sound uniquely encompasses a broad range of scientific disciplines including aerodynamics, thermodynamics, structural dynamics, and acoustics.

This chapter will develop the principles and mathematical relationships governing the generation, transmission, and radiation of sound by the ducted axial-flow fan. It includes basic theories and a review of previous research.

2.2 The Acoustic Wave Equation

Sound is defined as the mechanical radiant energy that is transmitted by longitudinal pressure waves in air or other material medium and is the objective cause of human hearing [2]. The mathematical description of acoustic phenomenon stems from the acoustic wave equation which is based on the properties of the medium and the principles that govern motion of the medium. For our purposes, it is important to emphasize the inextricable relationship between the generation of sound and the transmission of sound. We will show that spatial boundary conditions have significant influence on the nature of sound transmitted from a source.

In linear acoustics, we are concerned with small amplitude perturbations of a fluid about some steady value. We assume the fluid

to be inviscid and non-heat conducting. In general, it is adequate to assume the fluid to be Newtonian. The basic equations of acoustics follow from linearizing the full equations of mass and momentum conservation and the equation of state. Using tensor notation with the Einstein summation convention, Crighton [3] gives the continuity equation as

$$\frac{\partial \rho}{\partial t} + \frac{\partial}{\partial x_i} [\rho u_i] = 0 \quad . \tag{1}$$

We neglect all molecular relaxation and diffusion effects so that the stress on any fluid element consists simply of a normal pressure. Then, the momentum equation may be expressed as

$$\frac{\partial}{\partial t} [\rho u_i] + \frac{\partial}{\partial x_j} [\rho u_i u_j] = - \frac{\partial p}{\partial x_i} \quad . \tag{2}$$

We are only concerned with linear perturbations about the basic ambient states of the fluid. Therefore, ignoring the higher order perturbation terms and assuming the medium has uniform physical properties and is at rest, the continuity equation and the momentum equation may be expressed as, respectively,

$$\frac{\partial \rho'}{\partial t} + \rho_o \frac{\partial u_i'}{\partial x_i} = 0 \tag{3}$$

and

$$\rho_o \frac{\partial u_i'}{\partial t} + \frac{\partial p'}{\partial x_i} = 0 \quad . \tag{4}$$

Differentiating the continuity Equation (3) with respect to t and the momentum Equation (4) with respect to x_i, we obtain, respectively,

$$\frac{\partial^2 \rho'}{\partial t^2} + \rho_o \frac{\partial^2 u'_i}{\partial t \partial x_i} = 0 \qquad (5)$$

and

$$\rho_o \frac{\partial^2 u'_i}{\partial t \partial x_i} + \frac{\partial^2 p'}{\partial x_i^2} = 0 \quad . \qquad (6)$$

Subtracting these two equations yields

$$\frac{\partial^2 \rho'}{\partial t^2} - \frac{\partial^2 p'}{\partial x_i^2} = 0 \quad . \qquad (7)$$

We consider the fluid to be isentropic; therefore, the pressure of the fluid is a function of its density alone. A differential relation exists which Crighton [3] expresses as

$$dp = a_o^2 \, d\rho \quad , \qquad (8)$$

where a_o is the local sound speed. Thus, Equation (7) may be expressed as a partial differential equation in one variable,

$$\frac{1}{a_o^2} \frac{\partial^2 p'}{\partial t^2} - \frac{\partial^2 p'}{\partial x_i^2} = 0 \quad . \qquad (9)$$

A more common form of this equation is

$$\nabla^2 p - \frac{1}{a_o^2} \frac{\partial^2 p'}{\partial t^2} = 0 \quad , \qquad (10)$$

where ∇^2 is the Laplacian operator and equals $\partial^2/\partial x_i^2$.

Equation (10) is the homogeneous form of the acoustic wave equation. It mathematically describes the propagation of sound in a

region where there are no sources of sound present. To include their effect, acoustic source terms would be added to the right-hand side of Equation (10).

The form of Equation (10) is mathematically convenient. Before adding the effects due to sources in the spatial region of interest (annular duct), Equation (10) enables us to investigate the acoustic propagation characteristics of the region.

2.3 Sound Propagation in Annular Cylindrical Ducts

The axial-flow devices selected for study are not open rotors due to the presence of an annular shroud and support housing. The presence of the shroud has a very powerful effect on the acoustics of the axial-flow fan. Cumpsty [4] emphasizes the importance of this effect in his review paper, and Chandrashekhara [5] used a duct model for treatment of the noise generated by a shrouded rotor having a configuration similar to our devices. Therefore, we will treat the shroud as a duct.

Figure 1 illustrates the polar cylindrical coordinate system to be used for spatial representation of the annular duct geometry. Dimension "a" is the hub radius of the fan, and dimension "b" is the inner radius of the shroud. These radii do not change axially along the duct. For this analysis, it is assumed that these surfaces are acoustically rigid.

The Laplacian operator in the acoustic wave Equation (10) may be expressed in polar cylindrical coordinates. Skudrzyk [6] and others express the wave equation in cylindrical coordinates as

$$\frac{\partial^2 p'}{\partial r^2} + \frac{1}{r}\frac{\partial p'}{\partial r} + \frac{1}{r^2}\frac{\partial^2 p'}{\partial \theta^2} + \frac{\partial^2 p'}{\partial z^2} - \frac{1}{a_o^2}\frac{\partial^2 p'}{\partial t^2} = 0 \quad . \qquad (11)$$

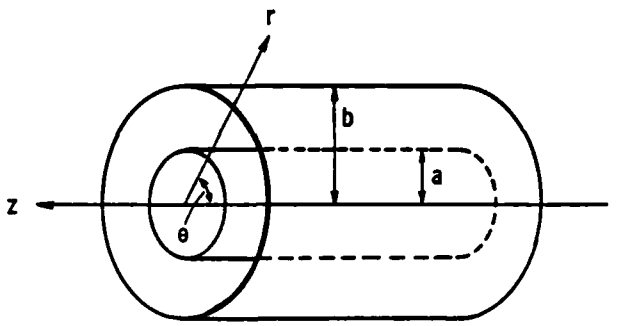

Figure 1. Polar Cylindrical Coordinate System.

This homogeneous partial differential equation may be solved using the separation of variables technique. By assuming a time-harmonic solution whose form is a product of functions of the independent variables, four ordinary differential equations are obtained which are related by three constants of separation. The constants are not independent of each other. Skudrzyk [6] obtains the general solution to Equation (11) using this approach; hence, it is unnecessary to review the details here.

For mathematical convenience, we express the solution in the general form

$$p'(r,\theta,z,t) = [\bar{A}J_m(k_r r) + \bar{B}Y_m(k_r r)]\exp[\pm i(m\theta + k_z z) + i\omega t] \quad , \tag{12}$$

where J_m is the Bessel function of the first kind of order m, Y_m is the Bessel function of the second kind of order m, m is the separation constant for the pressure variation in θ, k_r is the radial wave number, and k_z is the axial wave number. The coefficients $\bar{A}$ and $\bar{B}$ are complex numerical constants. The constants k_r and k_z are separation constants and are interrelated by:

$$k^2 = k_r^2 + k_z^2 \quad , \tag{13}$$

where $k = \omega/a_o$.

We may now apply the boundary conditions of the duct, illustrated in Figure 1, to the general solution, Equation (12). First, Equation (12) must be a single-valued function in θ because the duct is axisymmetric. Therefore, m must be an integer and we define m as the azimuthal mode number. Secondly, the duct has rigid walls, so the

radial particle velocity must vanish along these surfaces. To incorporate the effect of this boundary condition, we must establish the relationship between acoustic pressure and particle velocity.

In the absence of flow and with respect to the duct radius r, the linearized momentum equation, or Euler's equation, may be expressed as

$$\rho_o \frac{\partial u'_r}{\partial t} = - \frac{\partial p'}{\partial r} \quad . \tag{14}$$

We assume that the radial particle velocity is time harmonic, i.e., $u'_r \propto e^{i\omega t}$. Then, Equation (14) may be expressed as

$$i\omega\rho_o u'_r = - \frac{\partial p'}{\partial r} \quad . \tag{15}$$

Using Equation (15), we may apply the boundary conditions at the duct walls to Equation (12). Along the inner wall at r = a, the particle velocity vanishes. Therefore,

$$\frac{\partial p'}{\partial r}\bigg|_{r=a} = 0 = \bar{A} J_m'(k_r a) + \bar{B} Y_m'(k_r a) \quad , \tag{16}$$

where

$$J_m'(k_r a) = \frac{\partial}{\partial r}\left[J_m(k_r r)\right]\bigg|_{r=a}$$

and

$$Y_m'(k_r a) = \frac{\partial}{\partial r}\left[Y_m(k_r r)\right]\bigg|_{r=a} \quad .$$

Similarly, along the outer wall at r = b,

$$\frac{\partial p'}{\partial r}\bigg|_{r=b} = 0 = \bar{A} J_m'(k_r b) + \bar{B} Y_m'(k_r b) \quad , \tag{17}$$

where

$$J_m'(k_r b) = \frac{\partial}{\partial r}[J_m(k_r r)] \Big|_{r=b}$$

and

$$Y_m'(k_r b) = \frac{\partial}{\partial r}[Y_m'(k_r r)] \Big|_{r=b} \quad .$$

If Equation (12) represents a non-trivial solution to Equation (11), then the determinant of the coefficients, $\bar{A}$ and $\bar{B}$ in Equations (16) and (17), must be identically equal to zero. Therefore, we establish the relation

$$J_m'(k_r a)Y_m'(k_r b) - J_m'(k_r b)Y_m'(k_r a) = 0 \quad . \tag{18}$$

This relationship restricts k_r, the radial wave number, to certain values. These values specify the physically allowable radial wave numbers in the duct. These particular wave numbers are the so-called eigenvalues which satisfy Equation (18). The corresponding radial modes, obtained by substituting the eigenvalues into Equation (12), are the eigenmodes. For convenience, we now denote k_r as

$$k_r = k_{m\mu} \quad . \tag{19}$$

Here, m specifies the order of the Bessel functions in Equation (18) satisfied by k_r. The parameter μ is an ascending index starting at zero which identifies the member of a series of possible values of k_r satisfying Equation (18) for each value of m.

Recalling Equation (13), we may write

$$k_z = [k^2 - k_{m\mu}^2]^{1/2} \quad . \tag{20}$$

For boundedness of the general solution, Equation (12), when $k_{m\mu} > k$, we reject the positive square root of k_z. Thus, $p'(z) \propto \exp[-ik_z z]$ only and this result identifies a significant property of sound propagation in the duct. If k_z is imaginary, the sound field decays exponentially along the duct axis. If k_z is real, the sound field propagates along the duct axis. Therefore, we may write

$$k > k_{m\mu} \tag{21}$$

for the propagating modes in the duct. Morfey [7] obtains this result with his exact mathematical solution, although the approach taken is somewhat different than that presented here. We may non-dimensionalize Equation (21) by multiplying through by the outer radius of the duct, b. Recalling that $k = \omega/a_o$, we obtain

$$\frac{\omega b}{a_o} > k_{m\mu} b \tag{22}$$

as the requirement for propagation.

It is illustrative to review the expression we have obtained for the sound field,

$$p'(r,\theta,z,t) = \sum_{m=0}^{\infty} \sum_{\mu=0}^{\infty} [\bar{A}_{m\mu} J_m(k_{m\mu} r) + \bar{B}_{m\mu} Y_m(k_{m\mu} r)] e^{-ik_z z} e^{i(\pm m\theta + \omega t)} . \tag{23}$$

Physically, this represents characteristic radial pressure fluctuations whose surfaces of constant phase are rotating about the duct axis with angular velocity

$$\frac{\partial\theta}{\partial t} = \pm\frac{\omega}{m} = \Omega_m \text{ rad/sec} \quad . \tag{24}$$

For these fluctuations to propagate along the duct axis, z, Equation (21) must be satisfied. Otherwise, the fluctuations decay exponentially from the plane of their origin. The transition from non-propagating to propagating occurs when

$$k = \frac{\omega}{a_o} = k_{m\mu} \tag{25}$$

or at

$$f_{m\mu} = \frac{\omega}{2\pi} = \frac{k_{m\mu}a_o}{2\pi} \quad . \tag{26}$$

We now define $f_{m\mu}$ in Equation (26) as the cut-off frequency of the m,μ mode in the duct.

We will now review the significant result obtained by Tyler and Sofrin [8] in their famous study of ducted axial-flow compressor noise.

Recalling the governing relation for k_z from Equation (20), we may express k_z as

$$k_z = \left[\left(\frac{\omega}{a_o}\right)^2 - (k_{m\mu})^2\right]^{1/2} \quad . \tag{27}$$

Substituting the equality expressed in Equation (24),

$$k_z = \left[\left(\pm\frac{m\Omega_m}{a_o}\right)^2 - (k_{m\mu})^2\right]^{1/2} \quad . \tag{28}$$

If we denote M_m as the circumferential Mach number with which the m-lobed pressure pattern sweeps the outer wall of the duct at radius r = b, k_z may be finally expressed as

$$k_z = \frac{m}{b}\left[M_m^2 - \left(\frac{k_{m\mu}b}{m}\right)^2\right]^{1/2} \quad . \tag{29}$$

Tyler and Sofrin [8] define $(k_{m\mu}b/m)$ as the critical tip Mach number, M_m^*. They tabulate M_m^* for various m and μ by solving the transcental relation of Equation (18) for $k_{m\mu}$ at specified ratios of hub and duct radii.

Equation (29) redefines the requirement for sound propagation along the duct axis as

$$M_m > M_m^* = \frac{k_{m\mu}b}{m} \quad . \tag{30}$$

Solution of Equation (18) for $k_{m\mu}$ yields the result that, for all hub-duct ratios and all values of m and μ except $m = \mu = 0$, the critical tip Mach number, M_m^*, exceeds unity. Thus, if an m-lobed pressure distribution is to propagate along the duct axis, it must rotate about the duct axis at a supersonic rate, otherwise it will decay exponentially. The exception, $m = \mu = 0$, corresponds to a plane wave and this pressure distribution will propagate along the duct axis without attenuation.

We have described the form and characteristics of sound fields propagating in annular ducts. The resulting rotating fields are generated by compressors, propellers, and other forms of rotating blades. These sources will now be discussed.

2.4 The Generation of Propagating Acoustic Fields by Subsonic Tip-Speed Fans

Using the results obtained by Tyler and Sofrin [8], we have shown that a ducted rotor must generate a pressure field having supersonic phase velocity for that field to propagate along the duct. Accordingly, as Mather, Savidge, and Fischer [9] clearly point out, a

pressure field attached to and rotating with a subsonic tip-speed rotor cannot by itself produce acoustic energy in the far field.

We will now develop a physical description which illustrates the generation of a rotating supersonic pressure field by a subsonic rotor. This development closely follows that presented by Barry and Moore [10].

Consider a rotor with perfectly matched blades operating in a smooth, undistorted flow. Since the rotor speed is constant, rotation of the blades is periodic and we may express the circumferential, time-varying force distribution close to the rotor as a Fourier Series. Such an expression is

$$F(\theta,t) = \sum_{j=0}^{\infty} F_{jB} \cos[jB(\theta - \Omega t) + \phi_j] \quad , \tag{31}$$

where B is the number of rotor blades, Ω is the rotational speed of the rotor, j is the counting index which specifies each modal component of the total force, F_{jB} is the amplitude of the j^{th} component of the force, and ϕ_j is the phase of the j^{th} component of the force.

If there are slight irregularities between the blades, the force expression, Equation (31), must be modified. Physical variations between the blades will change the Fourier analysis of the force pattern near the rotor. The analysis will include all frequency components harmonically related to the rotational speed of the rotor and will not be limited to those that are multiples of the number of blades. Thus, the force distribution may be expressed as

$$F(\theta,t) = \sum_{s=0}^{\infty} F_s \cos[s(\theta - \Omega t) + \phi_s] \quad , \tag{32}$$

where s is the counting index based on rotor order, F_s is the amplitude of the s^{th} component of force, and ϕ_s is the phase of the s^{th} component of the force.

If the force on each blade varies as its position in the duct varies, the resulting force pattern will be circumferentially spatially modulated. These variations may be caused by the interaction of the rotor with the potential field of nearby stationary objects, such as stator vanes or struts, the interaction of the rotor with steady non-uniform circumferential inflow, and the interaction of the rotor with an annulus boundary layer shear flow which varies with circumferential position. A Fourier analysis of the distributed force may now be expressed as

$$F(\theta,t) = \sum_{s} \sum_{n} D_n F_s \cos[n\theta + \psi_n]\cos[s(\theta - \Omega t) + \phi_s] \quad , \quad (33)$$

where n is the counting index for the spatially modulated force distribution, D_n is the n^{th} harmonic of the variation in blade force per revolution divided by the steady blade force, and ψ_n is the phase of the n^{th} component of the force variation per revolution. Wright [11] refers to this circumferential force fluctuation as stationary asymmetric disc loading and denotes the Fourier components of this force as the Blade Loading Harmonics. Using the trigonometric identity for the product of cosines, expression (33) may be rewritten as

$$F(\theta,t) = \sum_{s} \sum_{n} \frac{D_n F_s}{2} \cos[(s \pm n)\theta - s\Omega t + \phi_s \pm \psi_n] \quad . \quad (34)$$

Thus, for each reduced frequency, $s\Omega$, two modes for each loading harmonic are generated and the speed of rotation of each mode is $\frac{s\Omega}{(s \pm n)}$.

Time-varying flow distortions will also cause the generation of Blade Loading Harmonics. Wright [11] refers to this phenomenon as non-stationary asymmetric disc loading. Temporal variation of the duct inlet conditions and/or an unsteady annulus boundary layer are examples of such distortions. The loading harmonics generated by these distortions will fluctuate as the distortions change with time.

Finally, if the distortions which cause the generation of Blade Loading Harmonics are rotating, non-rotational ordered frequencies will be generated. These distortions may be produced by blade vibrations or particular intake turbulence distributions which modulate the blade forces. Accounting for these effects, the rotating force distribution may be expressed as

$$F(\theta,t) = \sum_{s} \sum_{n} D_n F_s \cos[(s \pm n)\theta + (s\Omega \pm n\bar{\omega})t + \phi_s \pm \psi_n] \quad , \tag{35}$$

where $\bar{\omega}$ is the effective speed of rotation of the distortion relative to the fixed axis. The reduced frequencies generated are $(s\Omega \pm n\bar{\omega})$ with the corresponding modes of $(s \pm n)$ and the angular speed of rotation of each mode is

$$\frac{(s\Omega + n\bar{\omega})}{(s \pm n)} \quad . \tag{36}$$

If the speed of rotation is greater than sonic speed at the outer radius of the duct, the mode will propagate along the duct axis. Therefore, the modes, or blade loading harmonics, most likely to propagate along the duct axis and radiate as sound are those for which $(s \pm n)$ is small or equal to zero.

We have developed a physical description illustrating the generation of supersonic rotating pressure fields, or force distributions, by subsonic fans. These fields will propagate and radiate as sound. It is illustrative to review the radiation of the sound generated by these propagating fields from the end of the duct.

Using the coordinate system illustrated in Figure 2, Tyler and Sofrin [8] developed an approximate analysis for sound radiation from a duct. Modelling the end of the duct as a flexible membrane positioned in an infinite baffle, they calculated the far-field acoustic pressure using the simple source approach for spherically spreading, outgoing sound waves, viz., Morse [12]. Making these assumptions, the radiation problem may be treated in an analogous fashion to that for a piston source [12], where the normal surface velocity of the duct face is obtained from the pressure distribution specified by the propagating modes.

For our purposes, it is not necessary to review the mathematical details involved. The result for far-field acoustic pressure obtained by Tyler and Sofrin [8] is proportional to a directivity factor which we may express as

$$P_{m\mu}(\psi) \propto \text{D.F.} = \frac{k \sin\psi [J_{m-1}(kb\sin\psi) - J_{m+1}(kb\sin\psi)]}{(k_{m\mu}^2 - k^2 \sin^2\psi)} , \quad (37)$$

where $P_{m\mu}$ is the far-field acoustic pressure due to the m,μ mode, and k is the far-field acoustic wave number. Thus, propagating modes may be characterized by directional peaks in far-field sound level. Only modes of zero order and plane waves radiate sound along the duct axis

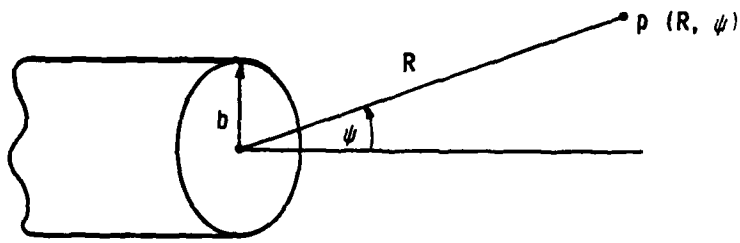

Figure 2. Cylindrical Duct Radiation Coordinates.

(After Tyler and Sofrin [8])

and their directivity is a function of the radiated sound wavelength relative to the width of the duct annulus, which is directly analogous to the piston source.

2.5 A Review of These Results and Previous Studies

We have identified some of the properties and characteristics for the generation, transmission, and radiation of sound from ducted, subsonic, axial-flow fans. For effective noise control, it is necessary to reduce the generation of supersonic rotating pressure distributions which are transmitted, or propagated, along the duct axis and radiate to the far field. Varying circumferential inflow is the principal cause of supersonic rotating pressure fields. In addition, variations in blade-to-blade loading, caused by physical differences between blades, blade vibration, or rotor eccentricity within the duct, generate pressure fields which propagate.

Following Barry and Moore[10], and Mugridge and Morfey [13], it is convenient to list the resulting characteristic noise generated by these mechanisms in tabular form, Table II. To produce a quiet rotor, the fluctuating forces listed in Table II must be removed or reduced. Thus, the steps towards effective noise control become very clearly identified.

So far, we have concerned ourselves solely with noise generation due to fluctuating forces on rotating blades, i.e., rotating acoustic dipoles. Wright [14] identifies this mechanism as the principal cause for discrete tonal sound radiation from periodic sources and asserts that fluctuating forces as small as one-thousandth of the steady-state thrust are sufficiently large to cause the rotor noise spectrum to be

TABLE II

NOISE SOURCES IN SUBSONIC FANS

Noise Spectrum	Generation Process (types of blade loading)	Examples of Sources of Loading
Constant Phase Blade-Passing	Steady Spatial Distortion Pattern	(a) Distortion due to intake imperfections. (b) Distortion due to cross flow at intake. (c) Boundary layer thickness varying with position. (d) Interaction with the potential field of nearby stationary objects.
Varying Phase Blade-Passing Frequency Tones	Time-Varying Spatial Distortion Patterns	(a) Boundary layer thickness with position in annulus in space and time. (b) Inlet turbulence. (c) Slowly varying intake distortions.
Rotational Frequency Harmonics	Differing Blade Loading	(a) Blade-to-blade tip clearance variations. (b) Blade-to-blade variation of stagger angle and/or skew. (c) Irregularly positioned blades. (d) Blade form imperfections. (e) Long-term blade boundary layer variations.
Non-Rotational Ordered Frequencies	Rotating Spatial Distortion Patterns	(a) Rotating intake distortions. (b) Mechanical vibration of blades.
Varying Frequency and Broadband Noise	Short-Term, Small Scale Distortions	(a) Detailed annulus boundary layer variations. (b) Short-term, small scale inlet turbulence. (c) Short-term boundary layer fluctuations.

tonal in character. In general, interference between lower order rotational harmonics of the blades causes cancellation of rotational orders not harmonically related to the blade-passing frequency and reinforcement of those which are.

However, in addition, rotors generate broadband sound. Since the early work of Yudin [15], this noise has been attributed to the shedding of vortices at the trailing edges of the blades. The vortices cause fluctuations in lift force which, depending on trailing edge Reynolds number, may be either periodic or random in nature. Another physical hypothesis for broadband sound generation was presented by Lilley [16]. He associated the sound with the turbulent boundary layers leaving the trailing edge of the blades. In general, it is believed that both of the physical descriptions are accurate, but at different rotor operating conditions.

For our purposes, broadband sound may be attributed to fluctuating blade forces whose higher frequency Fourier components, or loading harmonics, are sufficiently random in phase and frequency that cancellation between blades does not occur and these components propagate as zero order disturbances or plane waves. Thus, we are associating broadband sound generation with the same physical mechanisms responsible for discrete tonal sound generation.

Morfey [17] identifies the somewhat arbitrary nature of the distinction between tone and broadband sound radiation for a rotor in unsteady flow. If the inlet velocity fluctuations contain low-frequency components (compared with the blade-passing frequency), the radiated spectrum will exhibit a series of broad peaks; whereas higher frequency broadband turbulence tends to produce a more uniform spectrum.

Accurate prediction of rotor noise remains difficult because of the difficulty in measuring and/or predicting fluctuating blade loading. Indeed, Lowson and Ollerhead [18] have concluded that very high blade loading harmonics are important contributors to the sound field. Nevertheless, several investigators have achieved good agreement in critical experiments. For our purposes, accurate prediction of the generated noise is unnecessary. In light of the physical description we have assembled, knowledge of radiated sound will provide insight into the principal mechanisms responsible for the noise generation.

Numerous experimental studies have been conducted on the noise generated by axial-flow fans. Within these studies, many practical noise reduction schemes have been developed and evaluated. Instead of reviewing the details of this relevant work at this time, we will describe the experimental approach taken and the results obtained for this particular study and then incorporate the findings of other investigators as appropriate to meeting the goals of this program.

CHAPTER III

EXPERIMENTAL METHODS

3.1 Experimental Approach

The basic goal of this program was to demonstrate that reduction of discrete frequency noise generated by representative axial-flow devices could be achieved. Therefore, the experimental procedure and apparatus were designed towards meeting this goal.

Early in the program, it was determined that detailed aerodynamic flow measurements were unnecessary. Sufficiently detailed acoustic measurements would yield results which could be interpreted in light of the theory described in Chapter II. Additionally, comparison of the results obtained with other studies would aid in determining the mechanisms responsible for discrete frequency noise generation.

Having established these initial premises, a convenient approach was developed. The approach contained four stepwise phases comprising the remaining sections of this chapter.

3.2 The Test Facility

As an initial step, a test facility was designed and constructed at the Garfield Thomas Water Tunnel of the Applied Research Laboratory at The Pennsylvania State University. The facility consisted of three principal components: a fan duct, an anechoic chamber, and instrumentation for acoustic measurements.

3.2.1 The fan duct. A cross-sectional view of the fan duct is illustrated in Figure 3. The design of the duct is in accordance with the specifications outlined by Wells and Madison [19] with the exception of the static pressure tap. The pressure tap was flush-mounted with 25.4-mm (1-inch) square copper shim stock along the foam-lead-foam lining to minimize erroneous signals due to the turbulent shear flow adjacent to the foam. The static pressure in the duct was measured using a meriam fluid manometer connected to the tap and to ambient pressure within the anechoic chamber. As shown, the duct was configured with a throttle permitting regulation of the static pressure and the air flow. Additionally, as specified by Beranek, Reynolds, and Wilson [20], an anechoic termination was attached to the throttle to reduce the build-up of longitudinal standing waves within the duct. The termination consisted of a 20.3-cm (8-inch) diameter circular open-cell foam wedge whose overall length was 45.7 cm (18 inches). The duct was outwardly tapered near the anechoic termination in order to maintain a constant cross-sectional area along the duct axis.

The duct was fabricated from 4.8-mm (3/16-inch) thick PVC plastic tubing lined with a 25.4-mm (1-inch) thick foam-lead-foam composite material. This configuration was intended to reduce the build-up of transverse standing waves within the duct and proved to be resistant to any vibratory excitation generated by the test fans. The nominal inside diameter of the duct was equivalent to the diameter of the largest fan to be tested and a slip-over tapered reducer was used for testing units having smaller diameter.

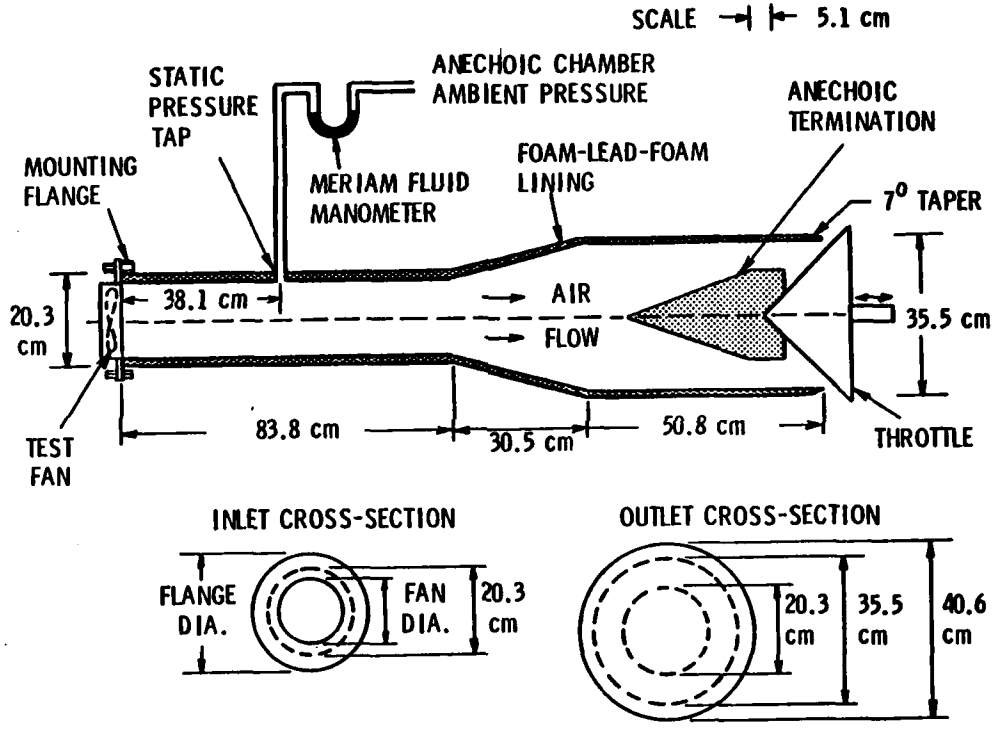

Figure 3. Cross-Sectional View of the Fan Test Duct.

3.2.2 The anechoic chamber. An anechoic chamber was used providing a free-field environment for acoustic measurements. This approach was selected because it permits identification of the directional characteristics of the noise radiated by the fans. As described in Chapter II, knowledge of these characteristics is very helpful in understanding the mechanisms responsible for fan noise generation. Additionally, use of the chamber permitted accurate and repeatable free-field measurements in a low noise environment. A detailed description of the chamber has been given by Marboe and Fitzgerald [21].

3.2.3 Facility assembly. The duct was mounted through a wall of the anechoic chamber, as shown schematically in Figure 4 and pictorially in Figure 5. The inlet of the duct was positioned 76 cm (29.92 inches) within the chamber. This positioning placed the duct outlet outside of the anechoic chamber. This arrangement minimized the interaction of inflow distortions, possibly generated by the foam wedges attached to the chamber walls, with the fan under test and prevented recirculation of the flow developed by the fan within the anechoic chamber.

3.2.4 Acoustic instrumentation. Acoustic data were obtained using the instrumentation set-up illustrated schematically in Figure 6. A B&K Type 4133 microphone was positioned 1 meter (39.4 inches) along the centerline of the test fan. This positioning was based on the free-field measurement methodology recommended by Beranek, Reynolds, and Wilson [20]. They recommend a distance not less than four times the diameter of the fan, and this has been the general approach adopted

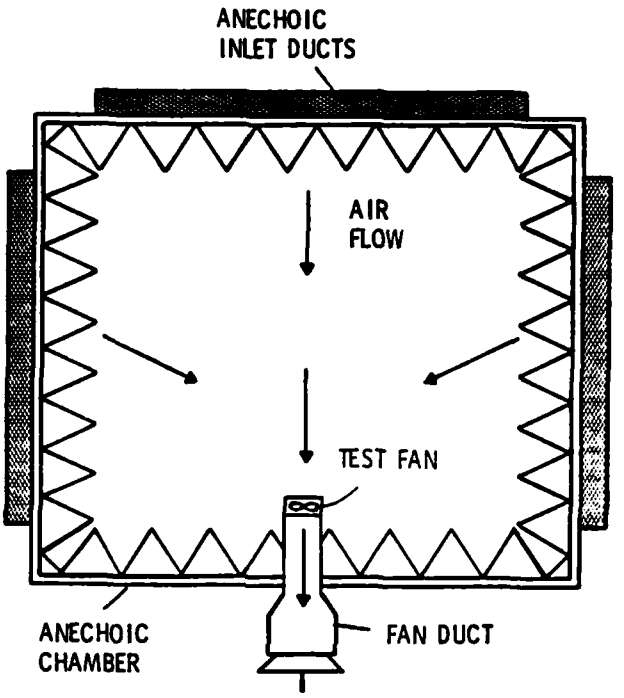

Figure 4. Test Facility Assembly and Flow Schematic.

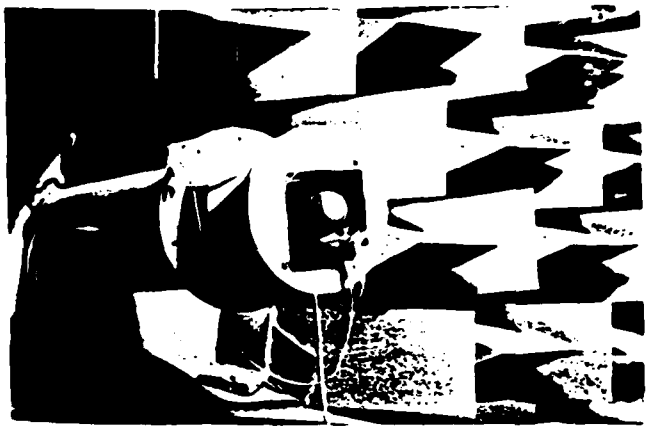

(a)

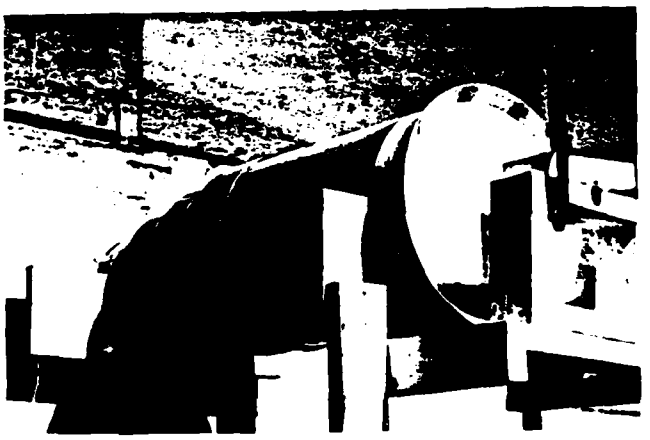

(b)

Figure 5. Fan Test Duct: (a) Inlet, and (b) Outlet.

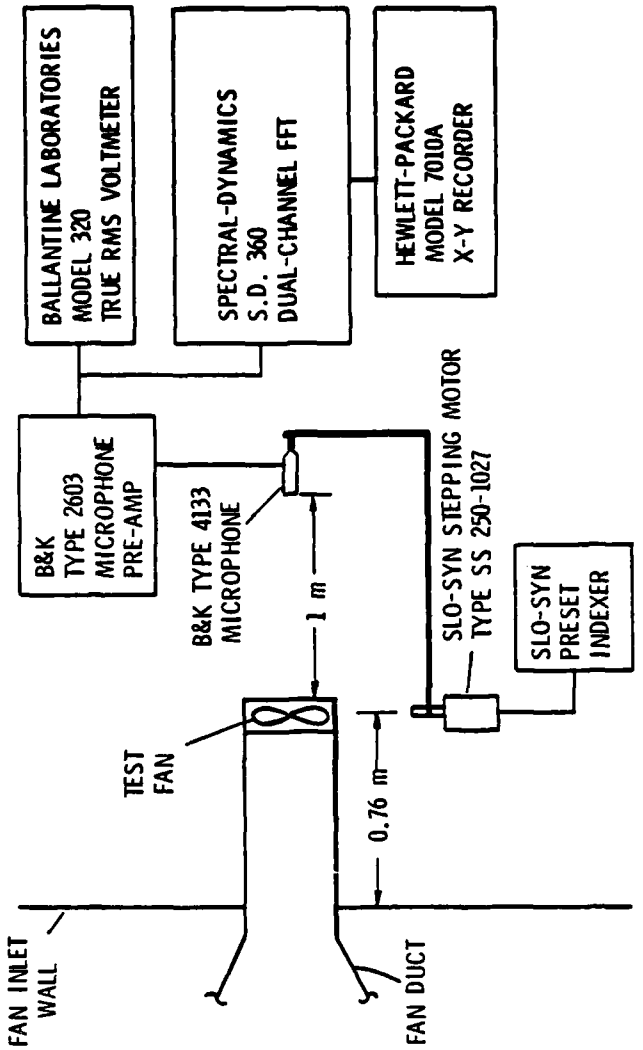

Figure 6. Acoustic Instrumentation Schematic.

by other investigators as well. The microphone was placed on a rotating boom whose azimuthal position could be changed in 1.8° increments using the stepping motor and indexer as shown in Figure 6. This set-up permitted measurements through the full frontal arc of the test fan.

To insure the accuracy and precision of the measurements obtained, a microphone calibration was conducted prior to and following each series of measurements. Calibrations were performed with a B&K Type 4220 Pistonphone which generates a 250 Hz tone having an amplitude of 124 dB (re 20 μPa). Because the B&K Type 4133 microphone has a linear frequency response over the frequency range of interest (essentially that for normal human hearing), a single tonal calibration was sufficient.

The amplified microphone output was supplied to the Ballantine voltmeter and the Spectral Dynamics S.D. 360 real-time FFT processor. Both of these instruments incorporate adjustable amplitude gain and in conjunction with the adjustable gain feature of the B&K Type 2603 Microphone Preamplifier, provided ample dynamic range for the fan noise measurements. Using the forward transform and averaging features of the FFT processor, a discrete frequency spectrum of the microphone voltage was obtained and recorded on paper using the Hewlett-Packard Model 7010A X-Y Recorder.

3.2.5 Test facility acoustic performance. Following assembly, the test facility background noise, transmission loss, free-field frequency characteristics, and free-field directivity were measured. The results are presented here as part of the description of the facility.

Background noise was measured with the microphone positioned along the duct axis and with the throttle of the duct open. As illustrated by the spectrum shown in Figure 7(a), low-frequency noise was present in the facility. To prevent distortion when conducting relatively low-amplitude measurements, a Krohn-Hite Model 3342 Filter was incorporated in the instrumentation set-up and adjusted for high-pass filtering at 80 Hz. The resulting background noise spectrum obtained is shown as Figure 7(b). The filter was used during all subsequent noise measurements.

Transmission loss measurements were conducted at several facility positions with the fan-duct throttle closed. The transmission loss exceeded 30 dB (re 20 μPa) for all frequencies about 250 Hz and 20 dB (re 20 μPa) for frequencies below 250 Hz.

To verify the free-field properties of the anechoic chamber, inverse square-law measurements were performed with the fan duct positioned in the chamber as described in Section 3.2.3. Figure 8 illustrates the results obtained for two source positions measured diagonally across the chamber. Based on these results, an anechoic field existed for all frequencies down to 200 Hz with a semi-anechoic field for lower frequencies.

Directivity measurements were performed to verify the symmetry of the free field within the anechoic chamber. A loudspeaker was positioned at the inlet of the fan duct and driven with pure tones ranging from 100 Hz to 1 kHz. The results obtained for lower frequencies are illustrated in Figure 9. A uniform sound field was measured for all frequencies, including those for which the chamber was only semi-anechoic.

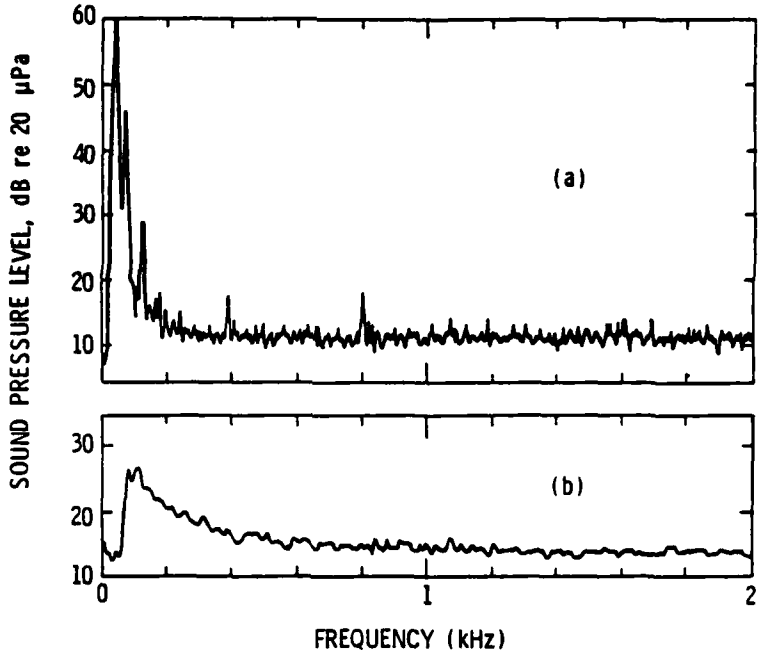

Figure 7. Facility Background Noise: (a) Ambient, and (b) With Low-Pass Filter.

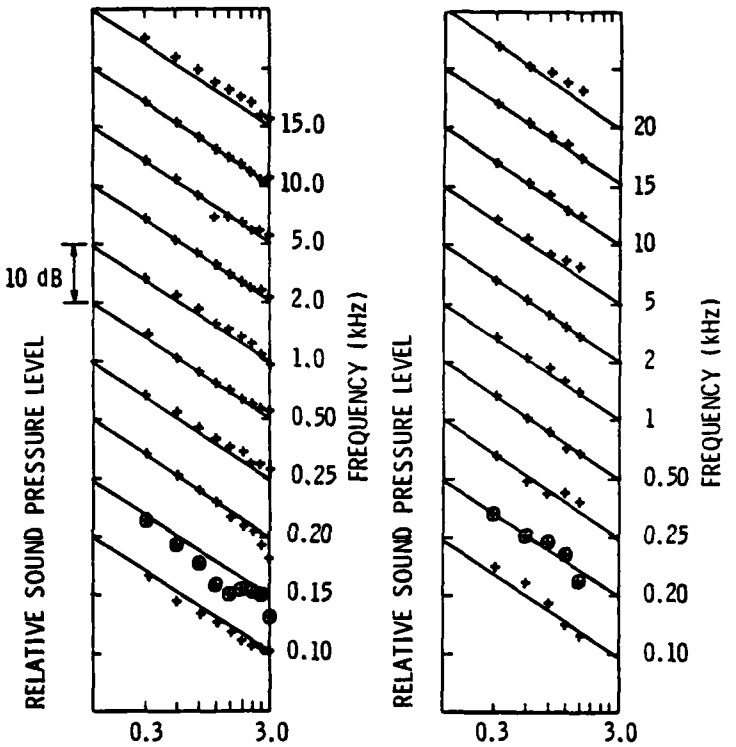

Figure 8. Inverse Square-Law Measurements for Two Source Positions.

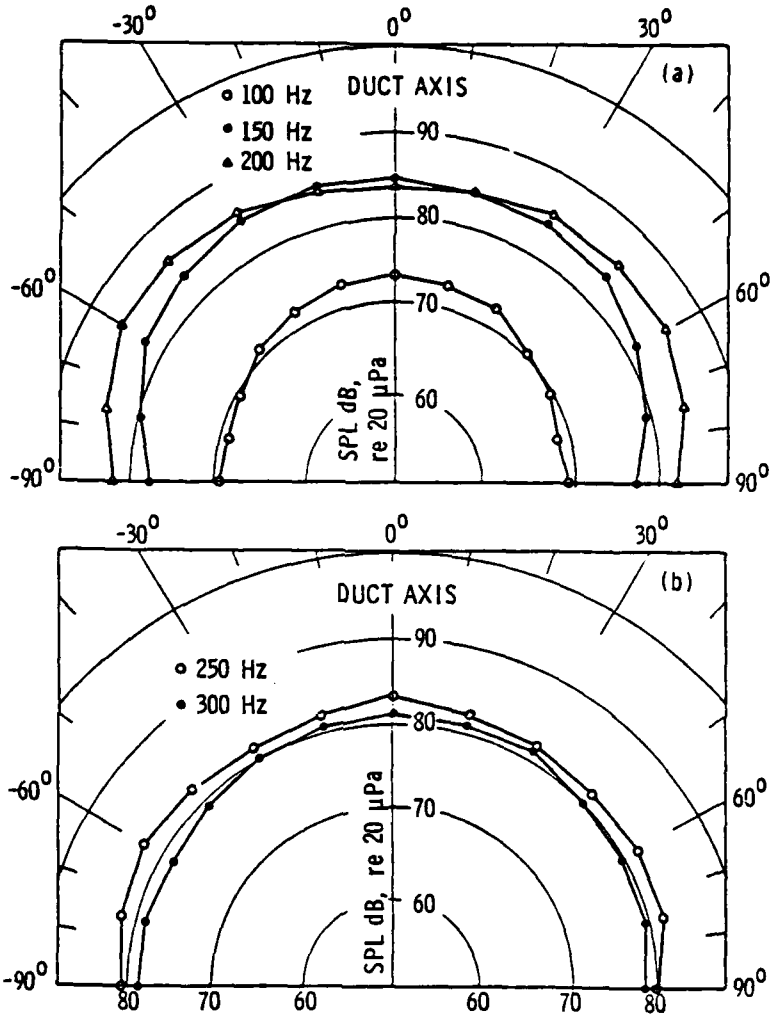

(a) at 100 Hz, 150 Hz, and 200 Hz frequencies

(b) at 250 Hz, and 300 Hz frequencies

Figure 9. Tonal Directivity Patterns at Various Frequencies.

Overall, the test facility was designed and assembled to provide a closely ideal operating environment for the fans. With this basic goal achieved, detailed measurement of the fan noise could be pursued.

3.3 Fan Noise Characterization

The purpose of this phase of the test program was to characterize the noise generated by the cooling fans at various operating conditions. Because of the basic premise to understand and reduce the generation of discrete frequency tonal noise, the experiments were designed to highlight these characteristics of the radiated sound.

Initially, the generated sound was measured as a function of static pressure rise for each of the four fans described in Chapter I and Appendix A. Table III lists the selected operating conditions based on static pressure alone. The operating conditions were based on the standard performance data provided by the manufacturer [22], which is included in Appendix A. The speed of rotor rotation was measured at each test condition listed with a Power Instruments Digistrobe strobe light.

At each test condition listed in Table III, discrete frequency sound pressure level spectra were obtained over various frequency ranges with the microphone positioned along the axis of the test fan and 1 meter (39.4 inches) from the plane of the rotor. The purpose of these measurements was to determine the influence of operating point on generated noise and identify the favorable and unfavorable operating points for each fan. Additionally, if discrete tones were present in the spectra obtained along the fan axis, the influence of operating point on their generation would be identified.

TABLE III

TEST CONDITIONS

Fan Model		Operating Static Pressure Rise ($mm-H_2O$)					
Muffin Mu 77 B1	max. obtain	7.6	5.1	2.5	min. obtain		
Muffin XL MX 2A1	max. obtain	7.6	5.1	2.5	min. obtain		
Patriot PT 77 B3	max. obtain	22.9	17.8	12.7	7.6	2.5	min. obtain
Tarzan TN 3A3	max. obtain	25.4	20.3	15.2	10.2	5.1	min. obtain

These initial measurements were limited to the on-axis microphone position to expedite the process of initial data acquisition. In addition, it was believed that this methodology was sufficiently detailed based on the theory presented in Chapter II. As discussed, sound radiation depends on the generation of supersonic rotating pressure distributions and/or the generation of zero-order non-rotating distributions. It was believed that the generation of zero-order distributions was most likely to occur because of the relatively very low speed of rotation of these fans and the apparent lack of flow modifiers to cause interaction with the fan blades. Only zero-order distributions contribute to the sound pressure on the fan axis, as discussed in Chapter II.

A detailed directivity survey was conducted for each fan at the most unfavorable operating condition identified. The survey consisted of the acquisition of discrete frequency sound pressure level spectra in 5.4° increments through the full 180° frontal arc of the fan.

To verify that the acoustical characteristics of given fans are repeatable and representative of the class, two additional assemblies of each fan model were procured and tested. The evaluation of these units consisted of the comparison of representative spectra and overall sound pressure levels at the critical operating conditions previously identified. In addition to these comparisons of on-axis data, measurements were conducted at 45° and 90° off-axis to insure the similarity of the directional characteristics obtained.

3.4 Fan Design Modifications

Following the acquisition of baseline characteristic acoustic data for each of the fans, redesign of the fans was undertaken to demonstrate that discrete frequency tonal noise reductions could be achieved. Chapter IV describes the details of these modifications, only the methodology is presented here.

The redesigns consisted of a series of modifications. Each modification was intended to reduce or eliminate the presence of a mechanism responsible for noise generation. The modifications were based on the results of the noise characterization tests, the results obtained by other investigators, and the theory described in Chapter II. A collection of five to ten principal modifications was assembled for each fan and included changes to the fan housing, support structure, and blades. Following review with the fan manufacturer, modifications deemed costly or impractical from a manufacturing standpoint were not attempted. Additionally, modifications which would greatly inhibit or alter the aerodynamic performance of the fans were not attempted.

Modifications were made to individual units on a prototype basis. When possible, assembly piece parts were modified and substituted in place of the original components. The fan manufacturer willingly supplied piece parts for modification and provided helpful information concerning the dismantling and the internal design of the fans.

3.5 Evaluation of Fan Design Modifications

The purpose of this phase of the approach was to test and evaluate the prototype design modifications incorporated on the cooling fans. The evaluation consisted of two principal steps which are now described.

3.5.1 Initial evaluation. Each modification was individually configured in a fan assembly and acoustically tested. The test consisted of operating the fan at the most unfavorable condition previously identified and obtaining discrete frequency spectra and overall sound pressure level measurements. Data were acquired with the microphone positioned on the axis of the fans and off-axis at the +45° and -45° positions.

Evaluation of each modification consisted of a review of the change in spectral character with particular emphasis placed on the discrete frequency noise components. It was recognized that the dominance of some mechanisms would prevent proper assessment of the changes provided by some modifications. Therefore, none of the modifications were rejected during the initial evaluation.

3.5.2 Amalgamation of modifications. Based on the results obtained in the initial evaluation, modifications were collectively incorporated into single fan assemblies. This process was conducted in a stepwise fashion beginning with modifications enhancing the spectral character of the generated noise to the greatest degree. The measurement requirements were the same as in the initial evaluation and the process continued until an acoustically "optimum" configuration was obtained for each fan.

Having obtained these configurations, detailed acoustic and aerodynamic performance tests were conducted. The acoustic tests consisted of the static pressure and directivity surveys described in Section 3.3. The aerodynamic tests were conducted in the manufacturer's performance test facility [23] permitting direct comparisons with the baseline reference performance units.

CHAPTER IV

EXPERIMENTAL RESULTS AND DISCUSSION

4.1 Approach

This chapter will present the results of the experiments described in Chapter III with a simultaneous discussion of their significance. The discussion will incorporate the theoretical aspects presented in Chapter II and the results of previous studies. Generally, the approach will follow the pattern established in Chapter III.

4.2 Characteristics of the Cooling Fan Noise

Characteristic on-axis discrete frequency sound pressure level (SPI) spectra obtained for each of the fans considered are shown in Figures 10 and 11. The spectra were obtained by taking 128 sequential averages of the radiated sound using the spectrum analyzer. The duct throttle was adjusted to minimize the flow restriction.

The spectra are clearly dominated by discrete tones. The presence of these tones directly along the axis of the fans indicates that zero-order pressure distributions are generated, as observed by Barry and Moore [10].

The frequencies indicated in Figures 10 and 11 are the blade-passing frequency (BPF) and harmonics for each of the fans. Rotational frequency harmonics and broadband sound are present but are generally lower in amplitude.

Based on these initial results, the measured frequency range was reduced to 3000 Hz for the remaining acoustic tests. This reduction

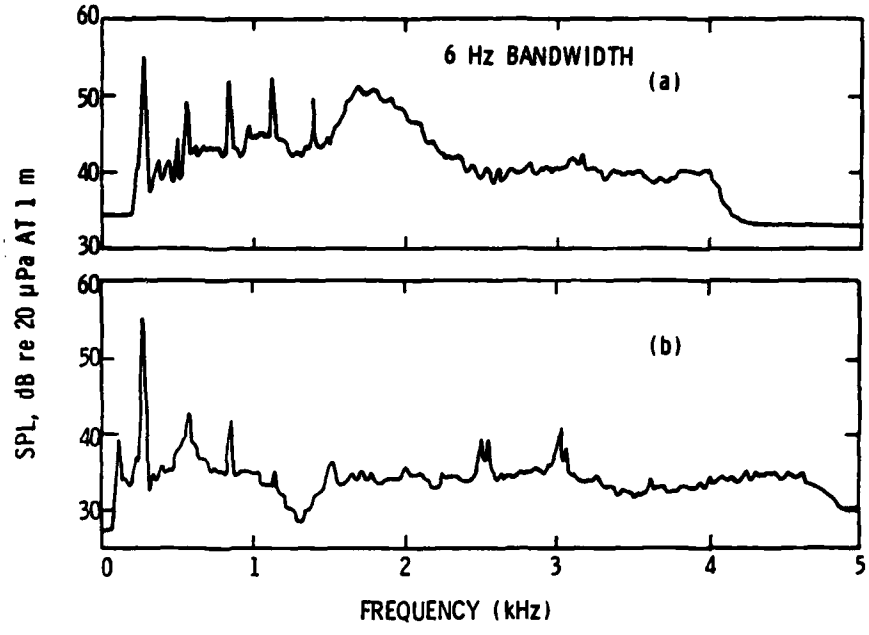

Figure 10. On-Axis Discrete Frequency SPL Spectra: (a) Tarzan, and (b) Patriot.

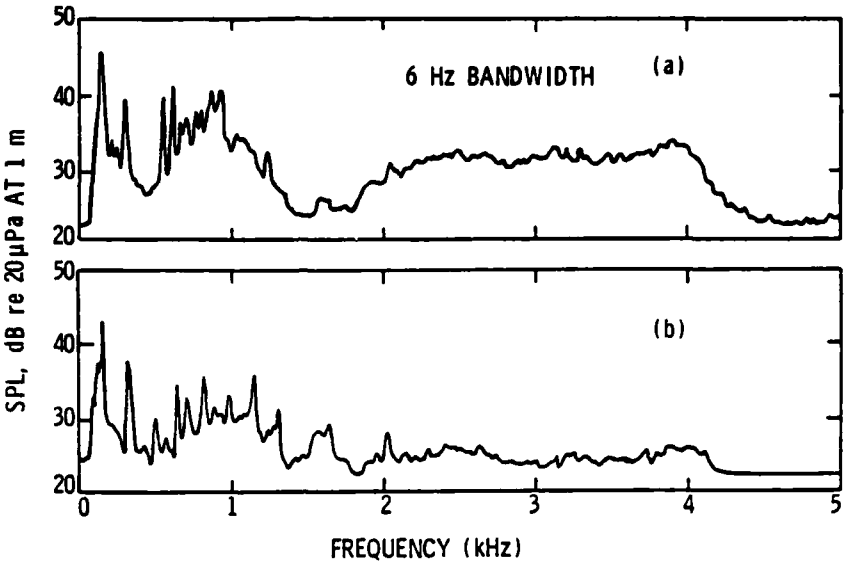

Figure 11. On-Axis Discrete Frequency SPL Spectra: (a) Muffin XL, and (b) Muffin.

the analysis bandwidth from 10 Hz to 6 Hz providing improved resolution of the discrete tones measured. Additionally, this frequency range was sufficient to include all of the principal tones generated by the fans.

It was necessary to take 128 sequential averages of the radiated sound to obtain repeatable spectra. Using this approach, the amplitudes of the discrete tones were found to repeat within 2 dB in successive measurements. The overall sound pressure level amplitudes were found to repeat within 0.5 dB in successive measurements. There were no additional variations observed during the tests.

4.2.1 Static pressure rise tests. The results obtained for the static pressure test of the Tarzan are shown in Figure 12. The spectra labels indicate the operating static pressure rise in millimeters of water (mm-H_2O), the airflow in liters per second (l/s), and the overall sound pressure level (OASPL) in decibels (dB re 20 μPa). The discrete tones present in the spectra are identified as the blade-passing frequency (BPF), harmonics of the blade-passing frequency (n, where n = 1,2,3,...), and rotational frequency harmonics (identified numerically).

While operating at a low static pressure rise, the generated sound is best described as tonal in nature with a broadband "hump" centered around the fifth harmonic of the BPF. The overall sound level decreases with increasing static pressure rise. Finally, at a critical point of operation shown as spectrum (d) in Figure 12, the sound becomes broadband in character having relatively high-amplitude low-frequency components.

The Patriot exhibits characteristics similar to the Tarzan, as shown in Figure 13. It does not radiate as many harmonics of the BPF or rotational frequency harmonics. The presence of higher frequency tones

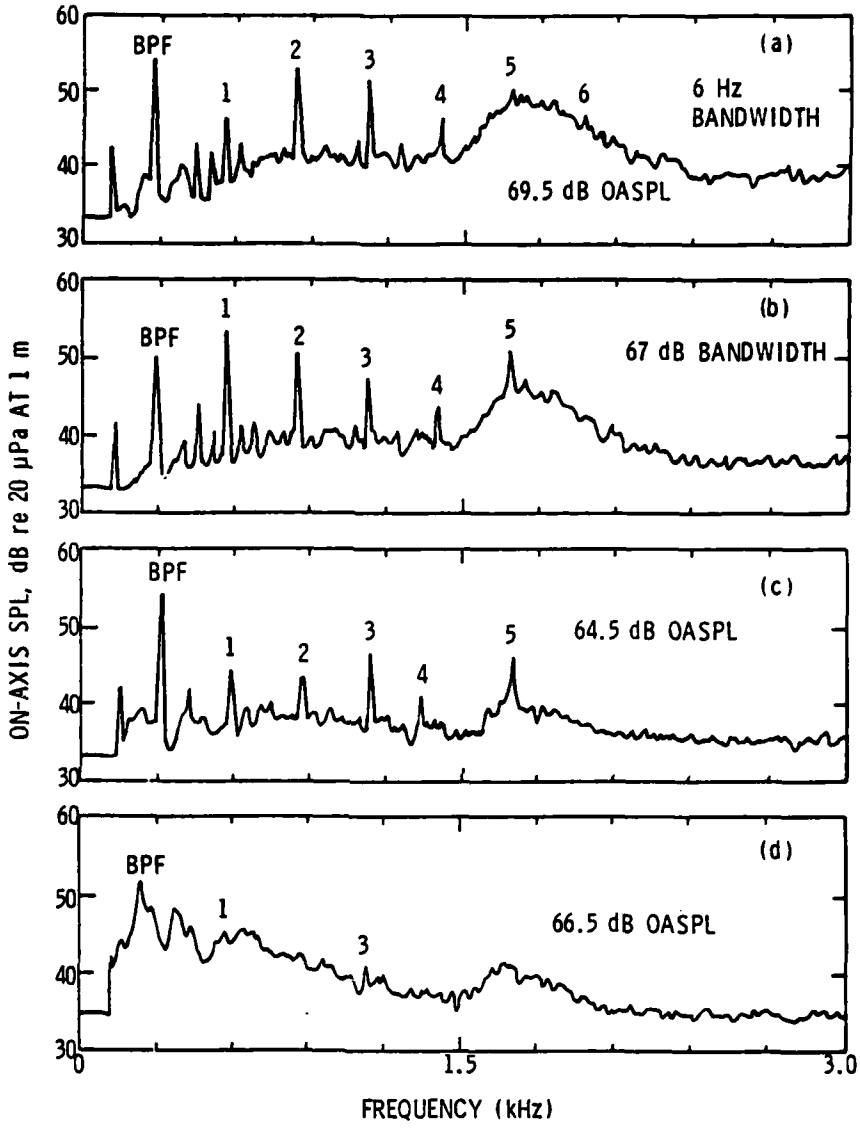

Figure 12. Tarzan On-Axis Discrete Frequency Spectra at Various Operating Conditions.

(a) 0.51 mm-H_2O and 160 1/s
(b) 5.59 mm-H_2O and 128 1/s
(c) 10.67 mm-H_2O and 83 1/s
(d) 11.94 mm-H_2O and 55 1/s

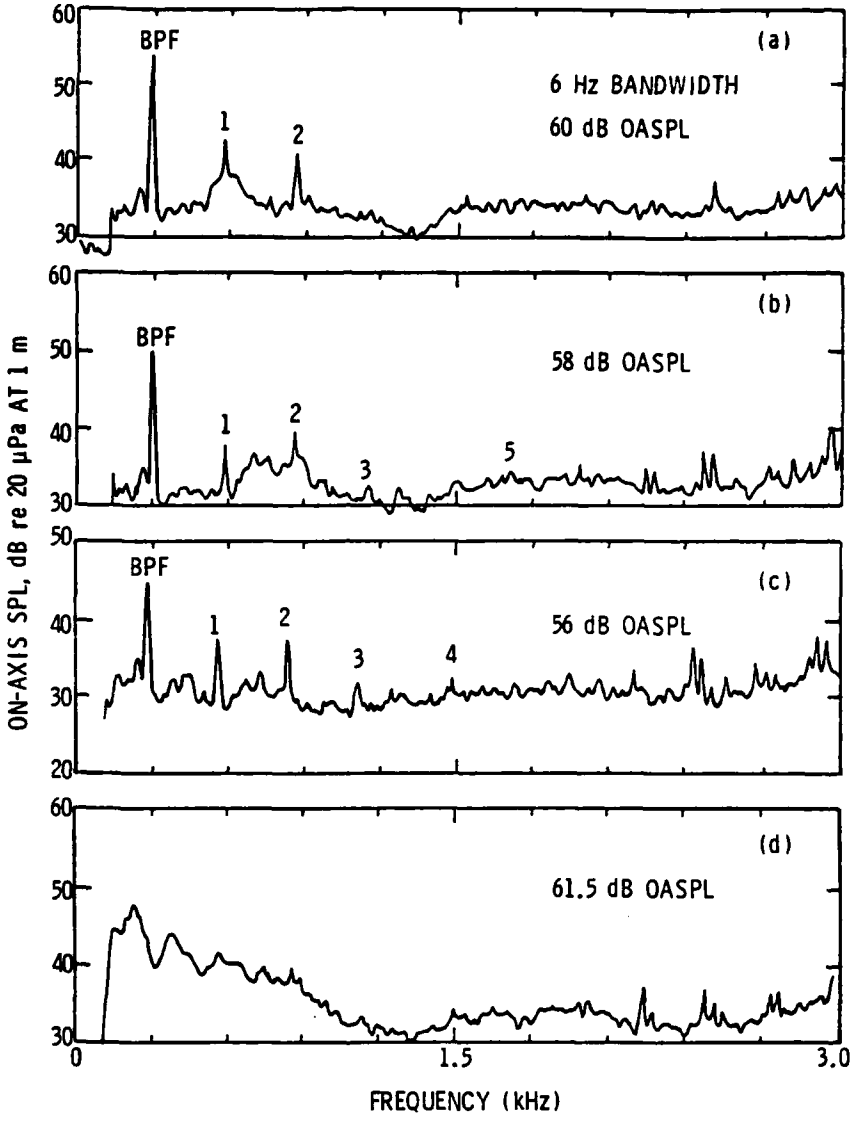

Figure 13. Patriot On-Axis Discrete Frequency Spectra at Various Operating Conditions.

(a) 0.25 mm-H_2O and 112 1/s
(b) 5.33 mm-H_2O and 87 1/s
(c) 9.14 mm-H_2O and 42 1/s
(d) 10.41 mm-H_2O and 39 1/s

above 2000 Hz is a unique characteristic of the Patriot. These tones are unaffected by variations in operating static pressure rise and it was observed during the course of the tests that they underwent temporal variations in frequency and amplitude. They are not rotational frequency harmonics, but may be a result of the trailing edge serrations on the fan blades, as described in Appendix A.

The results obtained for the Muffin XL are shown in Figure 14. The acoustic characteristics are very similar to those obtained for the Tarzan with the exception of the presence of high-amplitude rotational harmonics near the third, fourth, and fifth harmonics of the BPF. Although discrete tones dominate the levels of the spectra, higher-frequency broadband noise is also present above 2000 Hz.

Characteristic acoustic spectra obtained for the Muffin are shown in Figure 15. The principal tones generated are the BPF and its harmonics. These decrease in number and in amplitude as the operating static pressure rise is increased. As observed with the other fan models, a transition in the spectral character occurs at a specific point of operation. The sound level increases due to the generation of higher-amplitude low-frequency broadband components which mask and/or cancel the tones generated.

It is illustrative to review these results because each fan exhibits the same characteristics in varying degrees.

The generation of higher-amplitude low-frequency broadband sound at a critical operating static pressure rise is consistent and repeatable for all of the fans. Each fan exhibited remarkable sensitivity when operating near this condition, and the sharp transition obtained in

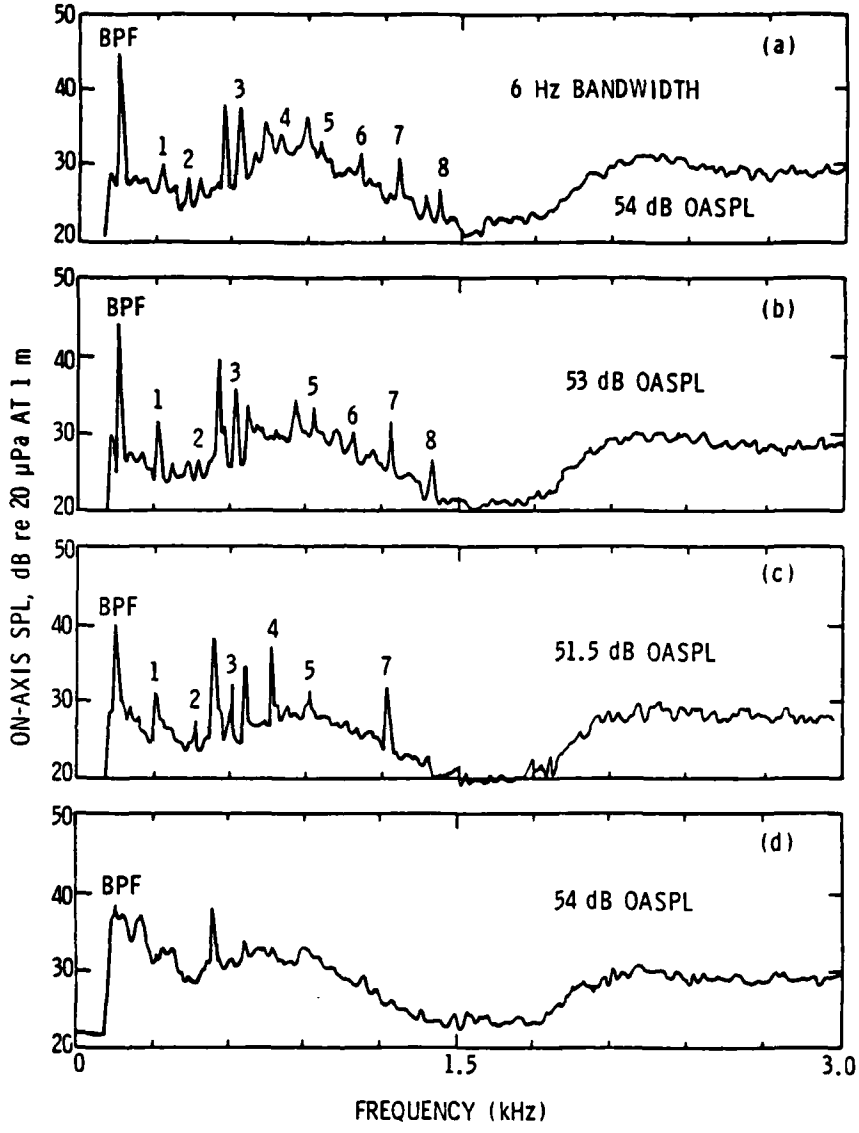

Figure 14. Muffin XL On-Axis Discrete Frequency Spectra at Various Operating Conditions.

(a) 0.0 mm-H_2O and 50 1/s
(b) 2.5 mm-H_2O and 36.5 1/s
(c) 3.3 mm-H_2O and 29 1/s
(d) 6.9 mm-H_2O and 4.5 1/s

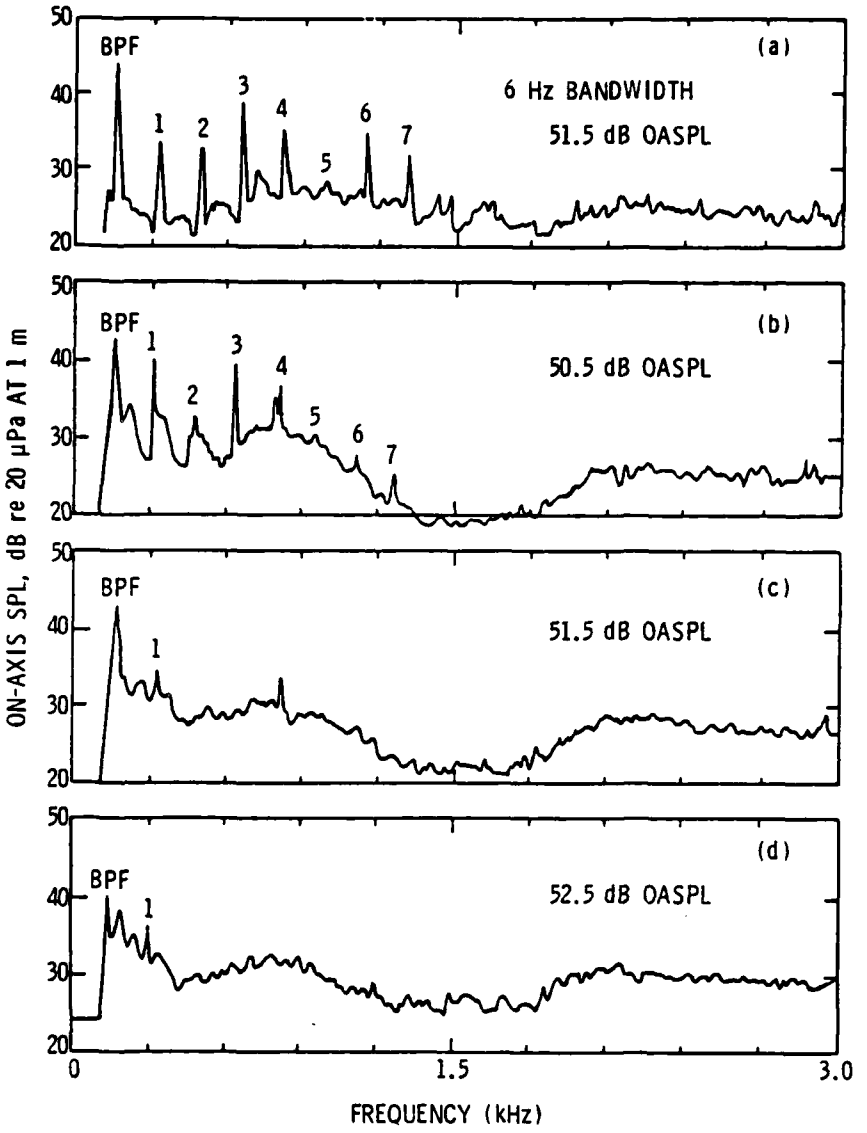

Figure 15. Muffin On-Axis Discrete Frequency Spectra at Various Operating Conditions.

(a) 0.0 mm-H_2O and 50 1/s
(b) 3.8 mm-H_2O and 19 1/s
(c) 5.1 mm-H_2O and 11 1/s
(d) 6.9 mm-H_2O and 1 1/s

spectral character is likely the result of a dramatic change in the air flow over the blades. A very similar trend was measured by Sharland [24]. He observed that the onset of blade stall produced a 10-dB increase in broadband noise level in the lower frequency part of the spectrum.

Additionally, operation at static pressure rise conditions higher than those included in Figures 12 through 15 resulted in a larger increase in low-frequency broadband noise generation. This behavior was measured by Longhouse [25]. He attributed the increase in noise level to the propagation of blade stall from a local region on the blade to the entire blade span. Based on the similarity of these results, it is likely that the fan blades are stalled when operating at these higher static pressure rises. It is advisable to avoid operation at these conditions.

Discrete frequency tones dominate the characteristic acoustic spectra at lower operating static pressure rises. Their generation is reduced and/or eliminated as static pressure rise is increased. These lower operating static pressure rises correspond to light blade loading with maximum air flow. Two important effects exist at these conditions. First, blade-load fluctuations reach their maximum value relative to the developed steady thrust. This enhances the generation of higher amplitude multiple blade-loading harmonics. Indeed, as illustrated by the spectra in Figures 12 through 15, the radiation of BPF harmonics reduces with increasing static pressure rise. Secondly, rotor inlet flow distortions and outlet flow interactions are greatest in magnitude and number with maximum air flow. As described in Chapter II, these are precisely the effects causing discrete tonal radiation along the axis of a multi-bladed rotor.

The discrete tones exhibit temporal variations in amplitude. In particular, the fundamental BPF generated by the Tarzan was observed to fluctuate as much as 6 dB in a ten-second time interval with corresponding fluctuations in the BPF harmonics. Higher-frequency fluctuating tones (above 2000 Hz) are radiated by the Partiot and Muffin XL. These tones occur randomly having amplitudes 10 dB above the broadband noise level, although their duration is no greater than a few seconds. To obtain repeatable spectra, 128 averaged ensembles were required. Barry and Moore [10] observed these high-frequency tonal excursions and associated this unsteady radiation with fluctuating distortions in the inlet flow.

Based on the noise radiated, an optimum point of operation exists for each of the fans. This point may be identified by combining the measured fan performance parameters, i.e., pressure rise, air flow, and speed, into a single nondimensional parameter and observing its influence on sound generation. Mellin [26] takes this approach using the flow coefficient, ϕ, which he gives as

$$\phi = \frac{(3.183 \times 10^5)\ Q}{N\ D_T^3} \tag{38}$$

where Q is the air-flow rate in m^3/min, N is the rotor speed in RPM, and D_T is the tip diameter of the rotor blades in centimeters.

Figures 16 and 17 illustrate the dependence of the overall sound pressure level on flow coefficient for each of the four fans. The resulting "U"-shaped curves are similar to those presented by Mellin [26] and their minima identify the optimum operating point for minimum noise. Discrete frequency rotational noise dominates the measured noise at high flow coefficients. Nonrotational broadband noise dominates at low flow

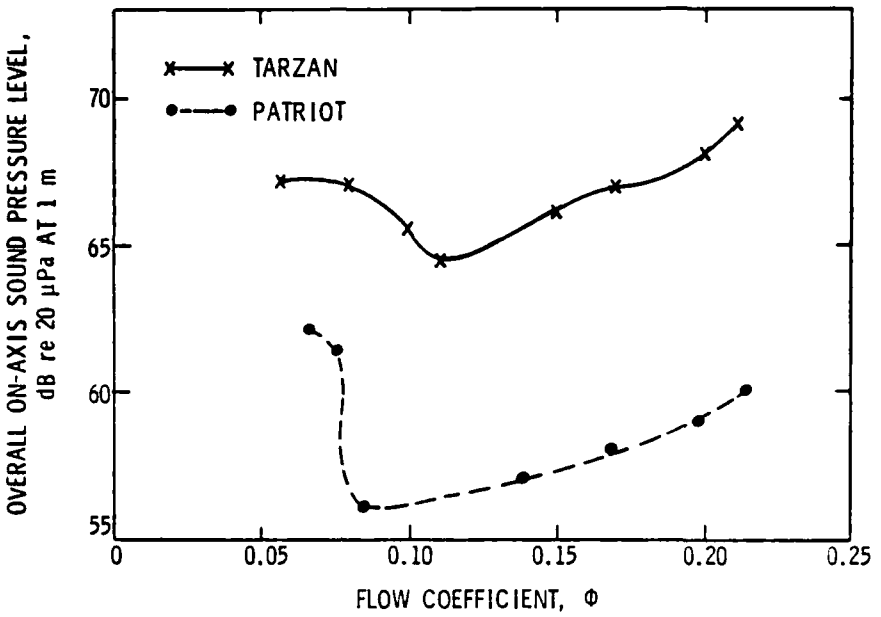

Figure 16. Measured SPL vs. Flow Coefficient for the Tarzan and Patriot.

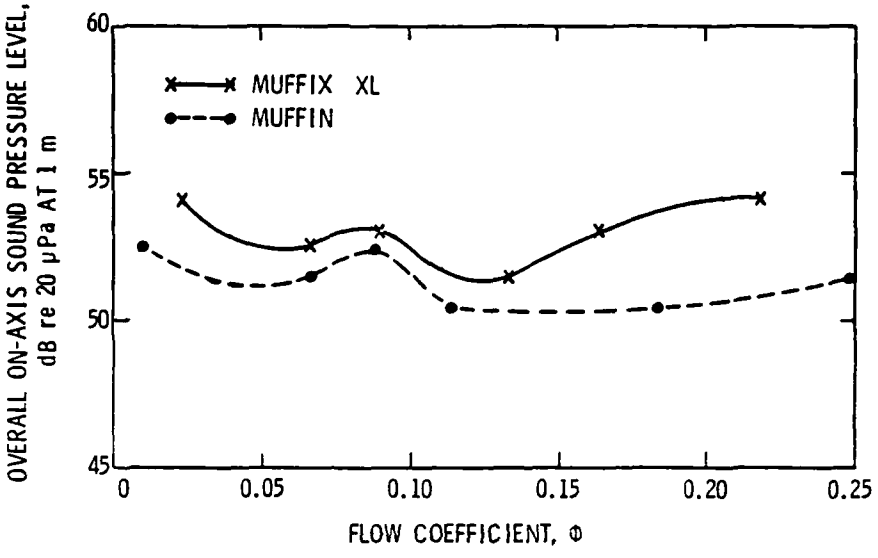

Figure 17. Measured SPL vs. Flow Coefficient for the Muffin XL and Muffin.

coefficients when the fan is heavily loaded. The noise minimum falls somewhere between these two extremes. This is the same trend observed by Longhouse [25].

Based on these results, the remaining acoustic tests were conducted with the fans operating at the minimum static pressure rise condition, i.e., maximum flow coefficient, to maximize discrete frequency noise radiation. The basic goal of the program would be best achieved under these conditions.

4.2.2 Directivity surveys. Directivity surveys were conducted as described in Section 3.3. The purpose of the surveys was to identify the directional characteristics of the radiated sound with particular emphasis on the discrete tones previously measured along the axis of the fans.

In the frontal 180° arc of all the fans, the maximum overall sound pressure level is radiated directly along the fan axis. This is due to the directional properties of higher-frequency broadband sound which has a maximum amplitude along the fan axis and reduces in level off-axis. Figure 18 illustrates a typical directivity pattern measured for this noise. The example shown is the average sound pressure level radiated by the Muffin XL over the frequency range of 2000 to 4000 Hz. The pattern radiated is indicative of zero-order pressure distributions which have directional properties similar to a piston source at higher frequencies. The radiated pattern is very similar to the "vortex noise" pattern given by Nagel [27] and verifies the approach developed by Tyler and Sofrin [8] for far-field radiation from a duct inlet.

Figure 19 illustrates the directivity patterns of several discrete tones radiated by the Tarzan. Shown are the BPF and its first three

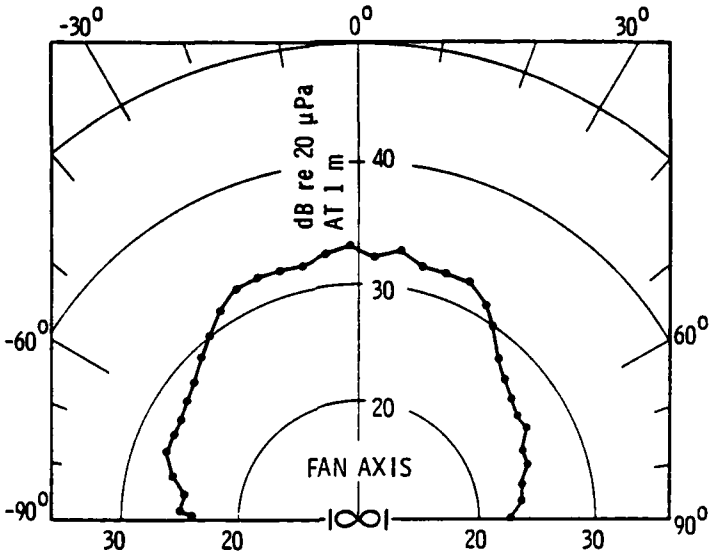

Figure 18. Typical Directivity Pattern for Higher-Frequency Broadband Sound.

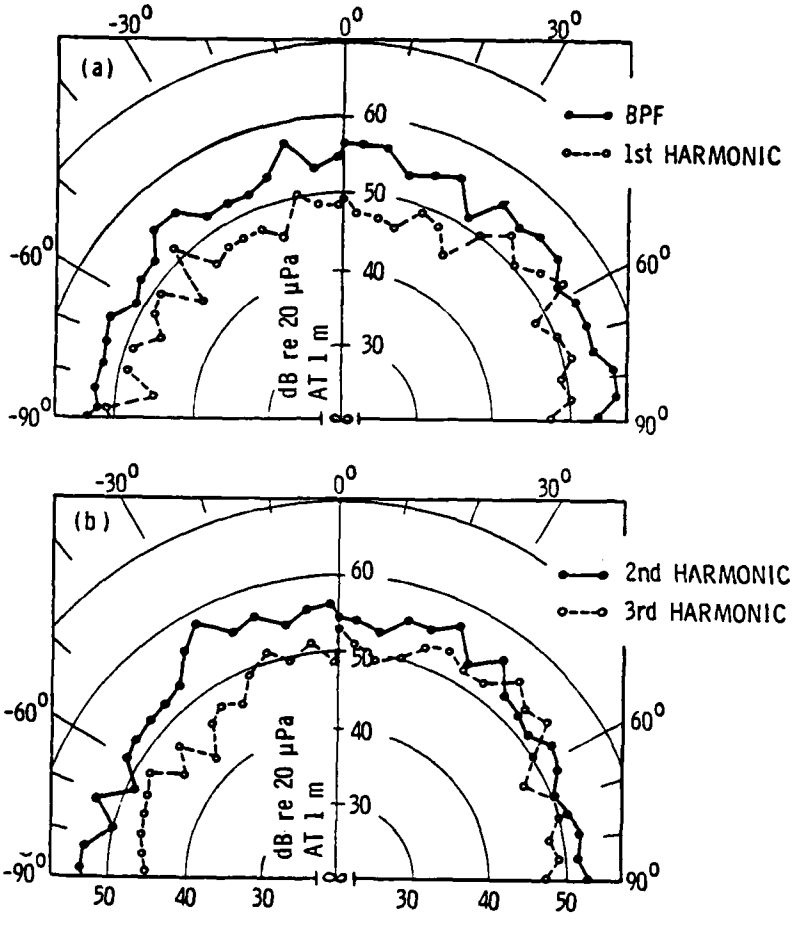

Figure 19. Tonal Directivity Patterns Radiated by the Tarzan at Various Frequencies.

(a) BPF (282 Hz) and 1st harmonic (564 Hz)
(b) 2nd harmonic (846 Hz) and 3rd harmonic (1128 Hz)

harmonics. These patterns are typical of the lower order discrete tones which radiate from the Tarzan. Higher-frequency tones, such as the fourth and fifth BPF harmonics, reduce in level off the axis of the fan as shown in Figure 20.

The directivity patterns for selected discrete tones radiated by the Patriot are shown in Figure 21. The patterns are generally uniform having some asymmetry at the BPF and its first harmonic. This tendency disappears at the higher-frequency discrete tones. From studies of the off-axis spectra, it can be stated that the Patriot does not radiate any additional BPF harmonics or rotational harmonics in directions off its axis.

As shown in Figure 22, this generally uniform tonal directivity behavior is exhibited by the Muffin XL as well. A partially-lobed pattern is radiated at the second harmonic of the BPF indicating the presence of a higher-ordered radiating pressure distribution at this frequency. The directivity of the rotational harmonics measured at 560 Hz and 880 Hz along the fan axis is uniform having the appearance of zero-order pressure distributions which reduce in amplitude off the axis of the fan.

The most atypical directivity characteristics are exhibited by the Muffin. For illustration of this behavior, the BPF pattern and the patterns of the first, fourth, and fifth BPF harmonics are shown in Figure 23. Clearly defined lobes are not present, but the directivity of these tones is nonuniform tending to radiate in an asymmetric fashion. The other BPF harmonics radiate uniformly with the higher-frequency tones reducing in amplitude off the axis of the fan.

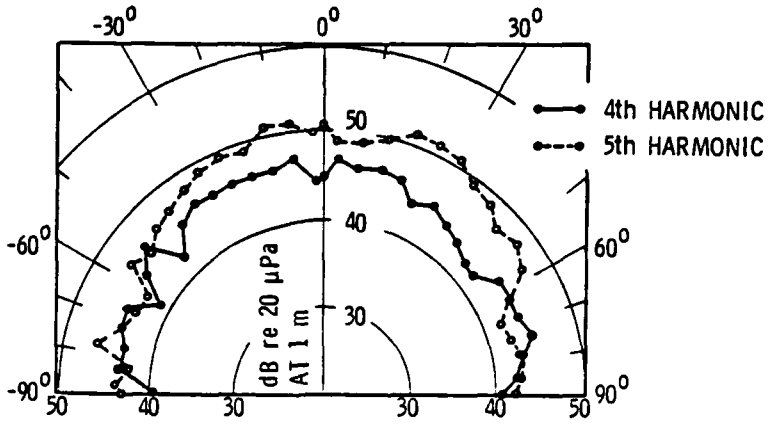

Figure 20. Tonal Directivity Patterns Radiated by the Tarzan at Various Frequencies.

(a) 4th harmonic of BPF (1410 Hz)
(b) 5th harmonic of BPF (1692 Hz)

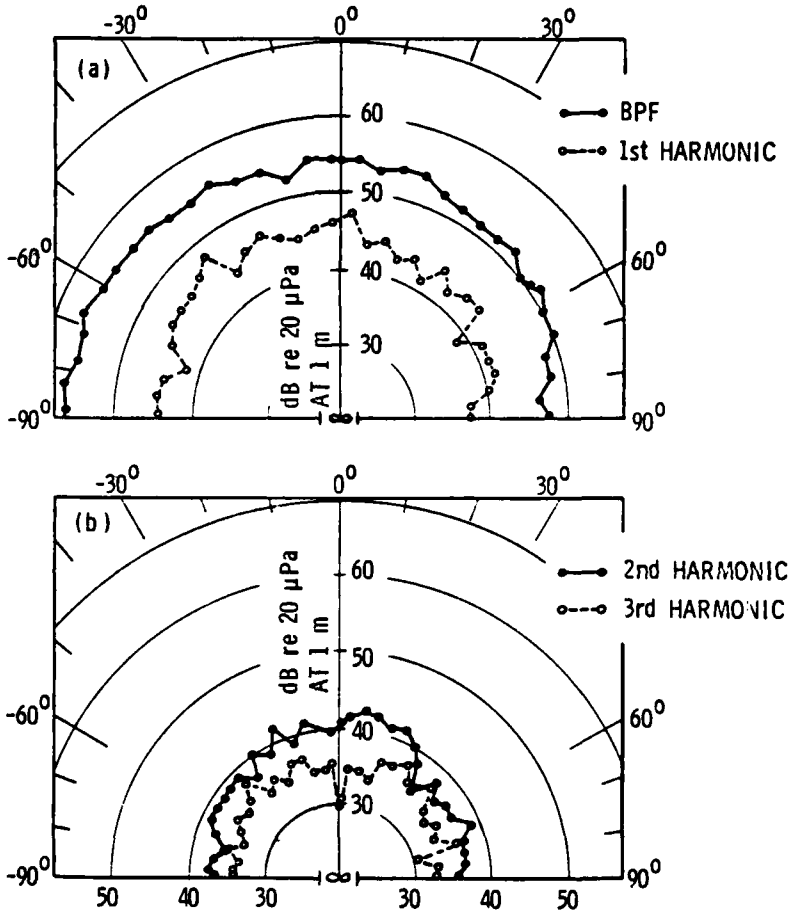

Figure 21. Tonal Directivity Patterns Radiated by the Patriot at Various Frequencies.

(a) BPF (288 Hz) and 1st harmonic (576 Hz)
(b) 2nd harmonic (864 Hz) and 3rd harmonic (1152 Hz)

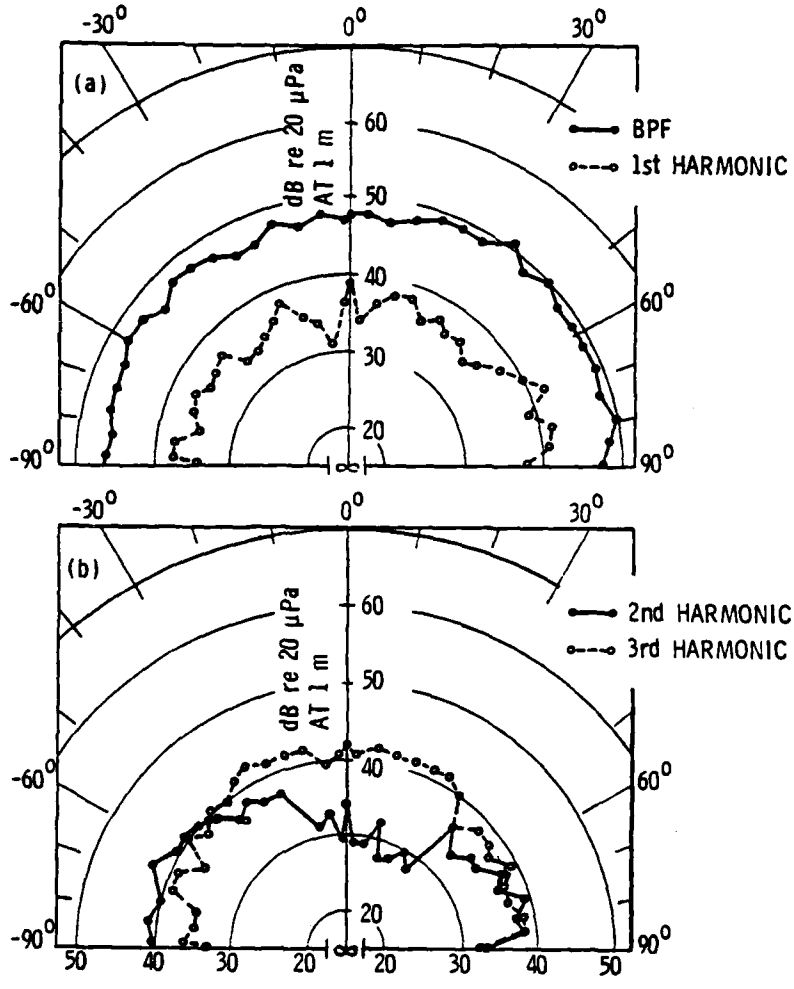

Figure 22. Tonal Directivity Patterns Radiated by the Muffin XL at Various Frequencies.

(a) BPF (156 Hz) and 1st harmonic (312 Hz)
(b) 2nd harmonic (468 Hz) and 3rd harmonic (624 Hz)

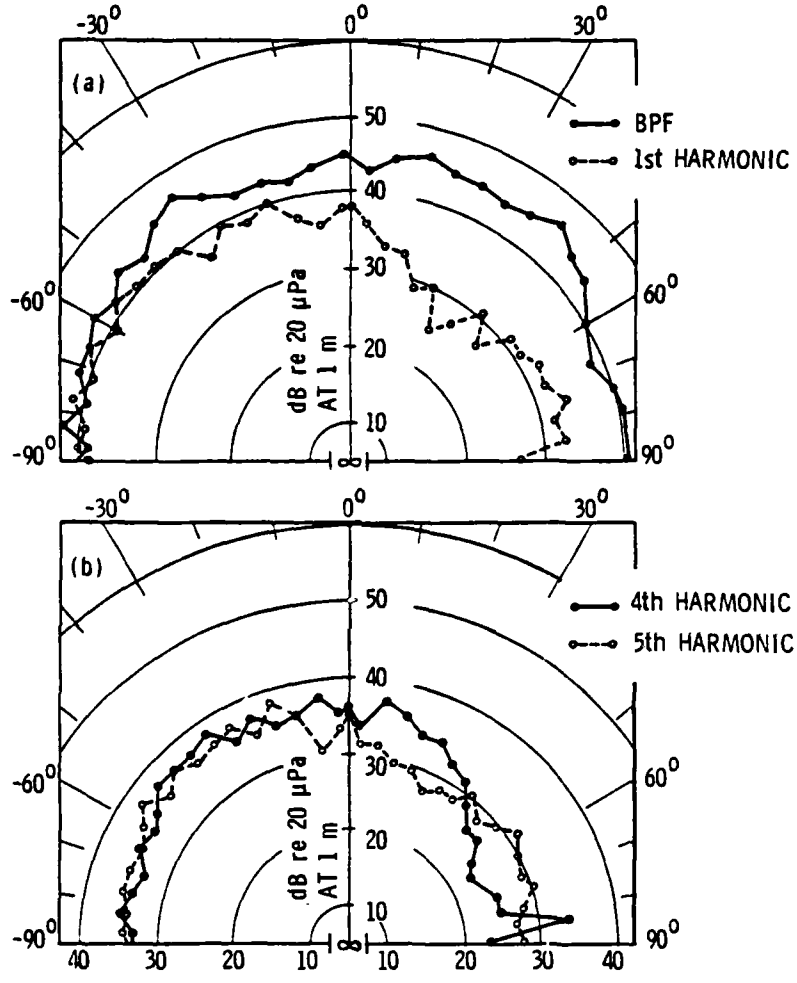

Figure 23. Tonal Directivity Patterns Radiated by the Muffin at Various Frequencies.

(a) BPF (162 Hz) and 1st harmonic (324 Hz)
(b) 4th harmonic (810 Hz) and 5th harmonic (972 Hz)

In summary, the fans radiate discrete tones in a generally uniform manner. The tones having greatest amplitude are the BPF, harmonics of the BPF, and rotational frequency harmonics. The uniform directivity patterns measured are characteristic of zero-order pressure distributions which can only be generated by the interaction of the rotor with nonuniform circumferential flow in the annulus of the fan. As described by Morfey [17], the directivity patterns resulting from this circumferentially unsteady-lift radiation are uniform having a figure-eight shape at higher harmonics.

4.2.3 Verification of the acoustic characteristics. Additional fan assemblies were procured and tested in accordance with the discussion of Section 3.3.

The results of these measurements indicate a remarkable level of quality control and consistency of product by the fan manufacturer. The overall sound pressure levels measured for the representative samples procured are within 0.5 dB of the levels measured for the original units. Every fan model exhibited this level of consistency.

Additionally, the discrete frequency spectra obtained for the samples are very consistent, exhibiting only minor differences in the various tonal levels. The distinct character and structure of the generated noise was consistent for every fan. Therefore, the acoustic characteristics measured and described here for each of the fans are truly representative of the class and the consistent acoustic performance obtained is in accordance with the findings of the fan manufacturer.

These consistent results are within the limits of the test set-up and measuring instrumentation. They eliminate an important experimental

variable permitting direct assessment of the design modifications incorporated on the fan assemblies. The design modifications will now be reviewed.

4.3 Fan Design Modifications

The results described in Section 4.2 indicate that the interaction of nonuniform circumferential flow with the fan rotor blades is the principal cause of noise radiation from these fans. As described in Chapter II, the fluctuating blade loading resulting from this interaction generates propagating acoustic pressure distributions which are either nonrotating or rotating with supersonic phase speeds.

Therefore, the design modifications are intended to eliminate and/or reduce the circumferential nonuniformity of the blade loading. For descriptive purposes, the modifications are divided into three groups: inlet, outlet, and rotor blades.

4.3.1 Inlet modifications. The principal cause of inlet flow distortion is the close-fitting shroud surrounding the fan rotor. Filleul [28] observed that the turbulent wake produced by the edge of a shroud increased the radiated sound of a free rotor by 6 dB. He was able to reduce this adverse effect by adding a bellmouth to the fan inlet. Therefore, bellmouths were designed for each of the fans and were based on the designs given by Wallis [29] and Bruce [30]. The inside diameter of each bellmouth is the same as the dimeter of the rotor annulus and the outside diameter of the bellmouth is two times this dimension. The radius of curvature of each bellmouth is one-quarter the rotor annulus diameter. The bellmouths are made from solid wood and a heated wax filler

was used to smooth the junction between the shroud and the bellmouth. Figure 24 illustrates the bellmouth design for the Muffin which was typical of those used.

The Tarzan incorporates four equally-spaced radial inlet support struts which are positioned 4.13 cm ahead of the leading edge of the rotor blades. Three of the struts are 4.78 mm wide and the fourth, which contains the electrical power leads for the motor, is 7.94 mm wide (width normal to the flow direction). The struts are very bluntly shaped. Using the approach given by Schlichting [31], there is a 99% velocity deficit of the mean flow directly behind the largest strut at the tip path plane of the rotor blades. To improve the inflow, strut modification is imperative.

The strut modification consists of filing the four original struts into a streamline shape having a 2.79 mm width. In order to provide a more uniform circumferential inflow, four additional hollow struts are added. These struts have a "teardrop" shape and are 2.79 mm wide and 6.4 mm long. They are equally spaced among the four original struts. It is noted that the total number of inlet struts has been changed to eight. There are five rotor blades and (8 - 5 = 3) which is not an even multiple of five. Therefore, minimal unsteady thrust is to be expected with this configuration. The power leads were fed individually through two of the hollow struts eliminating the need for a wider strut. This approach follows the recommendations given by Duncan, Dawson, and Hawes [32] for minimizing the noise generated by flow disturbances caused by inlet support struts.

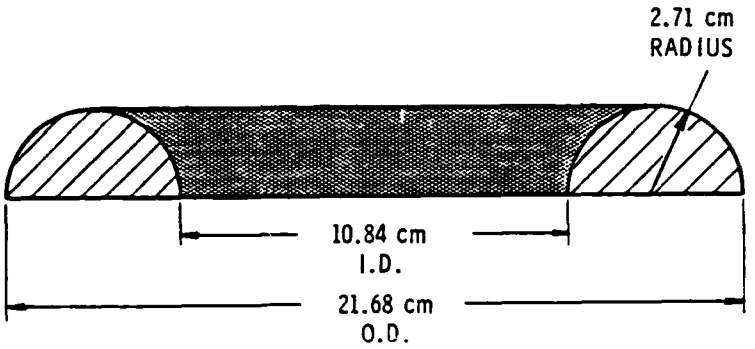

(Cross-section view of Muffin)

Figure 24. Typical Inlet Bellmouth Geometry.

Several investigators, including Filleul [28], have reported on the useful effectiveness of adding a stationary center hub cone ahead of the inlet of the fan rotor. This provides a smoother inflow at the blade roots which reduces noise radiation. Only the Tarzan has a stationary center hub at its inlet permitting the addition of a cone. The laminar flow coaxial cone shown in Figure 25 was designed for the Tarzan inlet. The cone is a symmetric solid wood piece whose laminar shape was acquired from Reference [33]. The coaxial shape permits air flow through the center hub for cooling the drive motor.

Another modification made to the Tarzan was the axial extension of the center hub support assembly over the motor. An aluminum tube was machined to a 9.35 cm outside diameter having a wall thickness of 1.73 mm. The length of the tube was 2.79 cm and it was cemented to the center support hub of the fan as shown in Figure 26. With this modification, the inside diameter of the fan's annulus remained constant up to the leading edge of the rotor.

4.3.2 Outlet modifications. On each of the fans, the outlet portion of the shroud was filled and smoothed with a heated wax filler. This resulted in a completely circular-shaped rotor annulus which, in conjunction with the smoothed bellmouth inlet, eliminated circumferential changes in the shape and diameter of the annulus.

Filleul [28] observed that a strut positioned downstream of a rotor produced an increase in radiated sound. Although not as significant as inlet struts, his results showed that outlet struts generate interactions with a rotor which cause fluctuating blade loads. Filleul [28] also observed that skewing of a strut away from the radial direction of

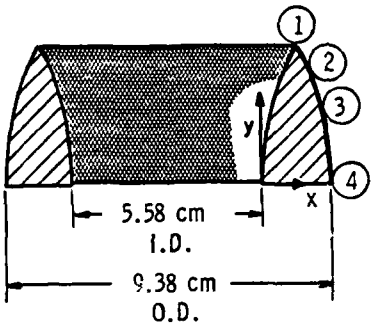

(Cross-sectional view and shape)

SHAPE COORDINATES (mm)

POSITION	x	y
1	9.5	40.2
2	6.4/12.8	34.6
3	3.2/16.0	24.0
4	0/19	0

Figure 25. Tarzan Stationary Center-Hub Piece.

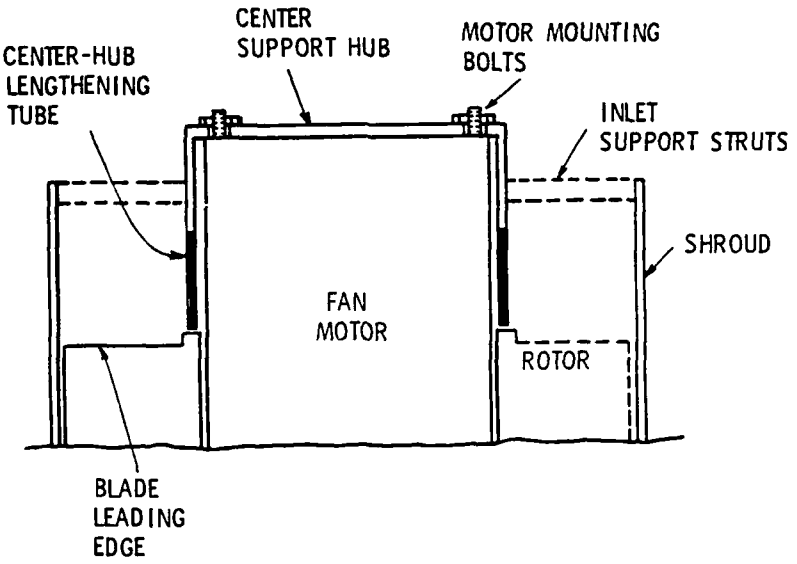

Figure 26. Cross-Sectional View of the Tarzan Inlet with Axial Extension of the Center-Support Hub.

the fan blades resulted in reduced radiated noise. The reduction in strut area instantly exposed to the blade wake, resulting from the tangential positioning, reduces the strength of the interaction between the blade and the strut. Additionally, to minimize this interaction mechanism, Duncan and Dawson [34] recommend a two-thirds ratio of strut number to blade number for low tip-speed fans.

The Patriot has three evenly spaced outlet support struts which tangentially mount the rotor hub to the shroud. Based on the number of struts and their mounting, this is a desirable configuration and any significant interaction with the five rotor blades results from the very blunt shape of the struts. Two of the struts are 5.56 mm wide (width normal to the flow direction) and are cylindrical in shape. The third strut houses the power leads for the drive motor and is a "U"-shaped hollow section 10.4 mm wide. In modified form, the width of the struts is reduced to 2.79 mm and they are filed to a "teardrop" aerodynamic shape. The power leads are individually taped along the trailing edge of the modified struts. Mold flashing, present near the struts on the hub and shroud of the fan, is filed to a smooth finish.

The Muffin XL and the Muffin both incorporate four evenly spaced outlet support struts. The struts are mounted tangentially to the hub on the Muffin XL and radially to the hub on the Muffin. Three of the struts are 4.78 mm wide on both fans. These are shaped cylindrically on the Muffin XL but are wedge-shaped, outwardly tapering in the flow direction, on the Muffin. The fourth strut, which contins the motor power leads, is 8.87 mm wide on the Muffin XL and 9.53 mm wide on the Muffin. This strut has a "U"-shape on both fans. In modified form, as recommended by Duncan

and Dawson [34], the number of struts is reduced to two and they are evenly-spaced on both fans. The two remaining struts, whose mounting orientation remains unchanged, are filed to a 2.79 mm width and are streamline in form on both fans. The motor power leads are taped along the trailing edges of the struts.

4.3.3 Rotor blade modifications. To investigate the presence of non-aerodynamic components in the generated noise, two mechanical modifications were made on each of the fans. First, the blades were removed from separate rotors and the fans were operated as "bare-hub" configurations, the purpose being to identify any significant components of noise related to the fan motors and/or bearings. Secondly, each of the baseline characteristic fans was dynamically balanced using a Stewart-Warner Model No. 2390-A portable industrial balancer. Although dynamic balancing of the rotors is a normal manufacturing process, it was possible to reduce the imbalance amplitude by 60 - 70% on each of the fans. Clay was attached to the rotor hub, away from the blades, to serve as a balancing weight.

Numerous studies have been conducted investigating the effects of physical design variations of rotor blades on radiated sound. These include variations in blade chord length, spanwise twist, sweep, skew, etc. It has been shown that proper blade design will reduce or relieve the forces inducing sound generation, but usually only under specific operating conditions. In addition, other studies have investigated respacing of the rotor blades. This alters the spectral character of the radiated sound adding lower amplitude rotational harmonics in place of BPF tones which reduces the annoyance of the noise. However, as pointed

out by Mugridge and Morfey [13], the spectrum obtained for low tip-speed axial-flow fans depends as much on the interacting flow distortions as on the geometry of the rotor itself.

Major redesign of the rotor blades and their geometry was deemed unnecessary for reducing the discrete tonal noise radiated by these fans. This decision was based on the unspecified use of the fans, the basic premise that original aerodynamic performance be retained, and the noise characterization tests which identified rotor-flow interaction as the most probable mechanism for sound generation.

Both the Muffin XL and the Patriot incorporate trailing edge serrations on their rotor blades. The purpose of the serrations is to disturb the coherent pattern of vortices shed at the trailing edge of the blades reducing "vortex-shedding" noise, as described by Patel [34]. To investigate their effectiveness, the serrations were filled with a plastic compound and smoothed to match the contour of the blades. These rotors were dynamically balanced to prevent excessive vibration.

Another modification made to the Patriot and Muffin XL rotor blades was a reduction in blade chord. With the trailing edge serrations filled, the blades were filed spanwise along the trailing edge to maintain the same total blade area as the rotor having unfilled serrations. This resulted in a 4.2% (2.59 mm) chord reduction on the Patriot and a 4.8% (2.14 mm) chord reduction on the Muffin XL.

The trailing edge of the Muffin blade sweeps backward (away from the direction of rotation) along its span. Figure 27(a) illustrates the swept appearance. In the region of maximum sweep near its outer radius, the trailing edge is cupped towards the pressure side of the blade. Since the blade is of constant thickness, it seemed probable that the

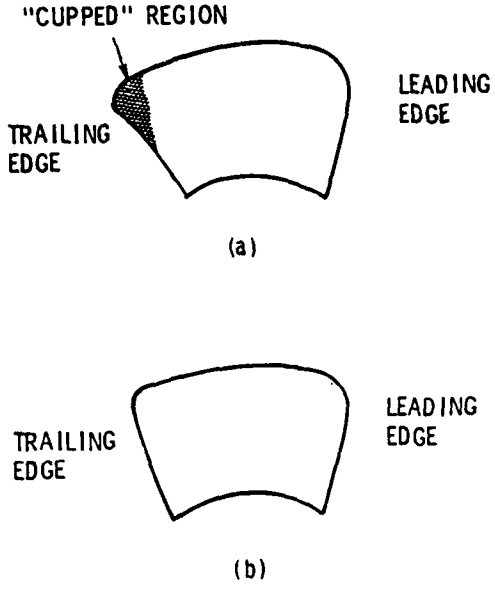

Figure 27. Muffin Blade Shapes: (a) Original, and (b) Modified.

air flow may separate in this region rendering this area of the blade inefficient for developing thrust. To investigate this assumption, a rotor having the blade shape illustrated in Figure 27(b) was configured. At its outermost radius, the modified blade has a 13.1% (5.9 mm) reduction in chord length. Prior to operation, the modified rotor was dynamically balanced.

Several studies have experimentally examined the effects of leading edge serrations and/or serrations positioned on the suction side of the blades. The works of Nagel [27] and Longhouse [36] are typical. These studies were primarily concerned with the reduction of vortex-shedding noise, but observed reductions in discrete frequency noise as well with the application of the serrations. As described by Longhouse [36], the serrations trip the laminar boundary layer on the suction side of the blade to a turbulent one which helps prevent laminar vortex shedding and separation near the trailing edge. Both studies found that the application of leading edge serrations to the blades reduced radiated noise, but also degraded aerodynamic performance. However, with suction-side serrations positioned at mid-chord, Longhouse measured a reduction in radiated noise and an improvement in peak efficienty. Based on these results, serrations were designed for each of the fans. Figure 28 illustrates the appearance of the serrations which were applied to the suction side of the blades and positioned at mid-chord with the notches pointing towards the leading edge. The serrations were made using Mancl Aluminum Company No. AL-3 Aluminum foil pressure sensitive tape which has a thickness of 0.179 mm. The tape adhered well to the surface of the blades and was trimmed along the blade tips to

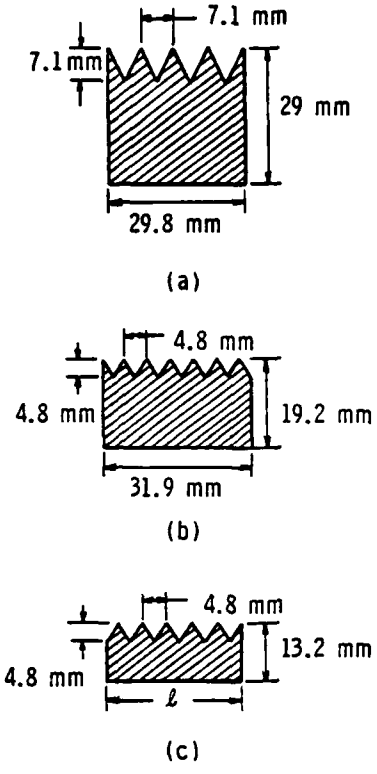

Figure 28. Serration Designs for Each of the Four Fans.

(a) Tarzan
(b) Patriot
(c) Muffin XL (1 = 28.9 mm) and Muffin (1 = 26.3 mm)

prevent rubbing against the shroud. To further investigate their effectiveness, additional rotor assemblies were configured with serrations applied to the pressure side of the blades and positioned slightly forward of the trailing edge. Prior to test and evaluation, all of these modified rotors were dynamically balanced.

Additional modifications considered were the reduction of rotor eccentricity and the blade-tip clearance within the fan shroud. As identified in Chapter II, rotor eccentricity imposes a steadily nonuniform load on the blades which may induce the generation of discrete tones. In addition, Longhouse [25] has identified the tip clearance vortex as a powerful noise source and demonstrated [36] that reduction of blade-tip clearance reduces this mechanism. These modifications were discarded based on discussions with the fan manufacturer. Their implementation would be prohibitively costly in full-scale manufacturing. Excessive rotor eccentricity was not observed on the fans received from the manufacturer. During bench-top assembly of the modified fans, rotor eccentricity was held to a practical minimum.

4.4 Evaluation of Modifications

A substantial amount of data was acquired during the test and evaluation of the various modifications. To facilitate the presentation of these results, they will be reviewed for each fan individually. The fundamental conclusions will be presented in Chapter V.

4.4.1 Tarzan. Operation of the Tarzan in the "bare-hub" configuration revealed the presence of a discrete tone at 1302 Hz whose amplitude is 44 dB (re 20 μPa) on the fan axis. As shown by Spectrum (b)

in Figure 29, additional tones having lower amplitude are also present. The 1302 Hz tone is the twenty-third harmonic of the rotational frequency and is not present in the baseline spectrum [Figure 29(a)] measured for the Tarzan fan. It is believed that the tone's generation is damped out of the radiated spectrum when the thrust load provided by the rotor blades is applied to the shaft bearings. The twenty-third harmonic is a non-multiplicative integer of the bearing-element number (the bearing contains seven rolling elements) and based on the calculation schemes for frequencies of rolling element bearing noise given by Warring [37], this tone may be indicative of a faulty irregular bearing and/or a resonance excited by bearing operation.

Dynamic balancing of the fan rotor did not alter the baseline spectrum of the radiated sound or change the measured sound pressure levels radiated by the baseline fan.

Spectrum (c) in Figure 29 illustrates the change due to the addition of the bellmouth at the fan's inlet. The spectrum is clearly tonal but limited to the BPF and the first three harmonics. These tones are likely caused by the steady nonuniform inflow generated by the four inlet support struts together with the shear flow imposed by the boundary layer formed on the bellmouth. Their higher amplitudes account for the 0.5 dB increase in overall sound pressure level. The other tones present in the baseline spectrum and the broadband hump centered around the fifth harmonic of the BPF have been reduced or eliminated.

The spectrum obtained with the inlet strut modification is shown as part (d) of Figure 29. The amplitude of the noisiest tones has been reduced from the baseline spectrum and the tonal energy is more evenly

Figure 29. Discrete Frequency On-Axis SPL Spectra for the Tarzan in Various Configurations.

(a) In unmodified original conditions.

(b) With the "bare-hub" rotor.

(c) With the inlet bellmouth.

(d) With the modified inlet support struts.

(e) With the bellmouth and support strut modifications.

(f) Configuration in (e) with the center-hub extension piece and the suction-side serrations on the blades.

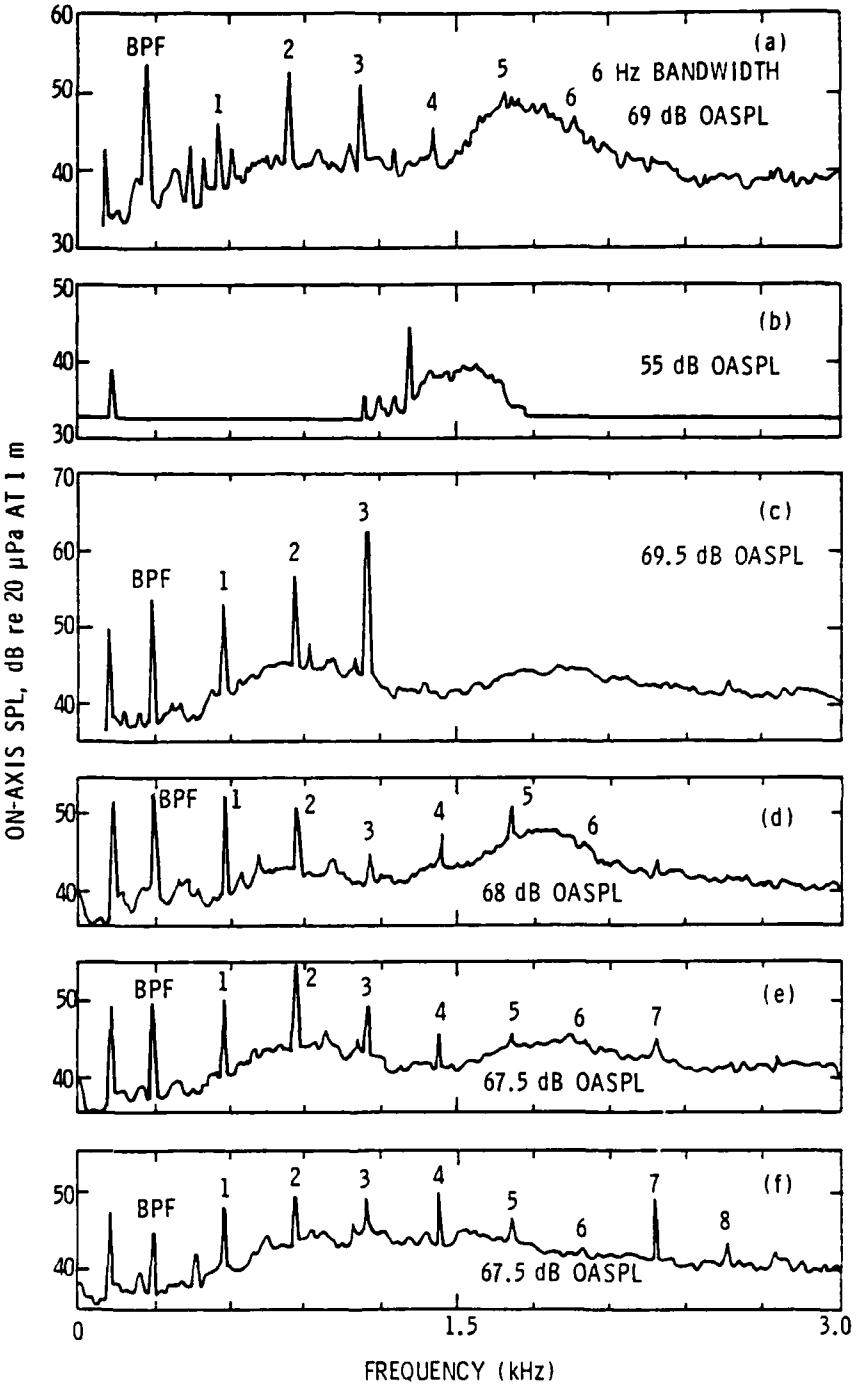
(a)
6 Hz BANDWIDTH
69 dB OASPL
BPF
1
2
3
4
5
6
(b)
55 dB OASPL
(c)
69.5 dB OASPL
(d)
68 dB OASPL
(e)
67.5 dB OASPL
7
(f)
67.5 dB OASPL
8
ON-AXIS SPL, dB re 20 μPa AT 1 m
FREQUENCY (kHz)
0
1.5
3.0

spread among the rotational haromonics and the harmonics of the BPF. The overall sound pressure level is reduced by 1 dB.

The bellmouth and the inlet support strut modification had the greatest individual effects on the radiated sound. The evaluation of other modifications was facilitated by having the bellmouth and the modified support struts incorporated in the test assembly. The combined effect of these two modifications is shown as Spectrum (e) in Figure 29. Except for the first and the second harmonics of the BPF, the amplitude of all the principal tones has been reduced.

The laminar-shaped center-hub piece, shown in Figure 25, caused an increase in the amplitude of the dominant radiated tones and increased the broadband noise level. Repositioning of the cone on the hub of the fan shifted the relative amplitudes of the discrete tones but did not provide an overall reduction in radiated sound. Evidently, the cone adversely affected the inflow to the rotor; therefore, this modification was discarded.

The center-hub extension tube, shown in Figure 26, caused a shift in the tonal energy from the lower BPF harmonics to the higher harmonics. The fundamental BPF was reduced by 4 dB and the second harmonic was reduced by 3 dB. However, there was an increase in the amplitudes of the fourth, fifth, sixth, and seventh harmonics of the BPF. This modification was retained because of the reduction in level of the second harmonic, the tone of highest amplitude. The overall on-axis sound pressure level increased by 0.5 dB.

The addition of the suction-side serrations to the blades had no effect on the radiated sound of the Tarzan. The serrations were

positioned at 50% chord and also at 33% chord (measured from the leading edge). Also, at the 33% chord position, the tips of the serrations were raised 4.4 mm above the surface of the blades and, in this form, the serrations produced a reduction in the radiated sound. Part (f) of Figure 29 illustrates the resulting spectrum. The higher BPF harmonics, whose amplitudes increased with the addition of the center-hub extension tube, remain unchanged in amplitude, but the second harmonic of the BPF is reduced by an additional 2.5 dB and the broadband noise, above 1.5 kHz, is also reduced. Thus, if the serrations are sufficiently thick to disturb the boundary layer on the blade surface, then a reduction in radiated sound can be achieved.

The addition of serrations to the pressure side of the blades caused an increase in the second, third, and fifth BPF harmonics by about 4 dB on the fan axis. The overall sound level did not change, which indicates that some reduction occurred in other frequency bands. Variations in chord-wise position and notch tip height did not significantly affect this result. Therefore, this modification was not incorporated.

Smoothing the outlet portion of the shroud, in combination with the bellmouth, the modified inlet support struts, the center-hub lengthening tube, and the suction-side serrations with raised tips, produced the most quiet modified configuration of the Tarzan. Figure 30 illustrates the on-axis spectrum measured for this configuration together with the original baseline spectrum. In this modified form, the overall on-axis sound pressure level is 2 dB lower than the original fan. The tonal energy is reduced and redistributed within the spectrum

AD-A118 439 PENNSYLVANIA STATE UNIV UNIVERSITY PARK APPLIED RESE--ETC F/G 13/1
DISCRETE FREQUENCY NOISE AND ITS REDUCTION IN SMALL AXIAL-FLOW --ETC(U)
MAR 82 J M FITZGERALD N00024-79-C-6043
UNCLASSIFIED ARL/PSU/TM-82-76 NL

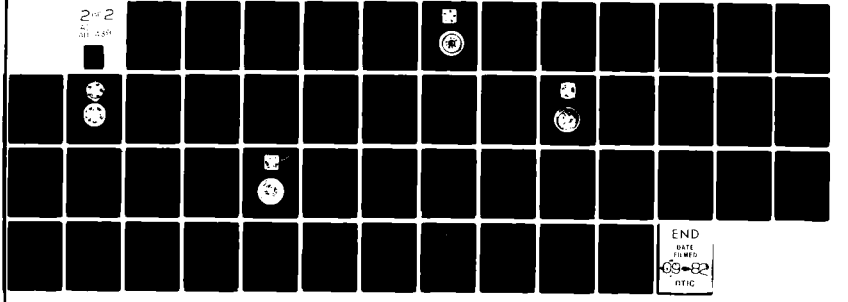

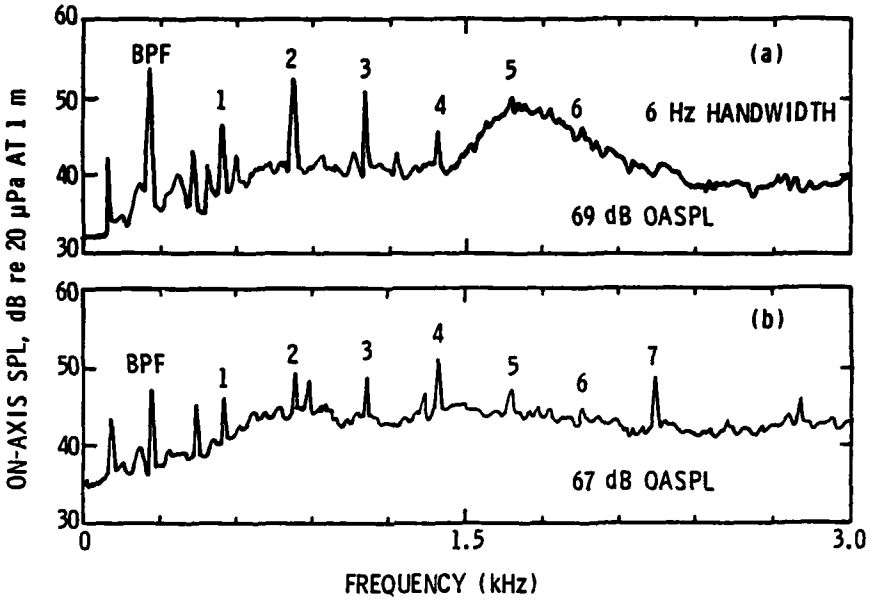

(a) in unmodified original condition

(b) with the bellmouth, modified inlet support struts, the center-hub extension piece, suction-side serrations, and the smoothed shroud outlet.

Figure 30. Discrete Frequency On-Axis SPL Spectra for the Tarzan in Various Configurations.

generated by the fan. The higher harmonics of the BPF radiated by the modified fan are generated by the four additional inlet support struts. With improved aerodynamic shape and tangential mounting of the struts to the center-hub, it is believed that further reductions in the amplitude of the radiated tones could be achieved.

Table IV lists the individual effects of the various modifications on the discrete tones radiated by the Tarzan. The changes in the on-axis sound pressure level amplitudes listed are all relative to the original baseline spectrum, in decibels.

A directivity survey of the noise radiated by the modified configuration of the Tarzan was conducted as described in Section 3.3. The directivity pattern of the BPF and its first seven harmonics was found to be generally uniform. However, the fourth harmonic exhibited an 8 dB lobe at -23° from the fan axis.

Using the directivity survey results, the sound power level of the radiated discrete tones can be determined. Wells and Madison [19] give an expression for calculating the sound power level in a particular frequency band from the sound pressure levels measured at discrete points in a semi-circle. The expression given is

$$L_w = \bar{L}_p + 20 \log_{10} r + 7.9 \quad ,$$

where L_w is the sound power level (re 10^{-12} watts), $\bar{L}_p$ is the sound pressure level averaged over space, and r is the measuring radius in meters. Table V lists the results for the original Tarzan and the modified Tarzan using this approach at the BPF and its first seven harmonics. Except for the fourth and seventh harmonics of the BPF, the

TABLE IV

EFFECTS OF THE MODIFICATIONS ON THE
DISCRETE TONES RADIATED BY THE TARZAN

Modification	Changes in the On-Axis SPL of the BPF Harmonics, dB							
	BPF	1	2	3	4	5	6	7
(1) Bellouth	-1	+6	+4	+11	-4	-6	-3	-1
(2) Inlet struts	-2	+5	-2	-7	+1	0	-2	+1
(3) Bellmouth and inlet struts	-5	+3	+2	-3	-1	-5	-2	+1
(4) Bellouth and inlet struts with laminar center-hub piece	-7	-4	+1	-4	+4	0	-1	+7
(5) Bellouth and inlet struts with center extension tube	-9	+2	-1	-2	+3	-1	0	+7
(6) Bellmouth and inlet struts with center extension tube and suction side serrations	-9.5	+2	-3.5	-2	+4	-4	-3	+7
(7) Bellouth and inlet struts with center extension tube and pressure side serrations	-9	+2	+2.5	+1	+3	+3	-1	+6
(8) Bellmouth and inlet struts with center extension tube, suction side serrations and improved outlet geometry	-7.5	0	-4	-2.5	+5	-4	-3	+6

TABLE V

DISCRETE FREQUENCY POWER LEVELS - TARZAN

Frequency	Sound Power Level dB (re 10^{-12} watts)		
	Original	Modified	Δ dB
BPF (282 Hz)	61.7	51.9	-9.8
1st Harmonic (564 Hz)	56.4	51.5	-4.9
2nd Harmonic (846 Hz)	61.3	54.2	-7.1
3rd Harmonic (1128 Hz)	56.8	51.4	-5.4
4th Harmonic (1410 Hz)	52.1	59.8	+7.7
5th Harmonic (1692 Hz)	54.8	53.4	-1.4
6th Harmonic (1974 Hz)	52.1	49.7	-2.4
7th Harmonic (2256 Hz)	48.9	51.9	+3.0

sound power radiated at discrete frequencies by the Tarzan has been reduced. The photographs shown in Figure 31 illustrate the differences in appearance between the original and modified fans.

4.4.2 Patriot. Operation of the Patriot in the "bare-hub" configuration showed no significant mechanical or electrical noise. Throughout the measured frequency range, the noise was 6 to 33 dB below that measured for the original fan. Dynamic balancing of the rotor did not alter the spectral character of the radiated sound or change its overall level. Therefore, the radiated sound is predominantly of aerodynamic origin.

As shown by Spectrum (b) in Figure 32, addition of the bellmouth did not significantly change the spectral character of the radiated sound. The high-frequency tones, present above 2000 Hz in the baseline Spectrum a), have been reduced, but the discrete tones measured at the BPF and its harmonics are increased somewhat by the bellmouth. As with the Tarzan results, this implies that circumferential variations of the inflow, caused by the geometry of the fan shroud, are responsible for the generation of the higher-ordered blade-loading harmonics radiated by these fans. The circularly-shaped inlet of the Patriot fan minimizes these variations.

The effect of the strut modification is shown by Spectrum (c) in Figure 32. The amplitude of the BPF has been reduced by 17 dB, although the amplitudes of the BPF harmonics are unchanged. The reduction of the BPF is most likely due to the decrease in width of the support strut which contains the motor electrical leads. The overall sound pressure level is reduced by 1 dB.

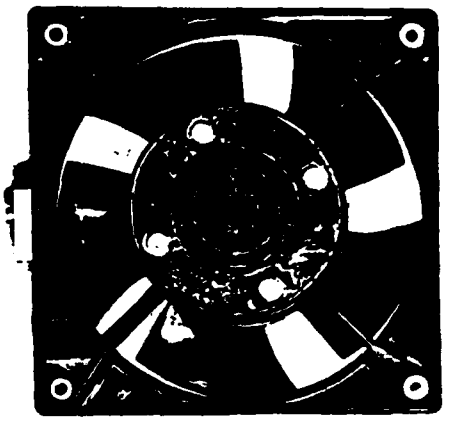

(a) original

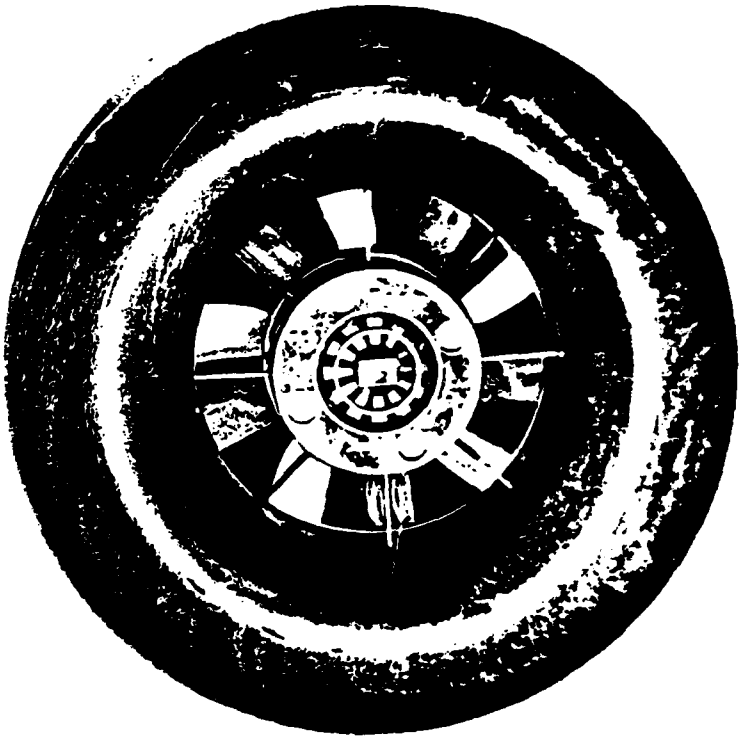

(b) modified

Figure 31. Appearance of the Original and Modified Tarzan Fans.

Figure 32. Discrete Frequency On-Axis SPL Spectra for the Patriot in Various Configurations.

(a) In unmodified original condition.

(b) With the inlet bellmouth.

(c) With the modified outlet support struts.

(d) Configuration in (c) and the Suction-side serrations.

(e) Configuration in (d) with the shorter blades.

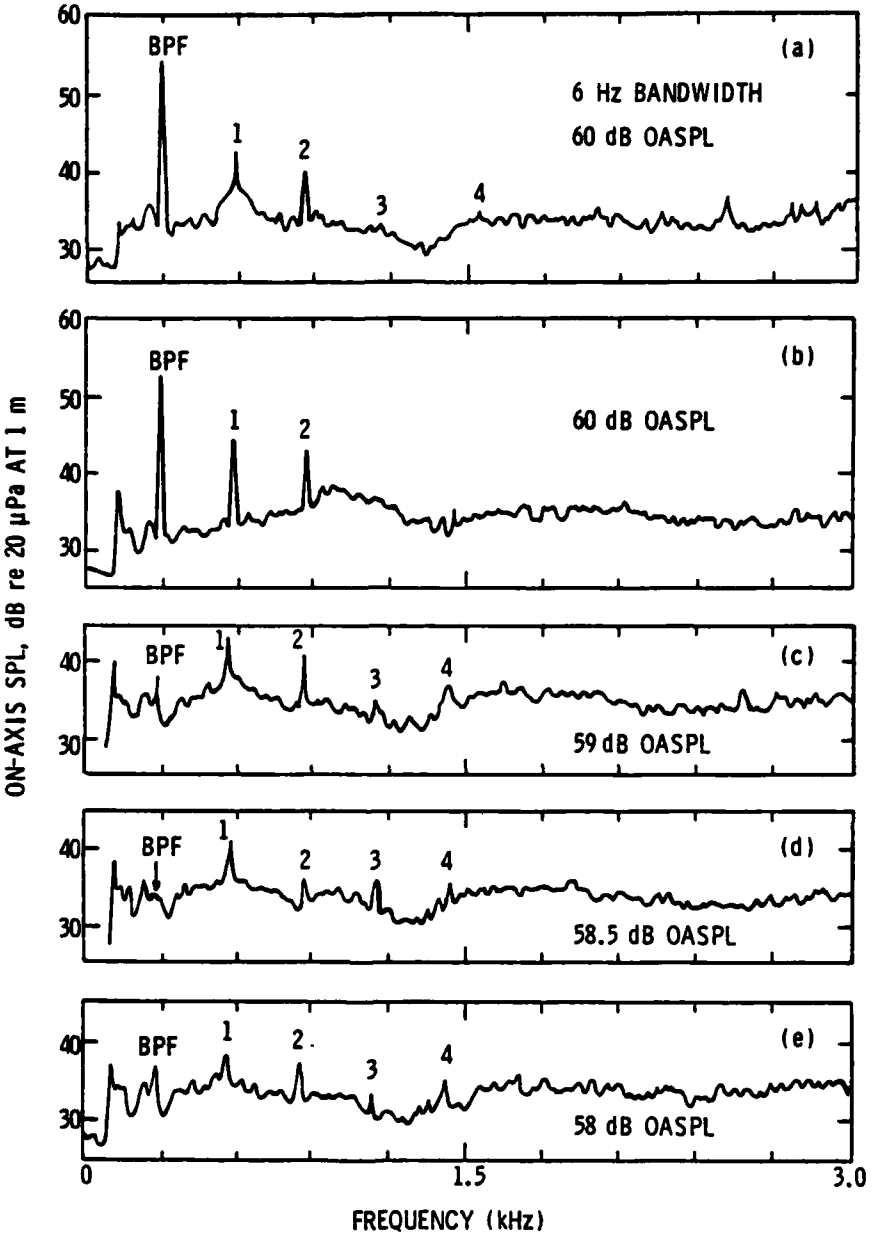
60
50
40
30
BPF
1
2
3
4
(a)
6 Hz BANDWIDTH
60 dB OASPL
(b)
60 dB OASPL
(c)
59 dB OASPL
(d)
58.5 dB OASPL
(e)
58 dB OASPL
ON-AXIS SPL, dB re 20 μPa AT 1 m
0
1.5
3.0
FREQUENCY (kHz)

Filling the trailing-edge serrations caused a 1 to 2 dB increase in the amplitude of the radiated tones. There was no change in the broadband sound level and no indication of vortex-shedding noise. The increased amplitude of the tones can be attributed to a more powerful interaction between the rotor and the outlet support struts. The wake shed by the blades without trailing-edge serrations is more powerful due to the increased blade area. The overall sound pressure level increased by 0.5 dB on the fan axis.

To enhance their effectiveness, the remaining modifications were evaluated on an assembly incorporating the modified outlet support struts. The bellmouth was discarded because its addition caused an increase in the amplitude of the discrete tones radiated by this assembly.

Shortening the blade chord as described in Section 4.3.3 reduced the amplitude of the radiated tones by 1 to 2 dB, but produced a broad "hump" in the sound spectrum which was centered at 2780 Hz. The overall sound level increased by 0.5 dB on the axis of the fan, but no increase in the overall sound level was measured at 45° off the axis of the fan. This behavior fits the vortex-shedding noise mechanism described by Longhouse [36]. If the blade chord is sufficiently small, the flow over the suction side of the blade will remain laminar up to a point near the trailing edge. Vortices due to laminar separation will be shed from the trailing edge causing the characteristic "hump" in the radiated sound.

The effect of the suction-side serrations is shown by Spectrum (d) in Figure 32. The BPF and its second harmonic are reduced by 4 dB, while the first and third harmonics of the BPF are reduced by 1 dB. Clearly, in addition to tripping the suction-side boundary layer into a turbulent

one, the serrations act to relieve or reduce the fluctuating blade forces which contribute to the generation of discrete tones.

Mounting the suction-side serrations on the rotor whose blades were shortened produced the most quiet modified configuration obtained for the Patriot. The serrations eliminated the broad "hump" in the spectrum generated by the shorter blades and, as shown in Figure 30(e), both modifications effectively reduce the amplitude of the discrete tones radiated.

Table VI lists the individual effects of the various modifications on the discrete tones radiated by the Patriot. The changes in the on-axis sound pressure level amplitudes listed are all relative to the baseline spectrum, in decibels.

In summary, incorporation of the modified outlet support struts, the shorter rotor blades with filled trailing-edge serrations, and the suction-side serrations into a single assembly produced the quietest modified configuration of the Patriot. The directivity patterns of the BPF and its first three harmonics radiating from the modified fan were found to be very uniform, indicating that the asymmetrical pattern observed for the BPF of the baseline fan [Figure 20(a)] is generated by the wide outlet support strut which contains the motor power leads.

Using the results of the directivity survey and the approach described in Section 4.4.1, the radiated power of the discrete tones can be calculated. Table VII lists the discrete frequency power levels calculated for the original and modified configurations of the Patriot at the BPF and its first three harmonics.

TABLE VI

EFFECTS OF THE MODIFICATIONS ON THE
DISCRETE TONES RADIATED BY THE PATRIOT

Modification	Changes in the On-Axis SPL of the BPF Harmonics, dB			
	BPF	1	2	3
(1) Bellmouth	-1.5	+2.5	+2.5	0
(2) Outlet struts	-17	0	0	+1
(3) Serrations filled	0	+1	+2	0
(4) Outlet struts and shorter blades	-17	-1	0	-2
(5) Outlet struts and suction-side serrations	-20	-1.5	-4	+1
(6) Outlet struts and shorter blades with suction-side serrations	-17	-3.5	-3	0

TABLE VII

DISCRETE FREQUENCY POWER LEVELS - PATRIOT

Frequency	Sound Power Level dB (re 10^{-12} watts)		
	Original	Modified	Δ dB
BPF (288 Hz)	60.7	44.9	-15.8
1st Harmonic (576 Hz)	51.1	46.3	-4.8
2nd Harmonic (864 Hz)	46.2	44.6	-1.6
3rd Harmonic (1152 Hz)	42.3	39.6	-2.7

The sound power levels of the discrete frequencies radiated by the Patriot have been reduced. Figure 33 illustrates the differences in appearance between the original and modified fans.

4.4.3 Muffin XL. Operation of the Muffin XL in the "bare-hub" configuration indicated the presence of discrete tones at 588 Hz, 882 Hz, and 1644 Hz. The tone at 1644 Hz is 2 dB below the baseline spectrum at this frequency. The other tones are 14 dB below the baseline spectrum. These frequencies are rotational harmonics. Based on discussions with the fan manufacturer, it is believed that these are natural frequencies of the electrical rotor bar which are excited by operation of the fan motor. The rotor bar is a compressed lamina which interacts with the magnetic field induced by the motor windings to power the fan rotor. During operation, the laminations can vibrate and radiate sound. An additional basis supporting this assumption is the fact that the Muffin XL incorporates an oil-impregnated sintered bronze sleeve bearing which does not contain any rolling elements.

Dynamic balancing of the rotor did not alter the spectral character of the radiated sound or change its overall level.

Spectrum (b) in Figure 34 illustrates the effect of adding the bellmouth to the fan's inlet. As was observed with the Tarzan, the addition of the bellmouth eliminates the generation of higher harmonics of the BPF, reduces the generation of higher-ordered rotational harmonics, and smooths the broadband noise portion of the spectrum. The overall sound pressure levels did not change.

The effect of the modified outlet support struts is shown by Spectrum (c) in Figure 34. The amplitude of the BPF is reduced by 9 dB,

(a) original

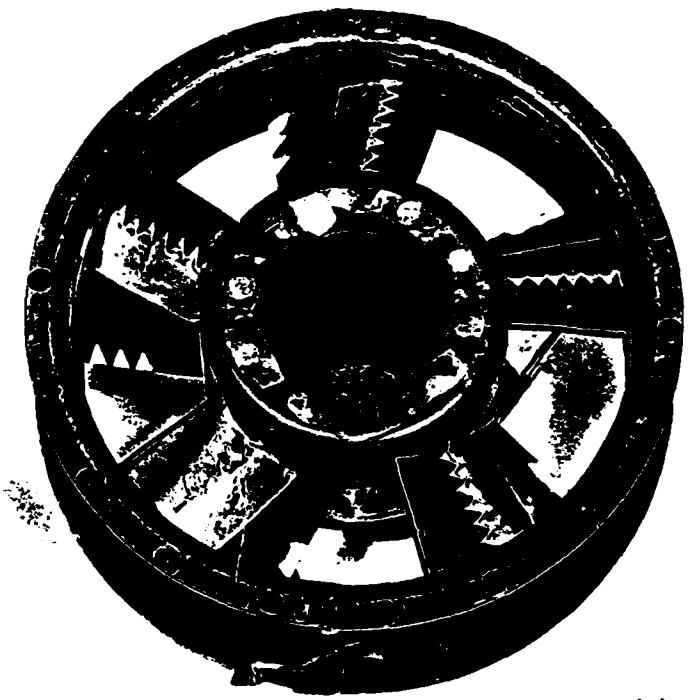

(b) modified

Figure 33. Appearance of the Original and Modified Patriot Fans.

Figure 34. Discrete Frequency On-Axis SPL Spectra for the Muffin XL in Various Configurations.

(a) in unmodified original condition
(b) with inlet bell-mouth
(c) with modified outlet support strut
(d) with suction-side serrations on the blade
(e) with bell-mouth modified strut and serrations
(f) configuration (e) and smooth shroud outlet

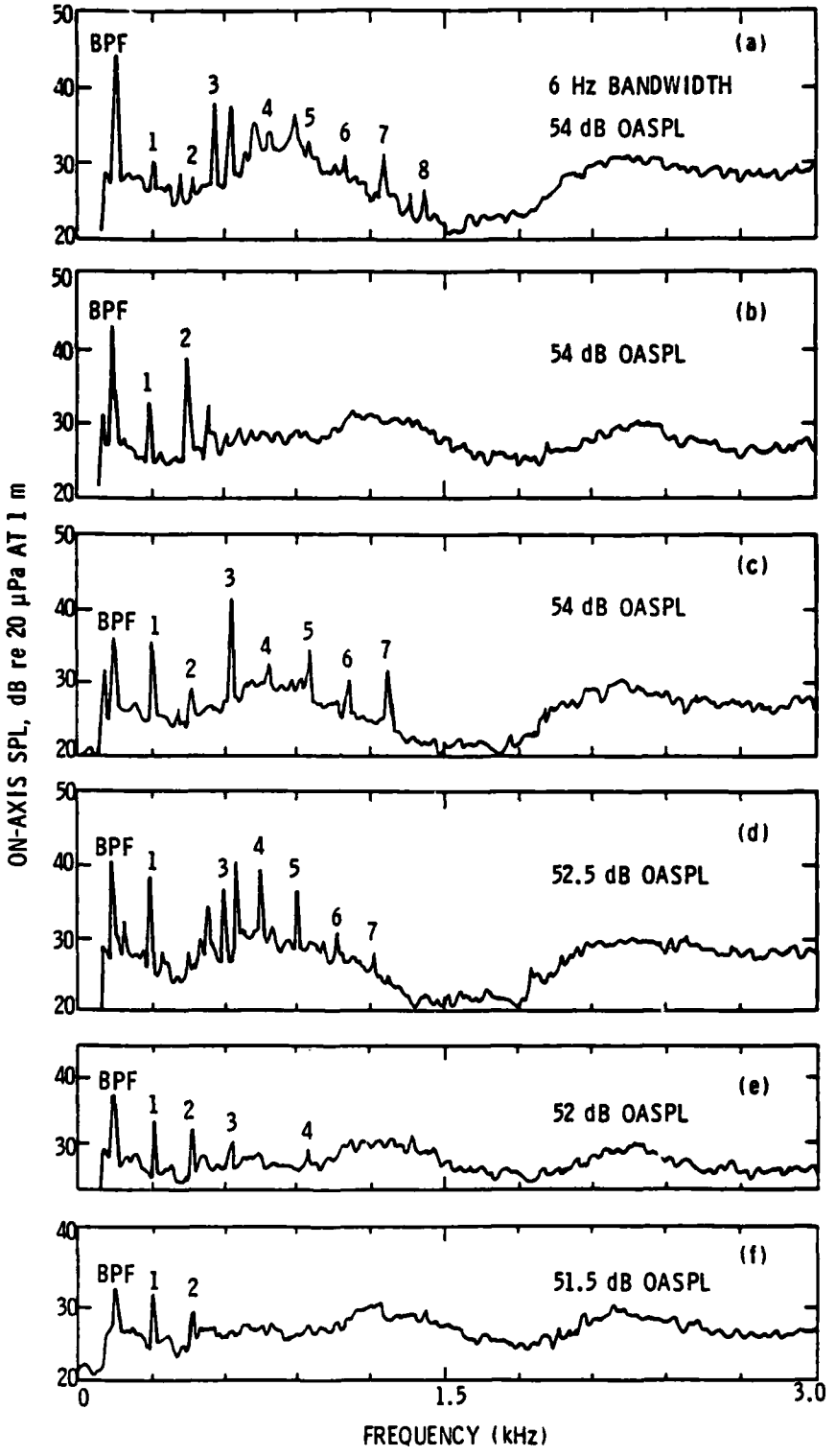
(a)
6 Hz BANDWIDTH
54 dB OASPL
(b)
54 dB OASPL
(c)
54 dB OASPL
(d)
52.5 dB OASPL
(e)
52 dB OASPL
(f)
51.5 dB OASPL
BPF
ON-AXIS SPL, dB re 20 µPa AT 1 m
FREQUENCY (kHz)
0
1.5
3.0

but the amplitudes of the first and third harmonics of the BPF are increased by 5 dB. The rotational frequency harmonics are not present and the overall sound pressure levels did not change.

Filling the trailing-edge serrations randomly shifted the amplitudes of the discrete tones but did not affect the broadband noise. There was no evidence of increased vortex noise. The overall sound pressure levels did not change.

Shortening the blade chord of the blades having filled trailing-edge serrations produced shifts in the amplitudes of the radiated tones. There was also no change observed on an assembly fitted with the bellmouth and the modified outlet support struts. Therefore, this modification was discarded.

The addition of the serrations to the suction side of the blades produced no effect on the radiated sound of the Muffin XL. The serrations were positioned at 50% chord and at 36% chord, where the blades have maximum thickness (15.9 mm from the leading edge). Also, at the 36% chord position, the tips of the serrations were raised 1.8 mm above the surface of the blades and, in this form, the serrations produced a reduction in the radiated sound. Spectrum (d) of Figure 34 illustrates the effect of the serrations. The broadband noise floor of the entire spectrum is reduced by about 2 dB. The relative amplitudes of the discrete tones are shifted exhibiting a more uniform distribution of the tonal energy, although the amplitude of the rotational harmonic present at 660 Hz has increased by 8 dB. The overall sound pressure levels measured at positions both on and off the axis of the fan are reduced by 1.5 dB.

The addition of the serrations to the pressure side of the blades produced no effect on the radiated sound. Experimentation with the

chord-wise position and tip height of these serrations did not yield any changes in the radiated sound. Therefore, this modification was discarded.

Spectrum (e) of Figure 34 illustrates the combined effect of the bellmouth, the modified outlet support struts, and the suction-side serrations, positioned and configured in the optimum manner described. The amplitudes of the significant discrete tones and the broadband noise (above 2 kHz) are reduced. The overall on-axis sound pressure level is reduced by 2 dB.

In addition to these three modifications, improvement of the circumferential outlet geometry of the shroud produced the most quiet modified configuration of the Muffin XL. Spectrum (f) in Figure 34 illustrates the effect of these four modifications on the acoustic characteristics of the fan.

Table VIII lists the individual effects of the various modifications on the discrete tones radiated by the Muffin XL. The changes in the on-axis sound pressure level amplitudes listed are all relative to the baseline spectrum, in decibels.

A directivity survey was conducted on the quietest modified assembly of the Muffin XL. The directivity curves at BPF and its harmonics were found to be uniform. The broadband noise "humps," evident within the on-axis spectrum near 1200 Hz and 2200 Hz [Figure 34(f)] were found to decrease in amplitude off the axis of the fan.

Using the results of the directivity surveys, the discrete frequency sound power levels were calculated as described in Section 4.4.1. Table IX lists the results for the original and modified configurations

TABLE VIII

EFFECTS OF THE MODIFICATIONS ON THE
DISCRETE TONES RADIATED BY THE MUFFIN XL

Modification	Changes in the On-Axis SPL of the BPF Harmonics, dB				
	BPF	1	2	3	4
(1) Bellmouth	-2.5	+3	+10	-6	-8
(2) Outlet struts	-9	+5	-1	+4	-5
(3) Serrations filled	-2	+2	+1	+2	+5.5
(4) Shorter blades	-3	+5	+6	-3	+3
(5) Suction-side serrations	-4	+7	+1	-2	+3
(6) Bellmouth and outlet struts with suction-side serrations	-7.5	+3	+3	-7.5	-6
(7) Bellmouth and outlet struts with suction-side serrations and improved outlet geometry	-11	+1.5	+1	-10	-6.5

TABLE IX

DISCRETE FREQUENCY SOUND POWER LEVELS - MUFFIN XL

Frequency	Sound Power Level dB (re 10^{-12} watts)		
	Original	Modified	Δ dB
BPF (156 Hz)	56.0	39.6	-16.4
1st Harmonic (312 Hz)	44.8	39.1	-5.7
2nd Harmonic (468 Hz)	43.5	35.1	-8.4
3rd Harmonic (624 Hz)	47.0	33.1	-13.9
4th Harmonic (780 Hz)	44.8	34.1	-10.7
560 Hz	43.2	32.3	-10.9
880 Hz	41.6	33.0	-8.6

of the Muffin XL at the BPF, the first four harmonics of the BPF, and the rotational frequency harmonics measured at 560 Hz and 880 Hz.

The sound power levels of the discrete tones radiated by the Muffin XL have been reduced. Figure 35 illustrates the differences in appearance between the original and modified fans.

4.4.4 Muffin. Operation of the Muffin in the "bare-hub" configuration indicated the presence of discrete tones throughout the entire spectrum of measurement. The tones are rotational harmonics of the shaft frequency and their amplitudes are 8 to 15 dB below the baseline spectrum. The likely source of these tones are the rolling contact elements of the ball bearings incorporated in the fan.

Dynamic balancing of the rotor did not alter the spectral character of the radiated sound or change its overall level.

Spectrum (b) of Figure 36 illustrates the effect of the bellmouth on the radiated sound. Unlike the Tarzan and the Muffin XL, the amplitudes of the higher harmonics of the BPF are not reduced by the addition of the bellmouth. In general, the amplitudes of the tones are increased, although there is a reduction in the broadband sound level above 2 kHz.

The effect of the modified outlet support struts is shown by Spectrum (c) in Figure 36. The BPF is reduced by 7 dB, but the third and fifth harmonics of the BPF are raised by about 6 dB. The amplitudes of the other BPF harmonics are substantially reduced.

The combined effect of the bellmouth and the modified outlet support struts produced Spectrum (d) in Figure 36. Spectrum (d) contains fewer discrete tones but has a large "hump" centered around the seventh

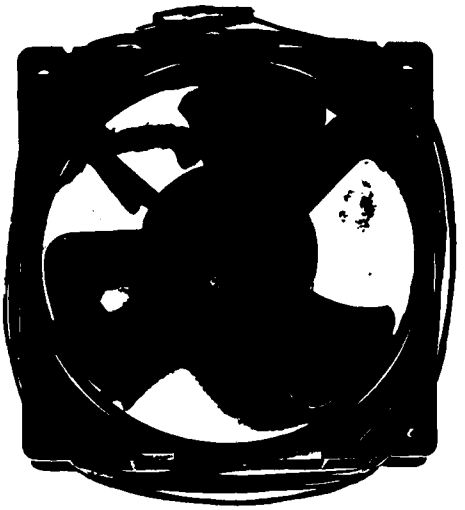

(a) original

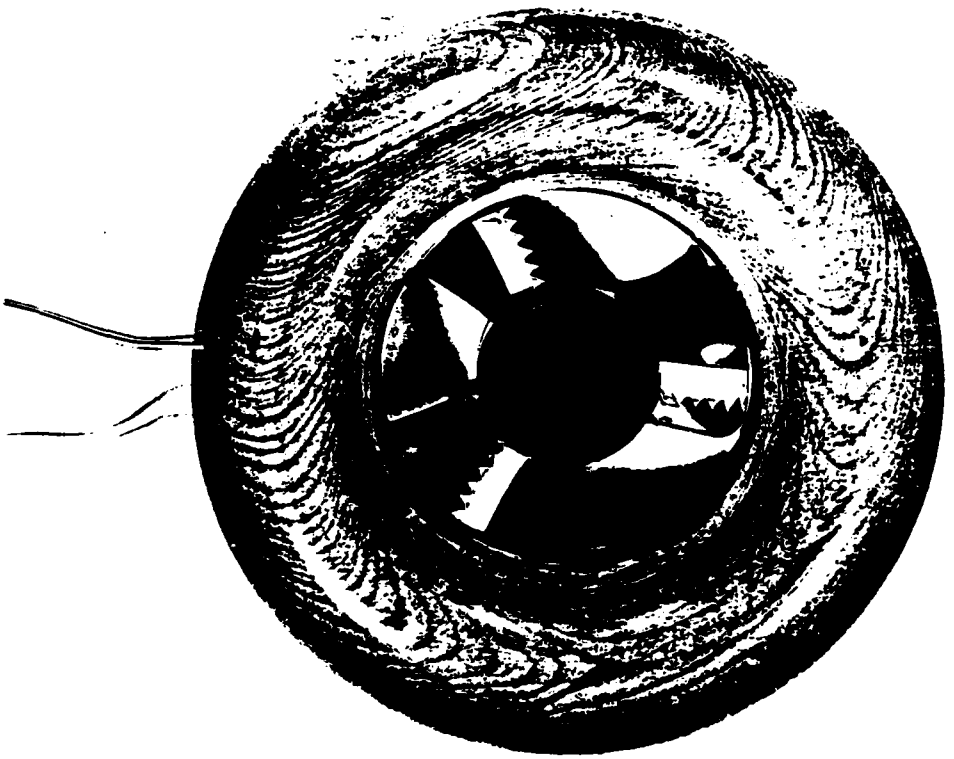

(b) modified

Figure 35. Apperance of the Original and Modified Muffin XL Fans.

Figure 36. Discrete Frequency On-Axis SPL Spectra for the Muffin in Various Configurations.

(a) In unmodified original condition.

(b) With the inlet bellmouth.

(c) With the modified outlet support struts.

(d) With the bellmouth and the modified struts.

(e) Configuration in (d) and the modified rotor blades.

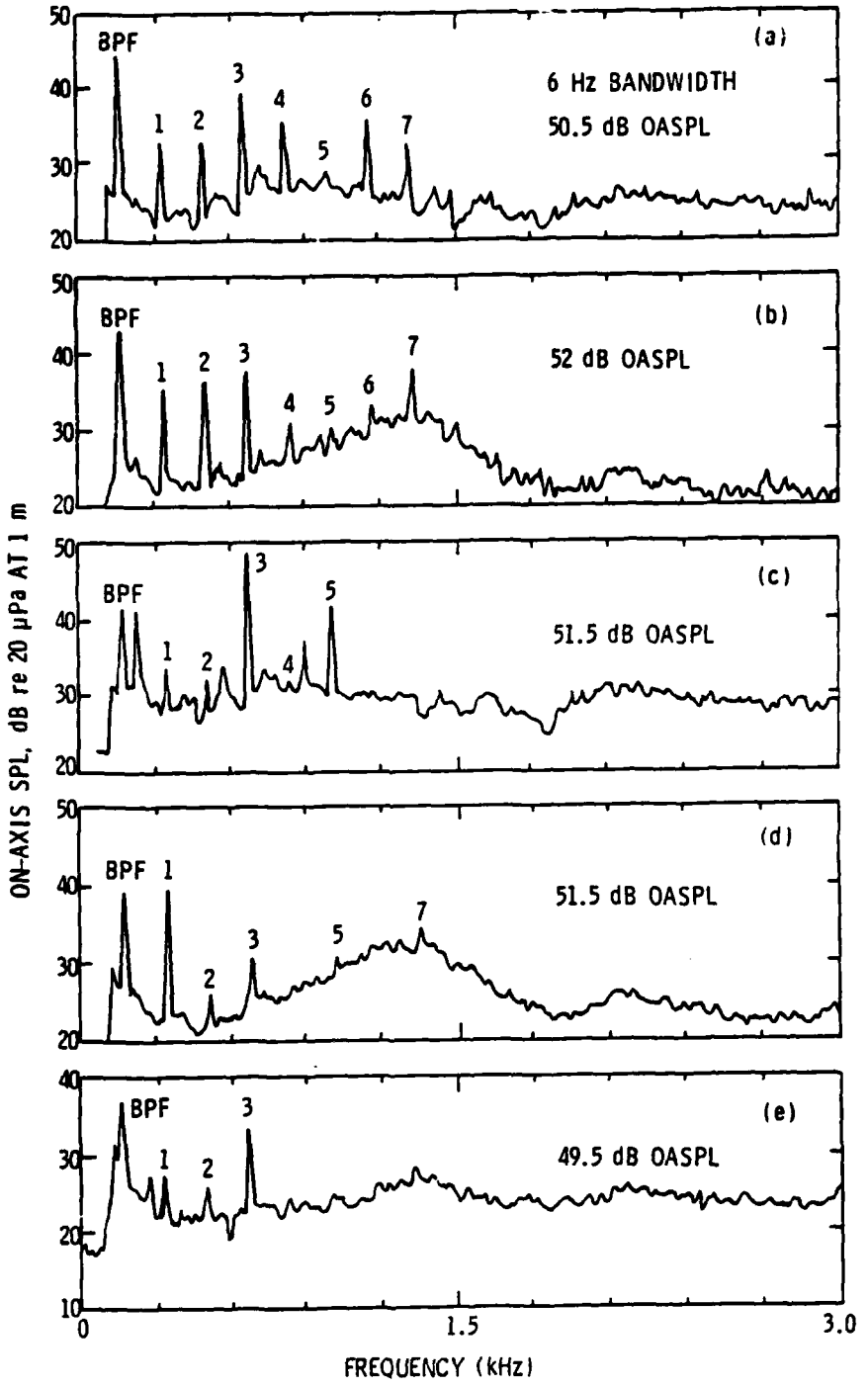
(a)
6 Hz BANDWIDTH
50.5 dB OASPL
(b)
52 dB OASPL
(c)
51.5 dB OASPL
(d)
51.5 dB OASPL
(e)
49.5 dB OASPL
BPF
ON-AXIS SPL, dB re 20 μPa AT 1 m
FREQUENCY (kHz)
0
1.5
3.0

harmonic of the BPF. This characteristic masks the higher-frequency discrete tones and is indicative of vortex-shedding noise as described by Longhouse [36].

During the evaluation of the additional design modifications developed for the Muffin, it became apparent that an abnormal or unaccounted flow condition was present. The somewhat predictable results obtained with the other fans were not demonstrated by the Muffin. Therefore, the modified blade shape illustrated in Figure 25 was evaluated. As described in Section 4.3.3, this modification was based on an assumption of the flow characteristics at the trailing edge of the blades. This assumption was indirectly supported by the acoustic measurements. To enhance its effectiveness, the modified blade shape was tested on an assembly incorporating the bellmouth and the modified outlet support struts.

Spectrum (e) in Figure 36 illustrates the combined effect of the bellmouth, the modified outlet support struts, and the modified blades. The BPF and its third harmonic remain in the spectrum, but the other discrete tones are reduced and/or eliminated from the radiated sound. The broad "hump" centered around the seventh harmonic of the BPF is reduced by 5 dB. This result exemplifies the value of acoustic measurements in assessing the aerodynamic properties of these fans. Although the radiated sound is a very small byproduct of the flow developed by the fan, a substantial change in the level and character of the radiated sound is indicative of an important change in the flow characteristics near the rotor blades.

The remaining modifications for the Muffin were evaluated on the fan assembly incorporating the bellmouth, the modified outlet support struts, and the modified rotor blade shape. Spectrum (b) in Figure 37 illustrates the improvement provided by circumferential symmetry at the outlet of the shroud which was obtained by filling the annulus with heated wax. Most apparent is the 8-dB reduction in the amplitude of the BPF as compared with Spectrum (e) of Figure 36.

The addition of the serrations to the suction side of the blades produced no change in the radiated sound until the notched tips were raised above the blade surface. The selected position for the serrations was 7.8 mm behind the leading edge (18% blade chord) of the modified blades and the tips were raised 1.8 mm above the surface of the blades. Based on the results obtained with the Tarzan and the Muffin XL, pressure-side blade serrations were not evaluated.

Spectrum (c) in Figure 37 illustrates the acoustic performance of the most quiet modified configuration of the Muffin. This assembly incorporates the bellmouth, the modified outlet support struts, the modified rotor blade shape, the improved shroud outlet geometry, and the suction-side serrations described above. Spectra (b) and (c) in Figure 37 illustrate the diminishing effect of the serrations once a uniform flow field is established near the rotor. Nevertheless, the serrations provided a 0.5 dB reduction in the overall on-axis sound pressure level.

Table X lists the individual effects of the various modifications on the discrete tones radiated by the Muffin. The changes in the on-axis sound pressure level amplitudes listed are all relative to the baseline spectrum, in decibels.

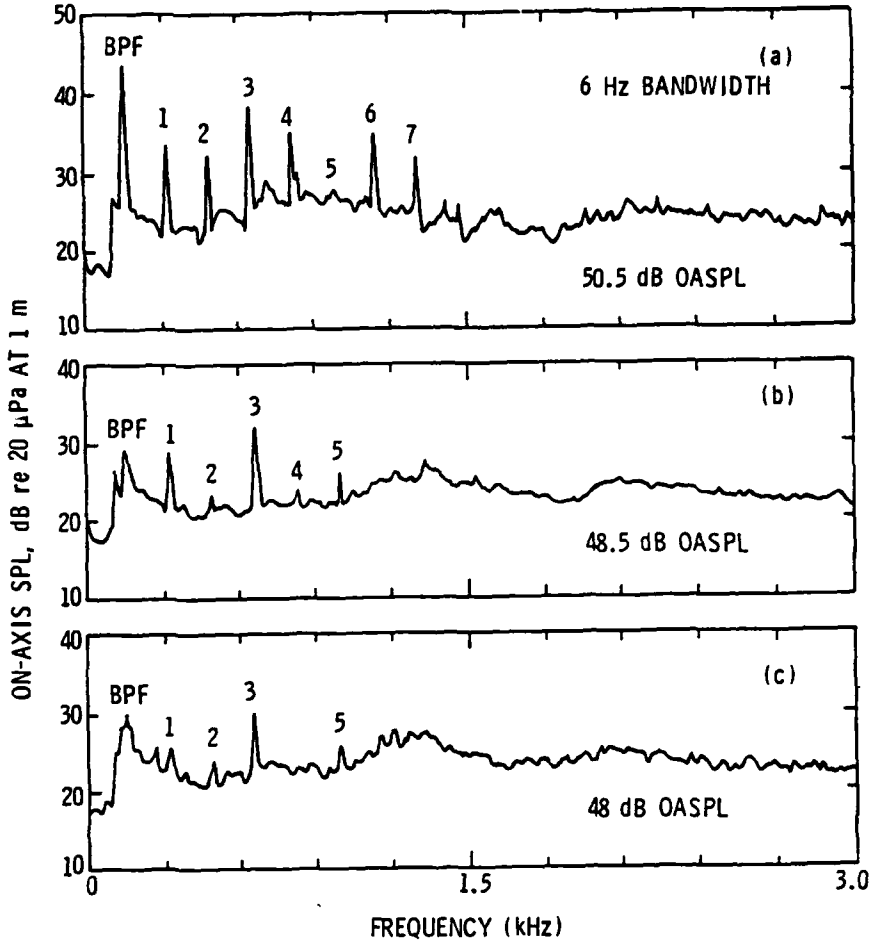

Figure 37. Discrete Frequency On-Axis SPL Spectra for the Muffin in Various Configurations.

(a) in unmodified original condition
(b) with the bellmouth, the modified struts, the modified blades, and the smoothed shroud outlet
(c) configuration of (b) with the suction-side serrations

TABLE X

EFFECTS OF THE MODIFICATIONS ON THE
DISCRETE TONES RADIATED BY THE MUFFIN

Modification	Changes in the On-Axis SPL of the BPF Harmonics, dB					
	BPF	1	2	3	4	5
(1) Bellmouth	-1	+2	+3	-1	-5	+2
(2) Outlet struts	-7	-5	-6	+5	-8	+7
(3) Bellmouth and outlet struts	-5	+6	-7	-8	-9	+1.5
(4) Bellmouth and outlet struts with modified blades	-7	-8	-7	-6	-11	-3
(5) Bellmouth and outlet struts with modified blades and improved outlet geometry	-14	-5	-9	-7	-11	-1
(6) Bellmouth and outlet struts with modified blades, improved outlet geometry and suction-side serrations	-13	-9	-9	-7	-12	-2

The directivity patterns of the discrete tones radiated by the modified assembly were found to be very uniform and displayed no evidence of the lobing present with the original unmodified fan. Using these results, the power levels of the radiated tones were calculated as described in Section 4.4.1. Table XI lists the results for the original and modified configurations of the Muffin at the BPF and the first five harmonics of the BPF.

The sound power levels of the discrete frequencies radiated by the Muffin have been reduced. Figure 38 illustrates the differences in appearance between the original and modified fans.

4.4.5 Aerodynamic performance. As described in Section 3.5.2, the aerodynamic performance of the modified configuration developed for each fan was determined.

The results of the performance evaluations are shown in Figures 39 and 40. The solid curve in each figure represents the typical baseline performance of the standard fan model. The dashed curve represents the performance of the modified fan. For each fan model, the apparent differences in performance between the baseline and modified configurations are within normal manufacturing performance tolerances. Therefore, the aerodynamic performance of the modified fans is essentially unaltered from the production norm and the discrete frequency noise reductions achieved to not penalize performance.

4.4.6 Static pressure rise tests. Static pressure rise tests of the modified fan configurations were conducted as described in Section 3.5.2 at the test conditions listed in Table III. The modified fans

TABLE XI

DISCRETE FREQUENCY POWER LEVELS - MUFFIN

Frequency	Sound Power Level dB (re 10^{-12} watts)		
	Original	Modified	Δ dB
BPF (162 Hz)	50.9	38.3	-12.7
1st Harmonic (324 Hz)	43.5	32.9	-10.6
2nd Harmonic (486 Hz)	43.2	30.7	-12.5
3rd Harmonic (648 Hz)	41.8	36.4	-5.4
4th Harmonic (810 Hz)	40.3	29.8	-10.5
5th Harmonic (972 Hz)	40.1	30.0	-10.1

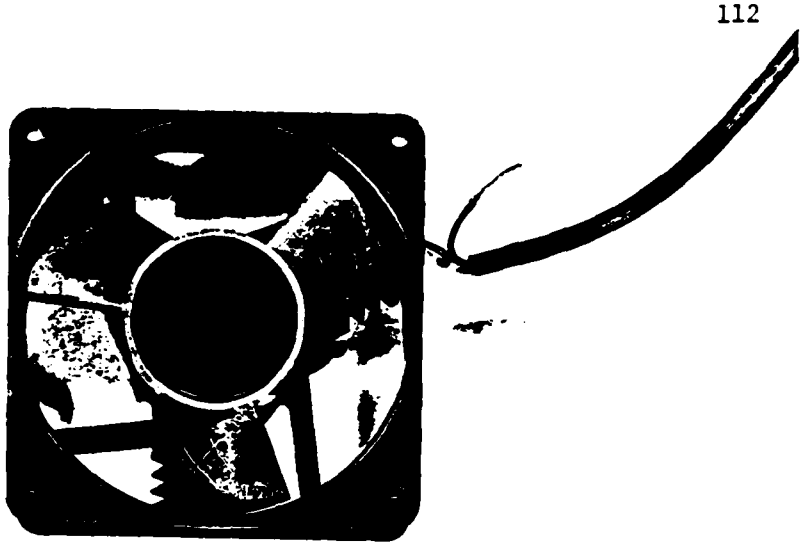

(a) original

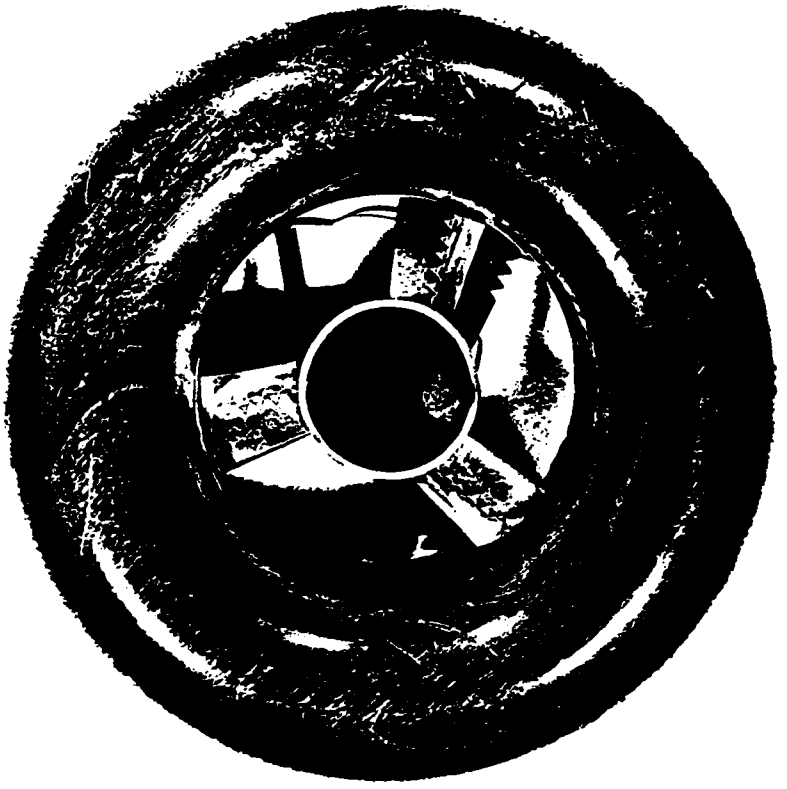

(b) modified

Figure 38 Appearance of the Original and Modified Muffin Fans.

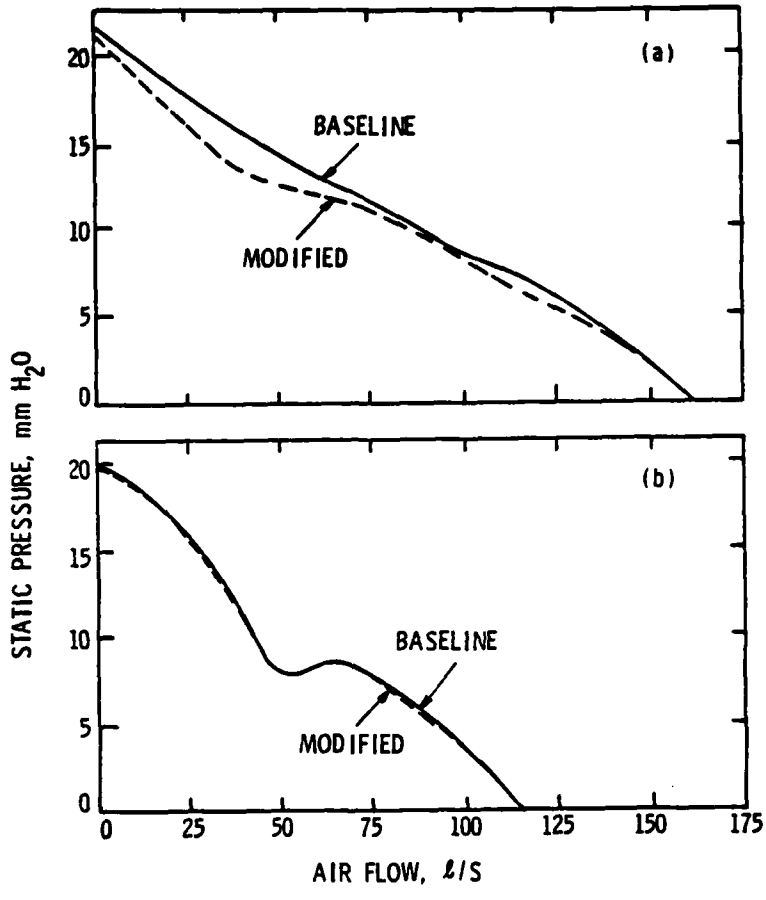

Figure 39. Aerodynamic Performance Characteristics: (a) Tarzan, and (b) Patriot.

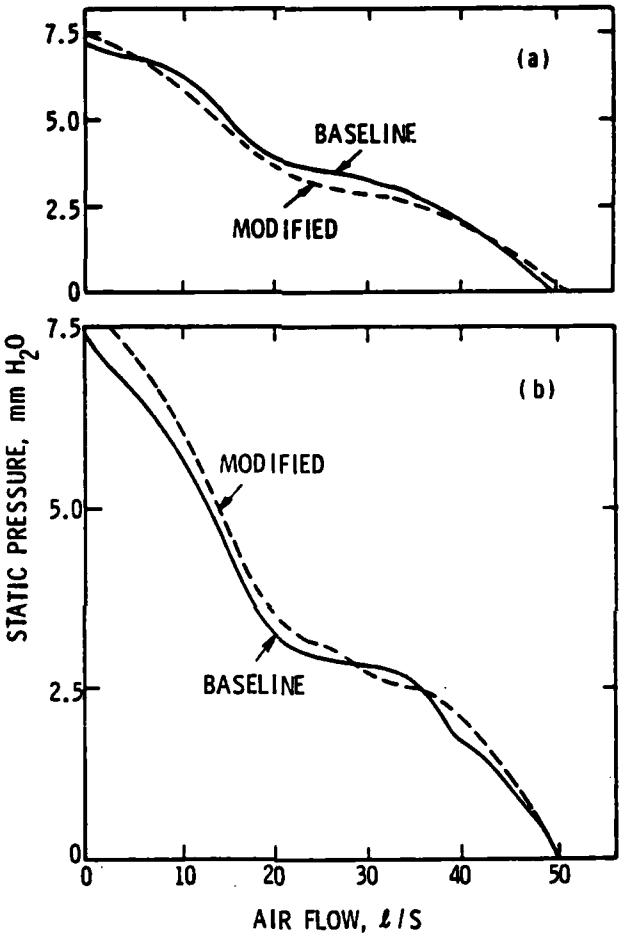

Figure 40. Aerodynamic Performance Characteristics: (a) Muffin XL, and (b) Muffin.

exhibited the same trends measured with the original fan configurations and described in Section 4.2.1. At low static pressure rises (high flow coefficients), discrete rotational tones dominate the radiated sound. The tones reduce in number and amplitude as the operating static pressure rise is increased. Finally, at a critical point of operation, the discrete tones are masked by low-frequency broadband sound which is characteristic of separated flow over the blades and blade stall.

As described in Section 4.2.1, an optimum point of operation can be determined using the nondimensional flow coefficient parameter. Figures 41 and 42 illustrate the dependence of the overall on-axis sound pressure level on the flow coefficient for the original and modified configurations of the four fans.

At low flow coefficients, the modified configurations of the Tarzan, the Muffin XL, and the Muffin radiate higher amplitude broadband sound than the unmodified configurations. These three fans incorporate inlet bellmouths and the increase in radiated sound is likely due to the shear flow imposed by the boundary layer formed on the bellmouth. The modified Patriot, which does not incorporate an inlet bellmouth, radiates less sound along its axis than the baseline Patriot at low flow coefficients. At high flow coefficients, where discrete tones dominate the radiated sound, the modified configuration of each fan radiates less sound along its axis than the original baseline configuration.

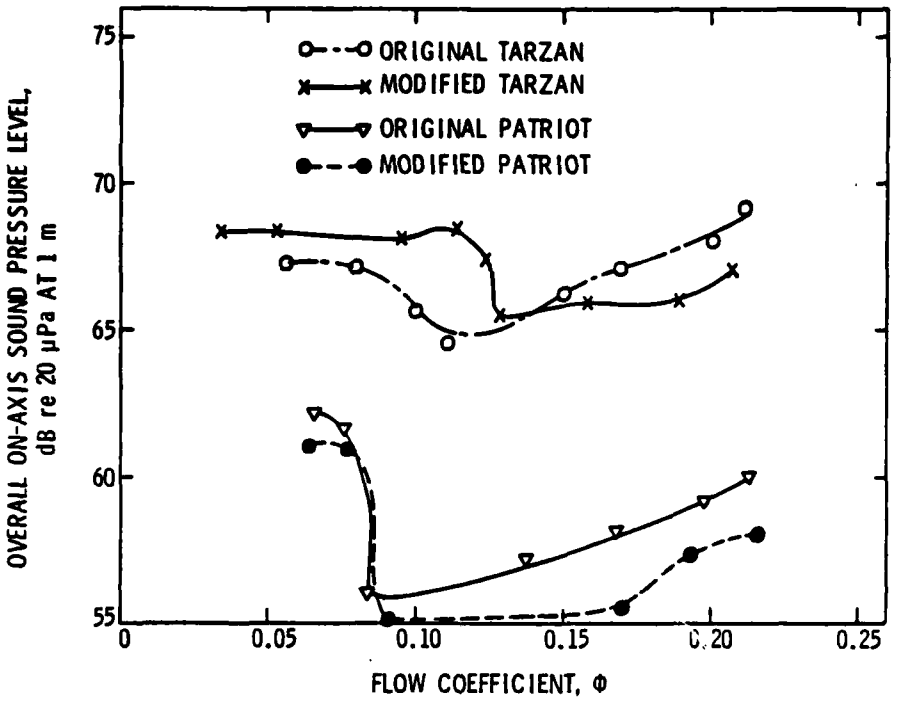

Figure 41. On-Axis SPL vs. Flow Coefficient for the Tarzan and Patriot Fans.

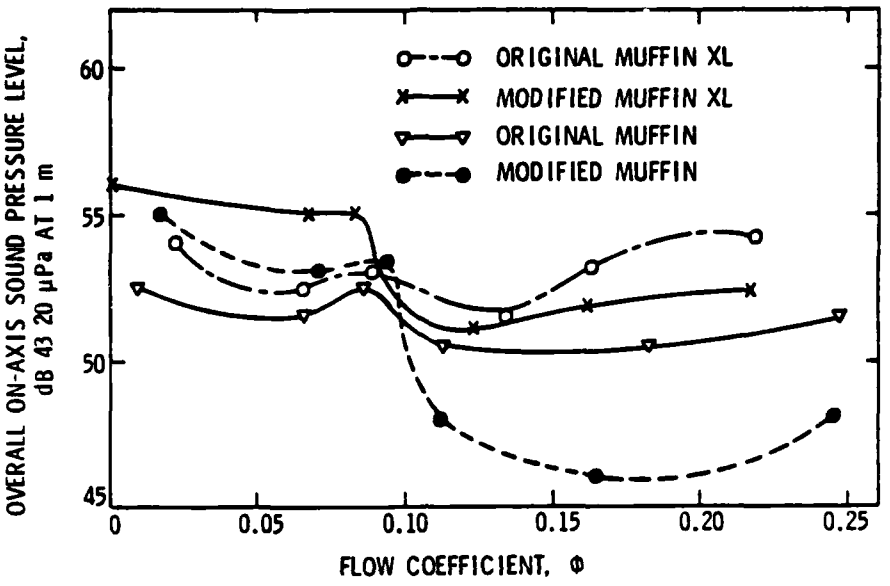

Figure 42. On-Axis SPL vs. Flow Coefficient for the Muffin XL and Muffin Fans.

CHAPTER V

CONCLUSIONS AND RECOMMENDATIONS

The following fundamental conclusions can be drawn from this study of the discrete frequency noise radiated by the axial-flow fans used in electronic equipment:

1. The maximum radiated amplitude of the discrete frequency noise occurs at high flow coefficients.
2. The radiated directivity of the discrete frequency noise is generally uniform.
3. The principal source of the discrete frequency noise is the interaction of the fan rotor with a circumferentially nonuniform flow. This interaction produces unsteady rotor blade loads which generate propagating acoustic pressure distributions.
4. Reduction of the radiated discrete frequency noise can be achieved by decreasing the unsteady blade loads. The unsteady blade loads are reduced by: improving the circumferential symmetry of the rotor annulus, inlet, and outlet; reducing the potential field of stationary objects in the rotor annulus; and adding flow modifiers to the rotor blades.
5. As observed by earlier investigators, the radiated discrete frequency noise has greater dependence on rotor inlet conditions than on rotor outlet ocnditions. The magnitude of the inlet flow distortions depends on the contraction

of the flow entering the rotor annulus and upstream strut configurations.

The following recommendations are offered as means to reduce the generation of discrete frequency noise by these types of axial-flow fans:

1. A circumferentially uniform shroud inlet geometry, such as a bellmouth, should be incorporated into the design of the fans.
2. The radial dimensions of the rotor annulus should be uniform along the rotor axis with no abrupt changes in curvature.
3. The center-hub support struts should be positioned downstream of the rotor at a maximum practical distance from the trailing edge of the rotor blades.
4. The center-hub support struts should be shaped aerodynamically and mounted tangentially or at least swept.
5. The design and use of blade-flow modifiers, such as the suction-side serrations, should be incorporated when feasible.
6. In applications of these fans, the local flow environment should be undistorted and uniform.

REFERENCES

1. Kryter, K. D., and Pearson, K. S., "Judged Noisiness of a Band of Random Noise Containing an Audible Pure Tone," Journal of the Acoustical Society of America, Vol. 38, July 1965, pp. 106-112.

2. Webster's Third New International Dictionary, copyright 1961 by G and C Merriam Company.

3. Crighton, D. G., "The Basic Principles of Aerodynamic Noise Generation," Prog. Aerospace Science, Vol. 16, No. 1, 1975, pp. 31-96.

4. Cumpsty, N. A., "Review - A Critical Review of Turbomachinery Noise," Journal of Fluids Engineering, Trans. ASME, Series I, Vol. 99, No. 2, 1977, pp. 278-293.

5. Skudrzyk, E. J., The Foundations of Acoustics: Basic Mathematics and Basic Acoustics, Springer-Verlag, New York-Wien, 1971, pp. 428-430.

6. Chandrashkhara, N., "Experimental Studies of Discrete Tone Noise from an Axial-Flow Fan," Journal of Sound and Vibration, Vol. 13, No. 1, 1970, pp. 43-49.

7. Morfey, C. L., "Rotating Pressure Patterns in Ducts: Their Generation and Transmission," Journal of Sound and Vibration, Vol. 1, 1964, pp. 60-87.

8. Tyler, J. M., and Sofrin, T. G., "Axial-Flow Compressor Noise Studies," S.A.E. Transactions, Vol. 70, 1962, pp. 309-322.

9. Mather, J. S. B., Savidge, J., and Fisher, M. J., "New Observations on Tone Generation in Fans," Journal of Sound and Vibration, Vol. 16, 1971, pp. 407-418.

10. Barry, B., and Moore, C. J., "Subsonic Fan Noise," Journal of Sound and Vibration, Vol. 17, 1971, pp. 207-220.

11. Wright, S. E., "Sound Radiation from a Lifting Rotor Generated by Asymmetric Disc Loading," Journal of Sound and Vibration, Vol. 9, 1969, pp. 223-240.

12. Morse, P. M., Vibration and Sound, copyright 1976 by The Acoustical Society of America, pp. 313, 326-328.

13. Mugridge, B. D., and Morfey, C. L., "Sources of Noise in Axial-Flow Fans," Journal of the Acoustical Society of America, Vol. 51, No. 5, 1972, pp. 1411-1426.

14. Wright, S. E., "Discrete Radiation from Rotating Periodic Sources," Journal of Sound and Vibration, Vol. 17, 1971, pp. 437-498.

15. Yudin, E. Y., "On the Vortex Sound from Rotating Rods," NACA TM 1136, 1947, National Advisory Committee for Aeronautics, Washington, DC.

16. Lilley, G. M., "On the Vortex Noise from Airscrews, Fans, and Compressors," Rolls-Royce Limited, Noise Panel Report, 1961 (as cited in Reference 17).

17. Morfey, C. L., "Rotating Blades and Aerodynamic Sound," Journal of Sound and Vibration, Vol. 28, 1973, pp. 587-617.

18. Lowson, M. V., and Ollerhead, J. B., "A Theoretical Study of Helicopter Rotor Noise," Journal of Sound and Vibration, Vol. 9, 1969, pp. 197-222.

19. Wells, R. J., and Madison, R. D., "Fan Noise," Handbook of Noise Control, edited by Cyril M. Harris, Chapter 25, McGraw-Hill Book Company, Inc., Copyright 1957.

20. Beranek. L. L., Reynolds, J. L., and Wilson, K. E., "Apparatus and Procedures for Predicting Ventillation System Noise," Journal of the Acoustical Society of America, Vol. 25, No. 2, 1953, pp. 313-321.

21. Marboe, R. C., and Fitzgerald, J. M., "The ARL/FED Anechoic Chamber," The Pennsylvania State University, Applied Research Laboratory TM81-164, August 1981.

22. Rotron Incorporated, Woodstock, NY, Commercial Product Catalog, February 1980, pp. Com 040, Com 043, Com 083, and Com 120.

23. Rotron Incorporated, Woodstock, NY, Fan Performance Test Facility, configured in accordance with AMCA Standard 210.

24. Sharland, I. J., "Sources of Noise in Axial-Flow Fans," Journal of Sound and Vibration, Vol. 1, 1964, pp. 302-322.

25. Longhouse, R. E., "Noise Mechanism Separation and Design Considerations for Low Tip-Speed Axial-Flow Fans," Journal of Sound and Vibration, Vol. 48, 1976, pp. 461-474.

26. Mellin, R. C., "Selection of Minimum Noise Fans for a Given Pumping Requirement," Noise Control Engineering, Vol. 4, No. 1, January-February 1975.

27. Nagel, R. T., "The Influence of Leading Edge Serrations on the Noise Radiated from a Statically Thrusting Rotor," The Pennsylvania State University, Ordnance Research Laboratory TM72-188, August 1972.

28. Filleul, N. Le S., "An Investigation of Axial-Flow Fan Noise," Journal of Sound and Vibration, Vol. 3, 1966, pp. 146-165.

29. Wallis, R. A., Axial-Flow Fans: Design and Practice, copyright 1961 by the Academic Press, p. 91.

30. Bruce, E. P., "The ARL Axial-Flow Research Fan - A New Facility for Investigation of Time-Dependent Turbomachinery Flows," ASME Publication 74-FE-27, May 1974.

31. Schlicting, H., Boundary-Layer Theory, copyright 1968 by McGraw-Hill Company, pp. 595-602.

32. Duncan, P. E., Dawson, B., and Hawes, S. P., "Design Techniques for the Reduction of Interaction Tonal Noise from Axial-Flow Fans," Report No. C116/75, copyright 1975 by the Institution of Mechanical Engineers.

33. Smith, R. H., "Aerodynamic Theory and Test of Strut Forms - II," NACA Report No. 335, 1929, National Advisory Committee for Aeronautics, Washington, DC.

34. Duncan, P. E., and Dawson, B., "Reduction of Interaction Tones from Axial-Flow Fans by Suitable Design of Rotor Configuration," Journal of Sound and Vibration, Vol. 33, 1974, pp. 143-154.

35. Patel, J., "Fan with Noise Reduction," United States Patent No. 4,089,618, May 16, 1978.

36. Longhouse, R. E., "Vortex Shedding Noise of Low Tip-Speed Axial-Flow Fans," Journal of Sound and Vibration, Vol. 53, 1977, pp. 25-46.

37. Warring, R. H., Handbook of Noise and Vibration Control, edited by R. H. Warring, copyright 1970 by Morden, Trade and Technical Publications.

APPENDIX A

DESCRIPTION OF THE REPRESENTATIVE FANS

The purpose of this Appendix is to provide a general description of each of the representative fans selected for this study. In their respective size and performance ranges, these fans are popularly used and represent the reference standards in the electronics industry. The photographs, layout sketches, and performance curves included here are taken from Reference [22].

A.1 Rotron Tarzan TN 3A3

The Tarzan is the largest fan selected for study. It is a five-bladed design fitted with an integral shroud and mounting structure as shown in Figure 43(b). The blades are of constant thickness and twisted having a nominal tip diameter of 16.2 cm, a nominal chord length of 7.3 cm, a 0.466 nominal aspect ratio, and are injection molded using black polycarbonate plastic. The rotor is powered by a 230 VAC single-phase motor which normally operates at 3325 RPM (60 Hz) and draws 73 watts. The blade tip Mach number is 0.087 while operating at free delivery. Figure 43 illustrates the appearance of the fan, the standard mounting dimensions and view, and the standard performance.

A.2 Rotron Patriot PT 77 B3

The Patriot is a five-bladed design incorporating a circularly shaped shroud with three tangentially mounted support struts as shown in Figure 44(b). The blades have a spanwise twist and are of variable thickness. The blade tip diameter is 14.3 cm. The blades have a

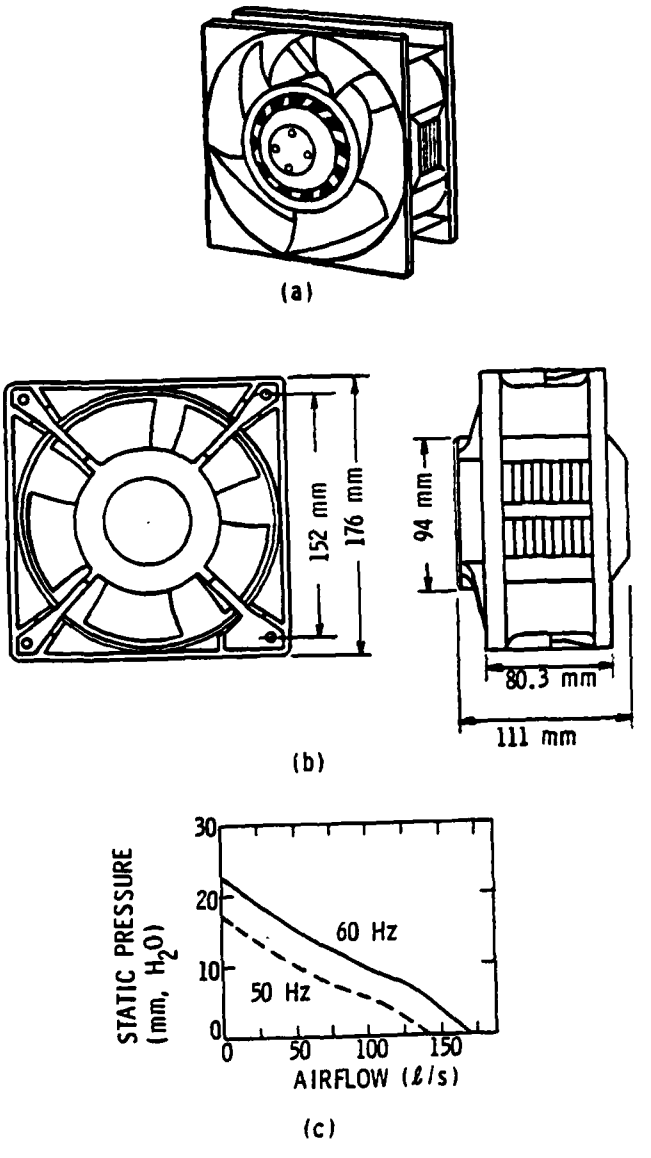

Figure 43. Tarzan Fan: (a) Appearance, (b) Dimensions and View, and (c) Performance.

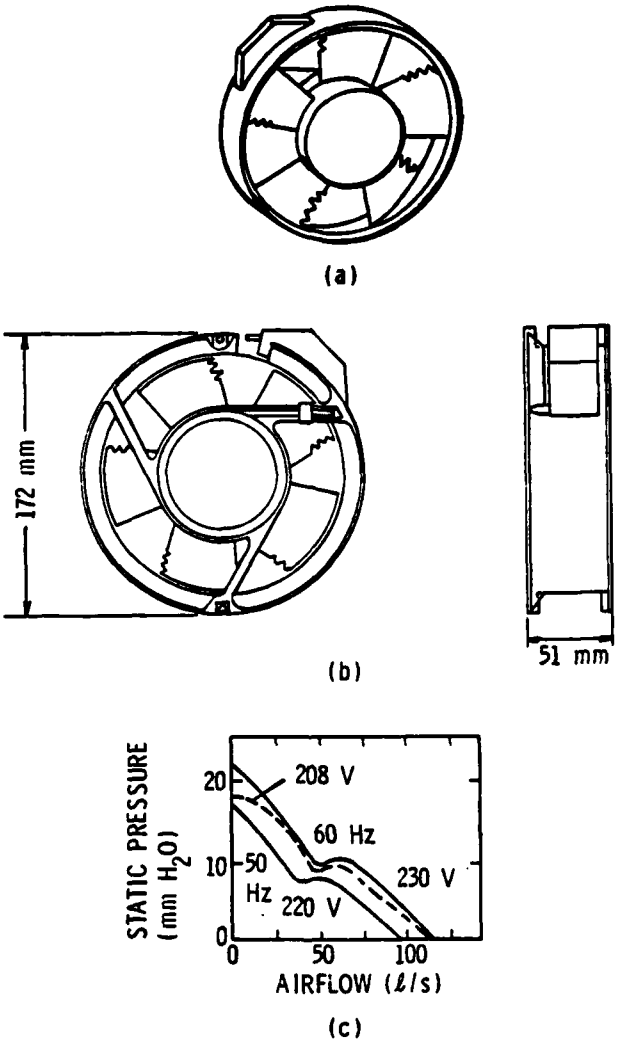

Figure 44. Patriot Fan: (a) Appearance, (b) Dimensions and View, and (c) Performance.

nominal chord length of 5.5 cm and an aspect ratio of 0.562. The blades incorporate training-edge serrations to reduce the generation of vortex-shedding noise as described by Patel [35] and are made from injection molded polycarbonate plastic. The rotor is powered by a 230 VAC single-phase motor which normally operates at 3350 RPM (60 Hz) and draws 35 watts. The blade tip Mach number is 0.076 while operating at free delivery. Figure 44 illustrates the appearance of the fan, the standard mounting dimensions and view, and the standard aerodynamic performance.

A.3 Rotron Muffin XL MX 2A1

The Muffin XL is the only fan selected for study which incorporates a sintered bronze sleeve bearing for rotation (the other fans incorporate ball bearings). It is a three-bladed design fitted with an integral shroud and four tangentially mounted support struts as shown in Figure 45(b). The blades are of variable thickness and are untwisted along their span. The blades have a nominal tip diameter of 11.1 cm, a 4.5 cm nominal chord length, and an aspect ratio of 0.67. The blades incorporate trailing-edge serrations to reduce the generation of vortex-shedding noise and are made from injection molded polypropylene plastic. The rotor is powered by a 115 VAC single-phase motor which normally operates at 3100 RPM (60 Hz) and draws 15 watts. The blade tip Mach number is 0.055 while operating at free delivery. Figure 45 illustrates the appearance of the fan, the standard mounting dimensions and view, and the standard aerodynamic performance.

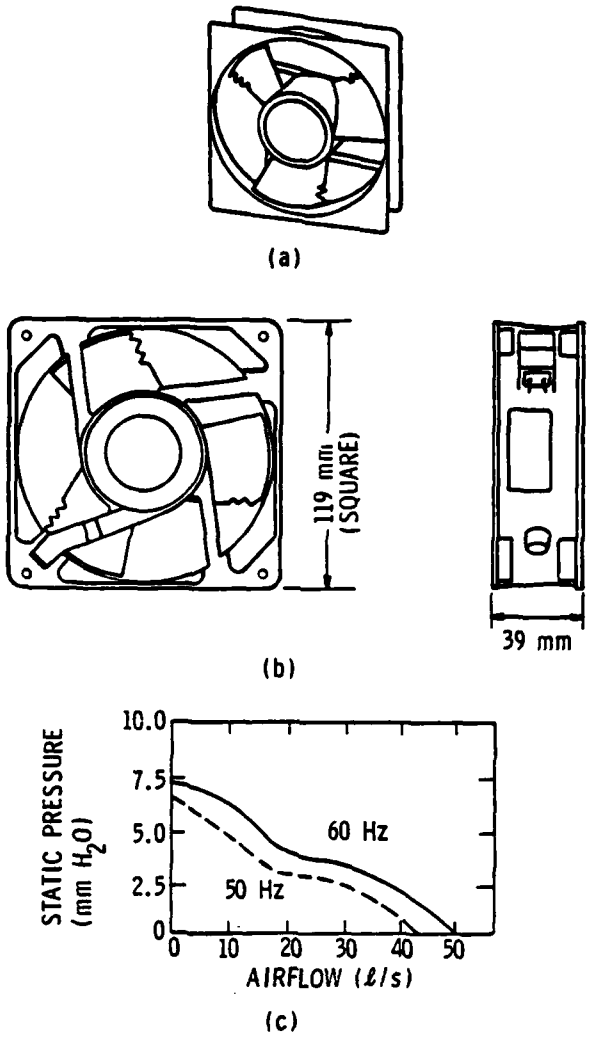

Figure 45. Muffin XL Fan: (a) Appearance, (b) Dimensions and View, and (c) Performance.

A.4 Rotron Muffin MU 77 B1

The Muffin is a three-bladed design fitted with an integral shroud and four radially mounted support struts as shown in Figure 46(b). The blades are untwisted and have constant thickness. The blades have a nominal tip diameter of 10.5 cm, a 4.5 cm nominal chord length, and an aspect ratio of 0.61. The blades are made from injection molded polypropylene plastic. The rotor is powered by a 230 VAC single-phase motor which normally operates at 3250 RPM (60 Hz) and draws 12 watts. The blade tip Mach number is 0.053 while operating at free delivery. Figure 46 illustrates the appearance of the fan, the standard mounting dimensions and view, and the standard aerodynamic performance.

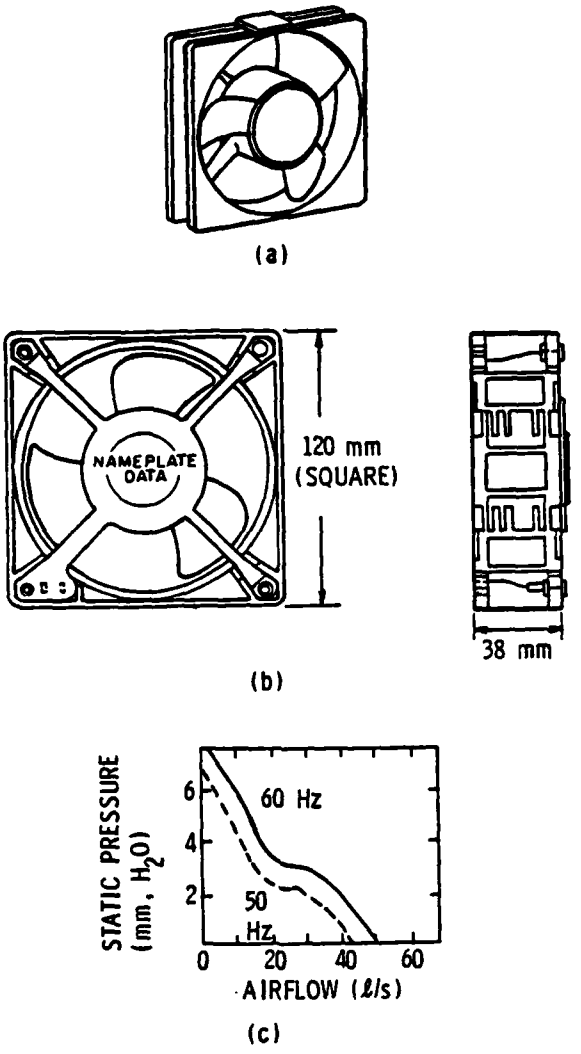

Figure 46. Muffin Fan: (a) Appearance, (b) Dimensions and View, and (c) Performance.

DISTRIBUTION LIST FOR UNCLASSIFIED ARL TM No. 82-76 by J. M. Fitzgerald dated March 2 1982.

Commander
Naval Sea Systems Command
Department of the Navy
Washington, DC 20362
Attn: Library
Code NSEA-09G32
(Copy Nos. 1 and 2)

Naval Sea Systems Command
Attn: R. Keane
Code NSEA-3213
(Copy No. 3)

Naval Sea Systems Command
Attn: F. E. Eissing
Code NDEA-05H
(Copy No. 4)

Naval Sea Systems Command
Attn: S. M. Blazek
Code NSEA-05HB
(Copy No. 5)

Naval Sea Systems Command
Attn: A. R. Paladino
Code NSEA-05H1
(Copy No. 6)

Naval Sea Systems Command
Attn: F. B. Peterson
Code NSEA-052P
(Copy No.7)

Naval Sea Systems Command
Attn: E. G. Liszka
Code NSEA-63R1
(Copy No. 8)

Naval Sea Systems Command
Attn: F. J. Romano
Code NSEA-63R3
(Copy No. 9)

Naval Sea Systems Command
Attn: T. E. Peirce
Code NSEA-63R31
(Copy No. 10)

Commanding Officer
Naval Underwater Systems Center
Newport, RI 02840
Attn: P. Corriveau
Code 3635
(Copy No. 11)

Naval Underwater Systems Center
Attn: D. Goodrich
Code 3634
(Copy No. 12)

Naval Underwater Systems Center
Attn: T. A. Davis
Code 36314
(Copy No. 13)

Naval Underwater Systems Center
Attn: B. J. Myers
Code 3630
(Copy No. 14)

Naval Underwater Systems Center
Attn: R. H. Nadolink
Code 3634
(Copy No. 15)

Naval Underwater Systems Center
Attn: Library
Code 54
(Copy No. 16)

Officer-in-Charge
David W. Taylor Naval Ship R&D Center
Department of the Navy
Annapolis Laboratory
Annapolis, MD 21402
Attn: J. V. Pierpoint
Code 2741
(Copy No. 17)

David W. Taylor Naval Ship R&D Center
Attn: J. Henry
Code 2741
(Copy No. 18)

David W. Taylor Naval Ship R&D Center
Attn: Library
Code 1505
(Copy No. 19)

David W. Taylor Naval Ship R&D Center
Attn: R. A. Cumming
Code 1540
(Copy No. 20)

David W. Taylor Naval Ship R&D Center
Attn: J. H. McCarthy
Code 154
(Copy No. 21)

DISTRIBUTION LIST FOR UNCLASSIFIED ARL TM No. 82-76 by J. M. Fitzgerald dated March 2 1982

David W. Taylor Naval Ship R&D Center
Attn: T. E. Brockett
Code 1544
(Copy No. 22)

David W. Taylor Naval Ship R&D Center
Attn: R. J. Boswell
Code 1544
(Copy No. 23)

David W. Taylor Naval Ship R&D Center
Attn: T. T. Huang
Code 1552
(Copy No. 24)

David W. Taylor Naval Ship R&D Center
Attn: Y. T. Shen
Code 1552
(Copy No. 25)

David W. Taylor Naval Ship R&D Center
Attn: M. M. Sevik
Code 19
(Copy No. 26)

David W. Taylor Naval Ship R&D Center
Attn: W. K. Blake
Code 1905
(Copy No. 27)

David W. Taylor Naval Ship R&D Center
Attn: R. A. Rippeon
Code 1908
(Copy No. 28)

David W. Taylor Naval Ship R&D Center
Attn: R. W. Brown
Code 1942
(Copy No. 29)

David W. Taylor Naval Ship R&D Center
Attn: T. M. Farabee
Code 1942
(Copy No. 30)

David W. Taylor Naval Ship R&D Center
Attn: F. E. Geib
Code 1942
(Copy No. 31)

David W. Taylor Naval Ship R&D Center
Attn: F. S. Archibald
Code 1942
(Copy No. 32)

Office of Naval Research
Department of the Navy
800 N. Quincy Street
Arlington, CA 22217
Attn: A. H. Gilmore
(Copy No. 33)

Office of Naval Research
Department of the Navy
800 N. Quincy Street
Arlington, CA 22217
Attn: R. E. Whitehead
Code 432
(Copy No. 34)

Commanding Officer
Naval Ocean Systems Center
San Diego, CA 92152
Attn: Library
(Copy No. 35)

Naval Ocean Systems Center
Attn: M. M. Reischmann
(Copy No. 36)

Naval Ocean Systems Center
Attn: D. Nelson
(Copy No. 37)

Defense Technical Information Center
5010 Duke Street
Cameron Station
Alexandria, VA 22314
(Copy No.s 38-43)

Naval Research Laboratory
Washington, DC 20390
Attn: Library
(Copy No. 44)

Naval Postgraduate School
The Presidio
Monterey, CA 93940
Attn: Library
(Copy No. 45)

DISTRIBUTION LIST FOR UNCLASSIFIED ARL TM No. 82-76 by J. M. Fitzgerald dated March 2 1982.

Professor P. Leehey
Dept of Ocean Engineering-Rm 5-222
Massachusetts Institute of Technology
77 Massachusetts Avenue
Cambridge, MA 02139
(Copy No. 46)

National Bureau of Standards
Aerodynamics Section
Washington, DC 20234
Attn: P. S. Klebanoff
(Copy No. 47)

Naval Research Laboratory
Washington, D.C. 20390
Attn: R. J. Hansen
(Copy No. 48)

Dr. John L. Lumley
Sibley School of Mechanical and
Aeronautical Engineering
Upson Hall
Cornell University
Ithaca, NY 14850
(Copy No. 49)

Dr. Allen Moore
Admiralty Research Laboratory
Teddington, Middlesex
England
(Copy No. 50)

University of Leeds
Department of Applied Mathematical Studies
Leeds LS29JT, ENGLAND
Attn: Dr. D. G. Crighton
(Copy No. 51)

The Pennsylvania State University
Aerospace Engineering Department
University Park, Pa. 16801
Attn: B. Lakshiminarayana
(Copy No. 52)

The Pennsylvania State University
Aerospace Engineering Department
University Park, Pa. 16801
Attn: P. J. Morris
(Copy No. 53)

The Pennsylvania State University
Applied Research Laboratory
Post Office Box 30
State College, PA 16801
Attn: R. E. Henderson
(Copy No. 54)

Applied Research Laboratory
Attn: D. E. Thompson
(Copy No. 55)

Applied Research Laboratory
Attn: E. G. Taschuk
(Copy No. 56)

Applied Research Laboratory
Attn: G. C. Lauchle
(Copy No. 57)

Applied Research Laboratory
Attn: W. S. Gearhart
(Copy No. 58)

Applied Research Laboratory
Attn: GTWT Files
(Copy No. 59)

Sone and Webster Engineering Corp.
245 Summer Street
Boston, MASS 02107
Attn: J. M. Fitzgerald
Environmental Eng. Div.
(Copy No. 60)

IBM Corp., Acoustics Laboratory
P.O. Box 390, Bldg. 704
Poughkeepski, NY 12602
Attn: Dr. W. W. Lang
(Copy No. 61)

IBM Corp.
Attn: Dr. G. C. Maling, Jr.
(Copy No. 62)

IBM Corp.
Attn: D. Yeager
(Copy No. 63)

ROTRON Corp.
Woodstock, NY
Attn: A. Bogess
(Copy No. 64)


FILME